NRC·CNRC Aerospace

Review of Aeronautical Fatigue and Structural Integrity Work in Canada (2015 - 2017)

Authors: Min Liao

Report No.: LTR-SMM-2017-0097

RDIMS No.: N/A

Date: April 2017

National Research Council Canada | Conseil national de recherches Canada

Canada

NATIONAL RESEARCH COUNCIL CANADA (NRC)

AEROSPACE

Review of Aeronautical Fatigue and Structural Integrity Work in Canada (2015 - 2017)

Volume 1 of 1

Report No.: LTR-SMM-2017-0097

RDIMS No.: N/A

Date: April 2017

Authors: Min Liao

Classification:	Unclassified	Distribution:	Unlimited
For:	International Committee on Aeronautical Fatigue and Structural Integrity (ICAF)		
Reference:	-		
Submitted by:	S. Béland, Director, Structures, Materials and Manufacturing Laboratory		
Approved by:	J. Komorowski, General Manager, Aerospace Portfolio		

Pages :	125	Copy No.:	N/A
Figures:	104	Tables:	3

EXECUTIVE SUMMARY

This report provides a review of aeronautical fatigue and structural integrity work in Canada during the period April 2015 to April 2017. All aspects of structural integrity, especially fatigue related work, are covered including: full-scale testing, life assessment and enhancement, load and usage monitoring, structural health monitoring and non-destructive inspection, environmental effect, as well as new material and manufacturing. This national review will be presented at the 35th International Committee on Aeronautical Fatigue and Structural Integrity (ICAF) Conference, which will be held in Nagoya, Japan, June 5th to June 6th, 2017.

Organization abbreviations used in this document are:

BA – Bombardier Aerospace
DRDC – Defence Research and Development Canada (DND)
DND – Department of National Defence
DTAES – Directorate of Technical Airworthiness and Engineering Support (DND)
IMP – IMP Aerospace
L-3 MAS – L-3 Communications (Canada) Military Aircraft Services (MAS)
NRC – National Research Council Canada
RCAF – Royal Canadian Air Force (CF)
RMC – Royal Military College of Canada (DND)

TABLE OF CONTENTS

ABBREVIATIONS

AE	Acoustic Emission
Al	Aluminium
ALEX	Aircraft Life Extension Program
AM	Additive Manufacturing
AP	Atmospheric Plasma
APES	Analytical Processes / Engineered Solutions
AR	Amplitude Ratio
ASIP	Aircraft Structural Integrity Program
ASTM	American Society for Testing and Materials
AU	Acoustic Ultrasonic
BOS	Baseline Operational Spectrum
BUS	Basic Usage Spectrum
BVID	Barely Visible Impact Damage
CC	Correlation Coefficient
CCC	Cross-Coupled Compensation
CBR	Center Barrel Replacement
CFH	Cumulative Flight Hours
CLT	Classical Laminate Theory
CMM	Coordinate Measuring Machine
CNR	Contrast-to-Noise Ratio
CP	Control Point
CR	Computed Radiography
CRIAQ	Consortium for Research and Innovation in Aerospace
CSG	Chameleon Skin Gauge
CX	Cold Expansion
DA	Durability Analysis
DADT	Durability and Damage Tolerance
DADTA	Durability and Damage Tolerance Assessment
DCB	Double Cantilever Beam
DCPD	Direct Current Potential Drop
DDTCP	Durability and Damage Tolerance Control Plan
DIC	Digital Image Correlation
DM	Damage Matrix
DOF	Degrees Of Freedom
DPHM	Diagnostics, Prognostics and Health Management
DRF	Damage Response Factor
DSA	Dynamic Strain Aging
DSG	Design Service Goal
DSTG	Defence Science and Technology Group Australia
DT	Damage Tolerance
DTA	Damage Tolerance Analysis
EB	Electron Beam
EBAM	Electron Beam Additive Manufacturing

EBH	Equivalent Baseline Hours
EC	Eddy Current
EDM	Electrically Discharged Machining
ELE	Estimated Life Expectancy
ENIQ	European Network for Inspection and Qualification
EPS	Equivalent Penetrameter Sensitivity
ER	Energy Ratio
FAA	Federal Aviation Administration
FARS	Fleet Average Reference Spectrum
FCC	Face-Centered Cubic
FCS	Flight Control Surfaces
FDR	Flight Data Recorder
FE/FEA/FEM	Finite Element/Finite Element Analysis/Finite Element Modelling
FMC	Full Matrix Capture
FOD	Foreign Object Damage
FS	Fuselage Station
FSCS	Flight State and Control System
FSFT	Full Scale Fatigue Test
FT	Fatigue Test
G	Gravity
GB	Gear Box
H-Stab	Horizontal Stabilator
HCP	Hexagon Close Packed
HOLSIP	Holistic Structural Integrity Process
HUMS	Health and Usage Monitoring System
IABG	Industrieanlagen-Betriebsgesellschaft mbH
IAT	Individual Aircraft Tracking
ICAS	International Council of the Aeronautical Sciences
ICFT	Integrated Creep-Fatigue Theory
IP	Imaging Plate
IQI	Image Quality Indicator
IR	Infrared
ISRV	Intermediate Support Readiness Validation
ISS	In-Service Support
K_t	Stress Concentration
L3-MAS	L-3 Communications (Canada) Military Aircraft Services (MAS)
LC	Laser Consolidation
LCF	Low Cycle Fatigue
LEFM	Linear Elastic Fracture Mechanics
LIF	Life Improvement Factor
LLI	Life Limited Items
LMA	Lockheed Martin Aeronautics
LPI	Liquid Penetrant Inspection
MHP	Maritime Helicopter Program
MAPoD	Model-assisted Probability of Detection
Mg	Magnesium

MRO	Maintenance, Repair and Overhaul
MSD/MED	Multi-site Fatigue Damage/Multiple Element Damage
N_f	Number of Cycles to Failure
NDI/NDE	Non-destructive Inspection/Non-destructive Evaluation
NDT	Non-destructive Testing
NPR	Negative Poisson Ratio
OEM	Original Equipment Manufacturer
OLM	Operational Loads Monitoring
PoD	Probability of Detection
PoL	Probability of Localization
PSE	Primary Structural Element
PZT	Piezoelectric Transducer
QETE	Quality Engineering Test Establishment
RAAF	Royal Australian Air Force
RCAF	Royal Canadian Air Force
RE	Rare Earth
RST	Residual Strength Test
RT	Room Temperature
SAM	Signal Approximation Method
SBI	Safety-by-Inspection
SBLM	Structural Base Level Maintenance
SDRS	Structural Data Recording Set
SEM	Spectral Element Method
SG	Stain Gauge
SIF	Stress Intensity Factor
SHM	Structural Health Monitoring
SLAP	Service Life Assessment Program
SMM	Structures, Materials and Manufacturing
SNR	Structure-to-Noise Ratio
SRM	Structural Repair Manual
SRP	Strategic Reform Program
SSI	Structurally Significant Items
ST	Structural Test
TF	Transfer Function
TFM	Total Focusing Method
TJ	Technical Justification
TMF	Thermal Mechanical Fatigue
ToF	Time of Flight
TR	Tail Rotor
TSA	Thermoelastic Stress Analysis
UCART	Usage Comparison and Reporting Tool
USN	United States Navy
USAF	United States Air Force
VCCT	Virtual Crack Closure Technique
WFD	Widespread Fatigue Damage

1.0 INTRODUCTION

Canadian Industries, universities and government agencies were solicited for information describing their fatigue technology and structural integrity related activities over the period April 2015 to April 2017. This review covers work performed or being performed by the following organizations (including some collaborative organizations):

- Bombardier Aerospace
- IMP Aerospace
- IHI Corporation, Japan
- L-3 Communications (Canada) Military Aircraft Services (MAS)
- Rolls-Royce Deutschland
- Siemens Canada
- School of Engineering, University of British Columbia
- Department of Mechanical and Industrial Engineering, Ryerson University
- Department of Mechanical & Aeronautical Engineering, Clarkson University
- Engineering, Harvard University
- Mechanical Engineering, University of Utah
- Department of National Defence (DND)
    - Defence Research and Development Canada (DRDC)
    - Royal Canadian Air Force (RCAF)
    - Director of Technical Airworthiness and Engineering Support (DTAES)
    - Royal Military College of Canada (RMC)
- Royal Australian Air Force (RAAF)
- United States Navy (USN)
- National Research Council Canada (NRC Aerospace)

Names of contributors (where available) and their organizations are included in the text of this review.

Full addresses of the contributors are available through the ICAF Canadian National Delegate at:

Min Liao, Ph.D.

Group Leader - Structural Integrity
Aerospace, National Research Council Canada
1200 Montreal Road, Building M14
Ottawa, ON, K1A 0R6, Canada
Tel: 1-613-990-9812
Email: Min.Liao@nrc-cnrc.gc.ca

2.0 FULL-SCALE STRUCTURAL AND COMPONENT TESTING

2.1 UPDATE ON CSERIES DURABILITY AND DAMAGE TOLERANCE TESTS

Bombardier Aerospace

The CSeries complete Aircraft Durability and Damage Tolerance (DADT) test started in mid-August 2014 at IABG in Dresden, Germany, shown in Figure 1.

Figure 1 CSeries full-scale test in Dresden, Germany

The main objective of the test is to demonstrate the damage tolerance and fatigue characteristics of the metallic components of the CSeries airframe. Other objectives include validation of:

1. Crack growth models for primary metal structures;
2. Inspection techniques and intervals; and
3. Typical repairs and allowable damage limits.

The main components covered by the Complete Aircraft DADT test, and shown in Figure 2, are:

- Complete fuselage including all doors and interfaces;
- Center and outer wing box primary metallic structure; and

- Vertical stabilator and rudder primary metallic structure and interfaces.

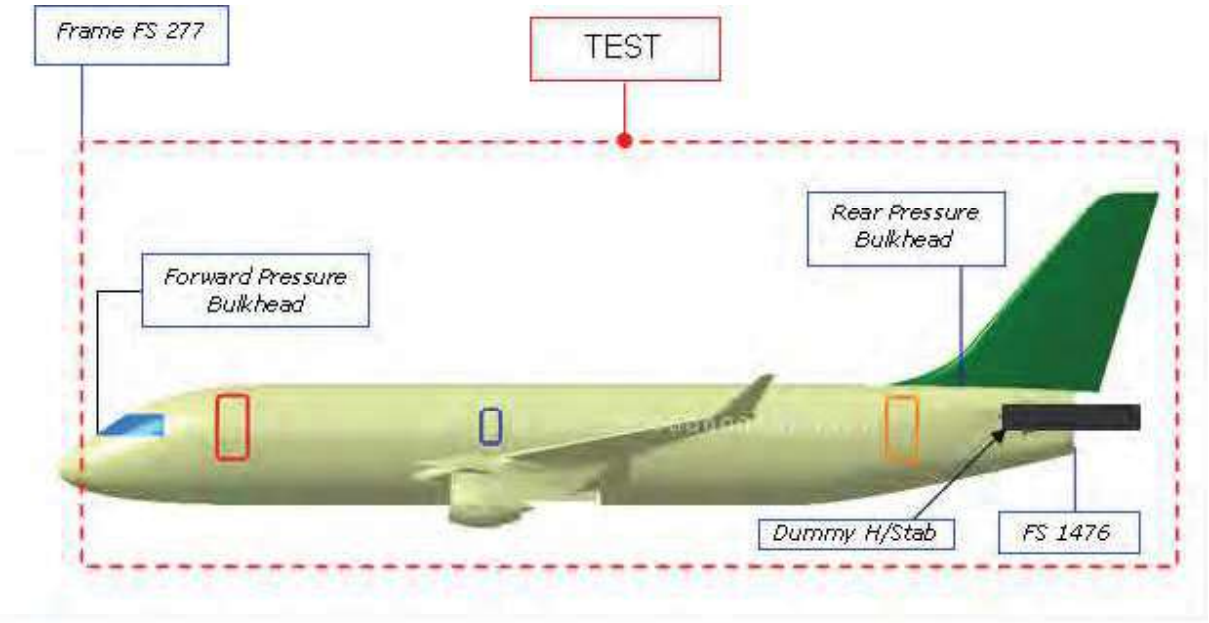

Figure 2 Schematic of main CSeries components

The aircraft structure will be subjected to a total of 180,000 flight cycles, which represent three times the Design Service Goal (DSG) of the aircraft. The test program is divided into three phases of testing and a final phase for teardown inspection:

1. Phase 1 – Durability testing: Two DSG of flight cycles (120,000 total flights) will be applied to the test article without any artificial damage.
2. Phase 2 – Damage Tolerance Testing: One DSG of flight cycles (60,000 flights for a total accumulated count of 180,000 flights) will be applied to the test article with the presence of artificial damage.
3. Phase 3 – Residual Strength Testing: A series of residual strength tests will be applied to the test article to demonstrate the structural integrity of standard repairs, confirm the critical crack lengths of the Damage Tolerance Analysis and demonstrate freedom from Widespread Fatigue Damage.
4. Phase 4 – Teardown inspection.

Close-ups of the wing and fuselage tests are shown in Figure 3 and Figure 4 respectively.

Figure 3 Close-up of wing test setup

Figure 4 Close-up of fuselage test setup

A mission with four flight types is applied to the test article. This mission was reduced and truncated to an equivalent of 268 end points, on average, per flight. The number of cycles required for Entry-Into-Service was reached at end of Nov 2014, with 2 lifetimes (120,000 flights) of cycling achieved in mid-January 2017.

In addition, there are multiple Durability and Damage Tolerance (DADT) bench tests for components that are not covered by the Complete Aircraft DADT Test. Table 1 contains a list of

the main metallic test rigs. These bench tests will also be tested for 180,000 flight cycles and will follow the same testing program as the Complete Aircraft DADT Test.

Table 1 List of subsequent metallic test rigs

TEST RIG (Metallic)
HORIZONTAL STABILIZER AND ELEVATOR DADT TEST
ENGINE PYLON DADT TEST
ENGINE MOUNTS (FWD AND AFT) AND THRUST LINKS DADT TEST
SLAT 2 BODY DADT TEST
SLAT 2 TRACKS DADT TEST
SLAT 4 BODY DADT TEST
WINGLET AND WINGLET ATTACHMENT DADT TEST
INBOARD FLAP BODY DADT TEST
INBOARD FLAP, INBOARD TRACK DADT TEST
OUTBOARD FLAP BODY DADT TEST
OUTBOARD FLAP, INBOARD TRACK DADT TEST
OUTBOARD FLAP, OUTBOARD TRACK DADT TEST
AILERON BODY AND SUPPORTS DADT TEST
GROUND SPOILER DADT TEST
MULTI-FUNCTION SPOILER 1 DADT TEST

As the CSeries structure is fabricated utilizing various metal alloys as well as Carbon Fiber Reinforced Plastic (CFRP) for its primary structure, other test rigs are being used to evaluate the durability and damage tolerance characteristics of the composite structure. These rigs are following a different testing program. A list of the main composite test rigs is provided in Table 2.

Table 2 List of composite test rigs

TEST RIG (Composite)
WINGLET AND WINGLET ATTACHMENT DADT TEST
INBOARD FLAP BODY DADT TEST
OUTBOARD FLAP BODY DADT TEST
AILERON BODY AND SUPPORTS DADT TEST
GROUND SPOILER DADT TEST
MULTI-FUNCTION SPOILER 1 DADT TEST
HORIZONTAL STABILIZER AND ELEVATOR DADT TEST
VERTICAL TAIL DADT TEST
WING BOX AND CENTRE WING BOX DADT TEST
BA500 REAR PRESSURE BULKHEAD DADT TEST
AFT FUSELAGE UPPER STRUCTURE DADT TEST

In conclusion, multiple CSeries DADT tests started in 2014. Three aircraft design lives (180,000 flight cycles) will be simulated to ensure the metallic structure meet the Damage Tolerance certification requirements, the requirements for Entry-Into-Service as well as the customer expectations. The number of cycles required for Entry-Into-Service was reached at the end of Nov 2014, with 2 lifetimes (120,000 flights) of cycling achieved in mid-January 2017.

2.2 GLOBAL 7000 DURABILITY AND DAMAGE TOLERANCE TESTS

Alain Charbonneau, Bombardier Aerospace, Product Development Engineering

The Global 7000, shown in Figure 5, flew for the first time last fall. Static testing is progressing and a limited number of sub-component durability and damage tolerance (DADT) tests, like forward and aft engine mount fittings and engine thrust fitting, are completed or well advanced. Testing performed on CSeries program helped reduce the number of development and lower level tests required for the Global 7000. Multiple durability and damage tolerance tests of major components are planned to start later this year.

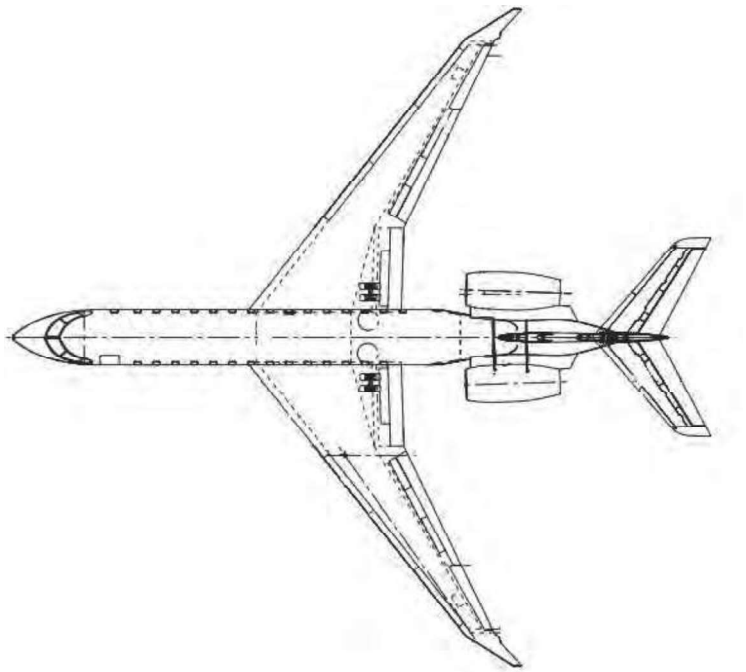

Figure 5 Global 7000

The plan on Global 7000 is to have a Complete Aircraft DADT test as well as many bench tests. The Complete Aircraft DADT test of the Global 7000 will cover the main structural components: complete fuselage, wing, engine mounts, vertical stabilizer and metallic parts of the horizontal stabilizer. It will also cover all doors, landing gear interfaces as well as the control surface and high lift devices attachment and backup structure within the wing box and horizontal and vertical stabilizer boxes.

In addition, there are multiple Durability and Damage Tolerance (DADT) bench tests for components not covered on the Complete Aircraft DADT Test. The main rigs will include:

- most critical slat body, tracks and attachment to the wing;
- inboard flap body, tracks and attachment to the wing;
- outboard flap body, tracks and attachment to the wing;
- most critical spoiler and attachment to the wing;
- winglet root joint;
- aileron and attachment to the wing;
- rudder and attachment to the vertical stabilizer; and
- elevator and attachment to the horizontal stabilizer.

The main objective of these tests is to demonstrate the damage tolerance and fatigue characteristics of the metallic components of the Global 7000 airframe, a model of which is shown in Figure 6. Other objectives include validation of:

1. Crack growth models for primary metal structure;
2. Inspection techniques and intervals; and
3. Typical repairs and allowable damage limits.

The aircraft structures will be subjected to a total of 51,000 flight cycles, which represent three times the Design Service Goal (DSG) of the aircraft. The test program is divided into three phases of testing and a final phase for teardown inspection:

1. Phase 1 – Durability testing: Two DSG of flight cycles (34,000 total flights) will be applied to the test articles, which include typical manufacturing and in-service damage and repairs.
2. Phase 2 – Damage Tolerance Testing: One DSG of flight cycles (17,000 flights for a total accumulated count of 51,000 flights) will be applied to the test article with the presence of artificial damage at specific Primary Structural Element (PSE) locations.
3. Phase 3 – Residual Strength Testing: A series of residual strength tests will be applied to the test article to demonstrate the structural integrity of typical repairs, confirm the critical crack lengths of the Damage Tolerance Analysis, and demonstrate freedom from Widespread Fatigue Damage.
4. Phase 4 – Teardown inspection.

As the Global 7000 structure is fabricated utilizing various metal alloys as well as Carbon Fiber Reinforced Polymer (CFRP) for its primary structure, other test rigs are being used to evaluate the durability and damage tolerance characteristics of the composite structure. These rigs are following a different testing program and are currently cycling. The following composite components are being tested:

- horizontal stabilizer;
- aileron;
- rudder; and
- elevator.

In conclusion, the DADT test rigs for the major metallic components of the Global 7000 will start this year. Three aircraft design lives will be simulated to ensure the metallic structure meet the Damage Tolerance certification requirements, the requirements for Entry-Into-Service as well as the customer expectations.

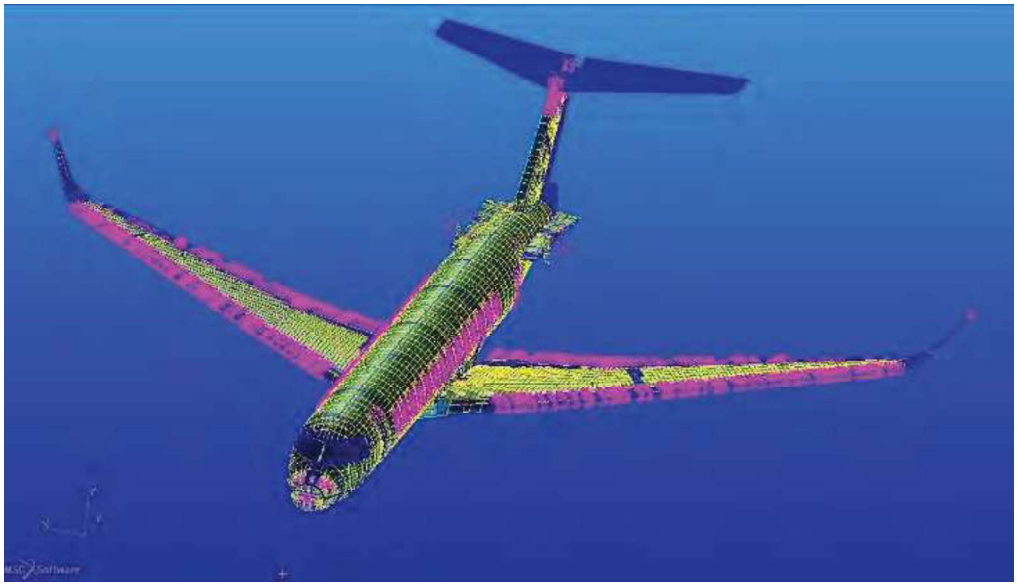

Figure 6 Global 7000 airframe

2.3 CF-188 (F/A-18) HORIZONTAL STABILATOR FATIGUE TEST (FT905) *

R.S. Rutledge, NRC Aerospace
* Paper and poster being presented at ICAF2017

As reported in the last ICAF symposium, the CF-188 aircraft are approaching or in some cases have already exceeded the Original Equipment Manufacturer (OEM) certification limits and Canada is currently testing the flight control surfaces to extend the certification basis. To ensure fleet operation and extend the certification basis to meet the new requirements for the CF-188 fleet and to avoid expensive control surface procurements, the Royal Canadian Air Force (RCAF), the National Research Council (NRC), Canada and L-3 Communications (L-3 Com) Military Aircraft Services (MAS) are performing a series of structural life extension fatigue tests.

NRC is currently in the process of conducting durability and damage tolerance (DADT), and residual strength testing of a retired United States Navy horizontal stabilator with representative service repairs and environmental / fatigue exposure. The stabilator, a hybrid composite skin / aluminium honeycomb core structure, has been durability fatigue tested to the equivalent of five lifetimes the RCAF new service usage requirement and will conduct a damage tolerance assessment and residual strength tests on the test article in the upcoming months. During testing the stabilator has been inspected at regular intervals. The NRC developed custom loading test rig for conducting this work on test article FT905 is shown in Figure 7.

For the damage tolerance portion, fatigue testing will be conducted after damages are introduced in the upper surface. All repair areas of the H-stab and damaged areas will be monitored for damage growth in the damage tolerance phase until the required life extension is achieved.

Residual strength tests to 120% design limit loads and ultimate loads are planned at the completion of the DADT testing.

(a) Test setup, side view

(b) Test setup, top view

Figure 7 Fatigue Testing FT-905 test configuration

2.3.1 REFERENCES

[1] R. S. Rutledge, D. S. Backman and A. Lehman Rubio, "Distributed Sensing Optical Fibres for Loads Monitoring during Full Scale Fatigue Testing", The 29th International Committee on Aeronautical Fatigue (ICAF) Symposium, 6/7/2017 - 3/9/2017, Nagoya, Japan.

[2] C.A. Beltempo, R. Rutledge, M. Yanishevsky, D. Backman, M. Genest, A. Roussel, and J. Juurlink, "F-18 Flight Control Surface Life Extension Testing - CF-18 Horizontal Stabilator", The 29th International Committee on Aeronautical Fatigue (ICAF) Symposium, 6/7/2017 - 3/9/2017, Nagoya, Japan.

2.4 CF-18 AILERON FATIGUE TEST (FT370)

R.S. Rutledge, NRC Aerospace

NRC is also currently conducting durability and damage tolerance (DADT), and residual strength testing of a RCAF retired aileron with representative service repairs and environmental / fatigue exposure. The aileron, a hybrid aluminium skin / aluminium honeycomb core structure, is being durability fatigue tested to the equivalent of five lifetimes the RCAF new service usage requirement and will conduct a damage tolerance assessment and residual strength test the article at the end of the project. During testing the aileron has been inspected at regular intervals. The NRC developed a custom loading test rig for conducting this work on test article FT370, which is shown in Figure 8.

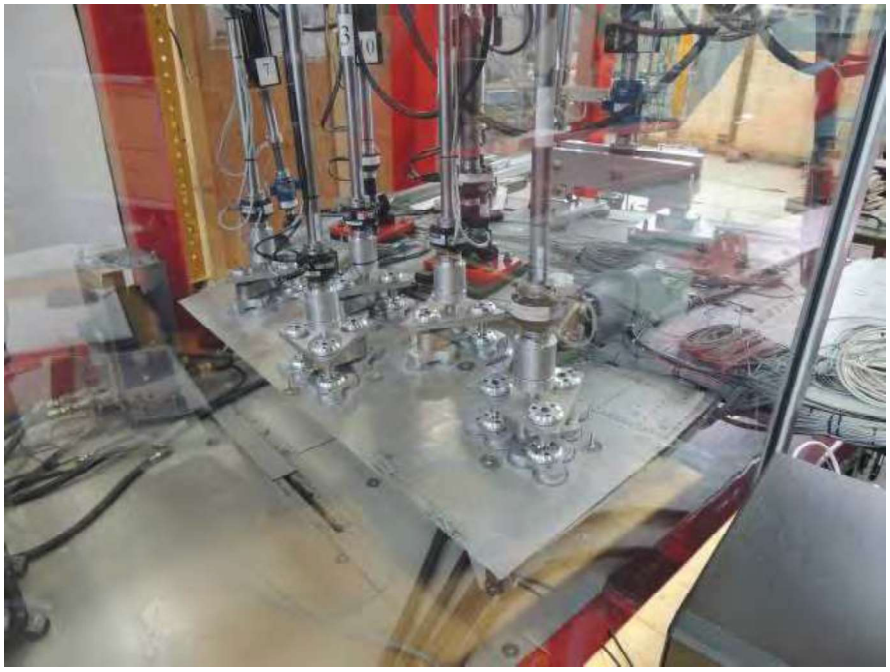

(a) Test setup side view-1

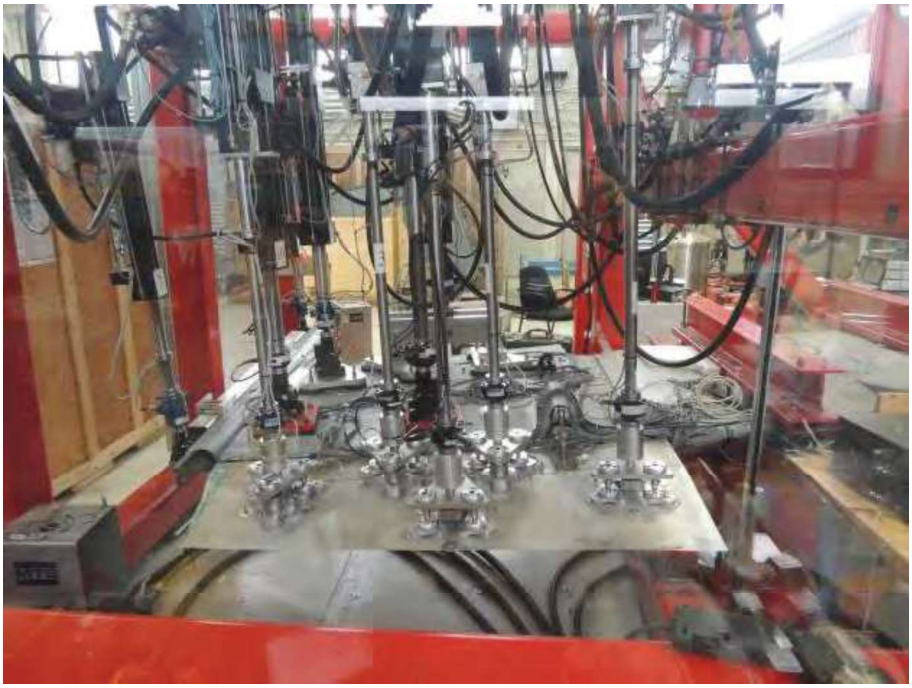

(b) Test setup side view-2

Figure 8 Fatigue testing FT370 test configuration

2.5 A CERTIFICATION TEST FOR CHALLENGER 350 WINGLET

R.S. Rutledge, NRC Aerospace

The Challenger 350 is Bombardier's newest entry in the super midsize business jet class, and was launched on May 20, 2013, with worldwide leader in private aviation NetJets® as the launch partner at the European Business Aviation Conference and Exhibition (EBACE) in Geneva, Switzerland. The Challenger 350 features increased performance from new engines and a new canted winglet design. But before the aircraft could be approved for sale, the outer wing and winglet needed to be tested to meet Transport Canada certification requirements. These tests were necessary to validate Bombardier's analyses, and demonstrate the strength of the new components under the highest expected service loads.

In collaboration with L3-MAS and Bombardier, NRC completed a static test on Challenger 350 winglet. The test rig was designed by L-3 MAS with NRC input and delivered to NRC Ottawa. Following this, the developmental winglet was joined to an existing wing at L-3 MAS, and safety of flight loading tests, shown in Figure 9, were successfully conducted at NRC Ottawa's full scale test facility, demonstrating that the developmental winglet was certified as safe to

undergo a series of test flights on Bombardier's flight test aircraft in Wichita (http://www.youtube.com/watch?v=yy0iRQBSEpQ).

Figure 9 Winglet certification test setup for the Challenger 350

During this test, NRC specialists installed over 100 strain gauges on the new wing for a total of 240 channels of data acquisition; and the assembly was tested to its limit flight loads. These loads were intended to simulate the loads that the outer wing and winglet will see once in the aircraft lifetime. In 2014, in the presence of Bombardier and Transport Canada personnel, the wing was bent to its ultimate strength, 50% above the once-in-one-lifetime limit load, with no permanent deformation. Furthermore, in order to find out how far the wing could go, a failure test was attempted, shown in Figure 10, which pulled the wing to a 96% above its once-in-one lifetime load, shown in Figure 11, or almost twice what it is ever likely to see in service. This load bent the wing by almost 2 feet, but the wing survived without any significant catastrophic failures.

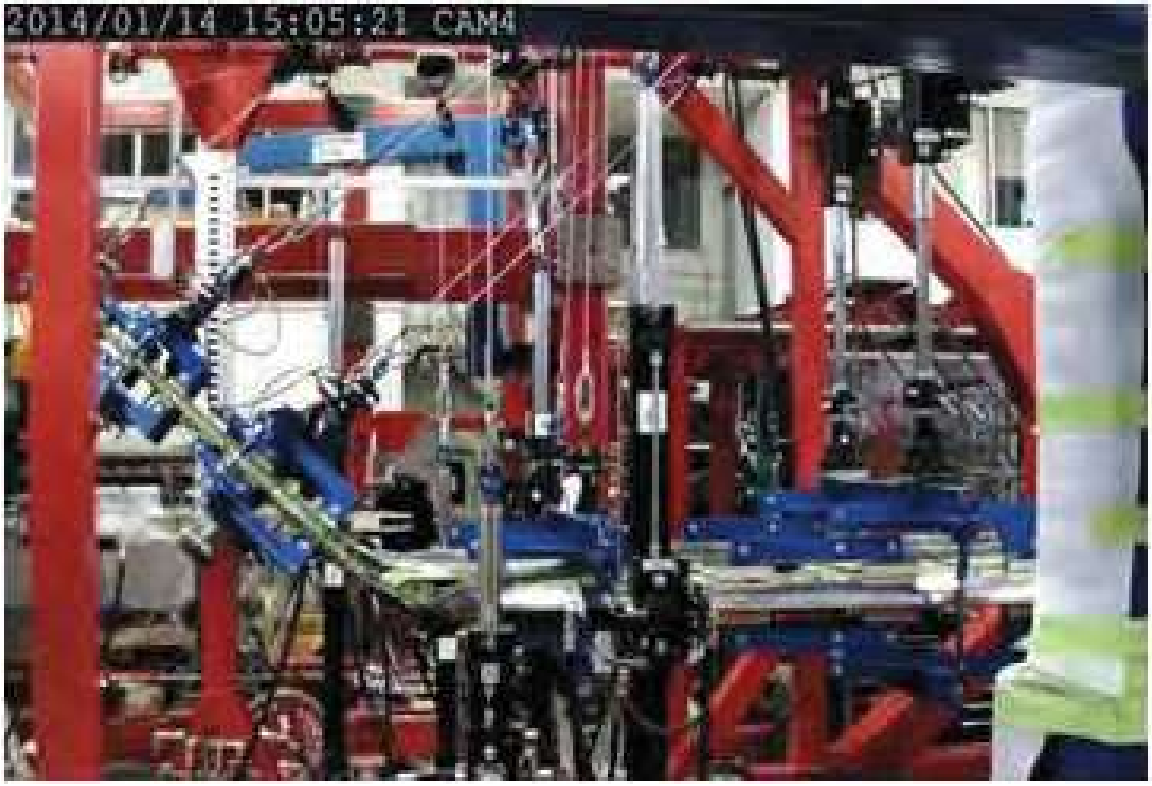

Figure 10 Wing at zero load

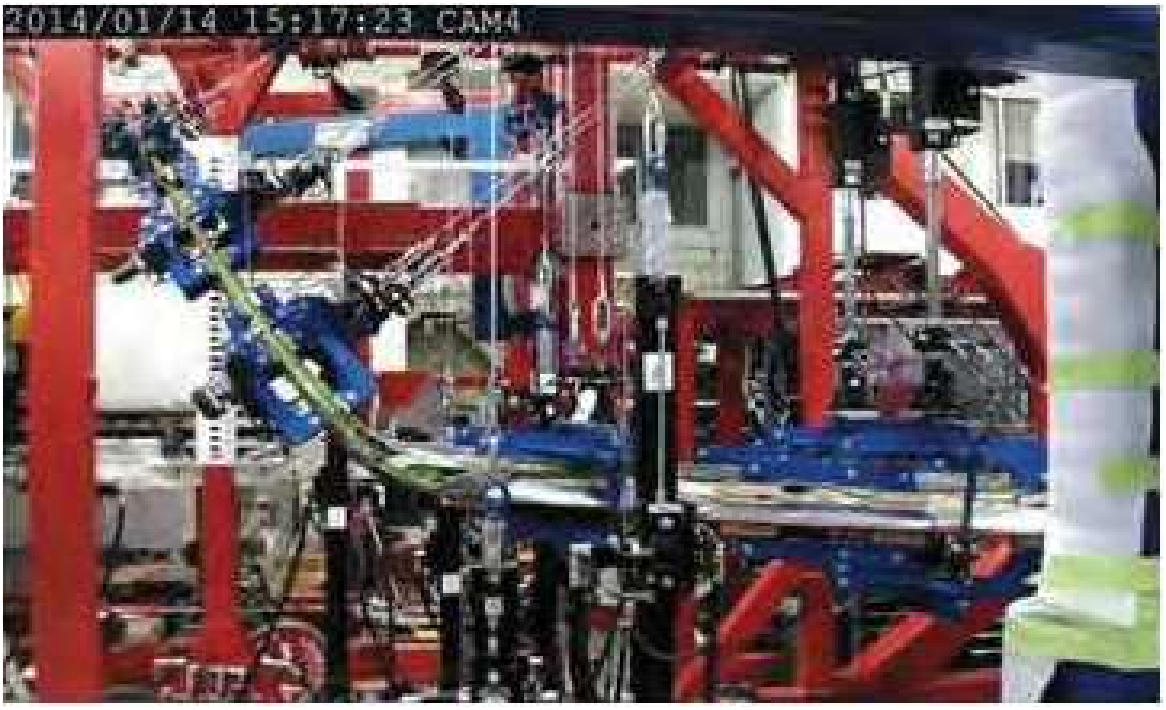

Figure 11 Wing at 96% above its design load (196% of Limit load)

2.6 APPLICATION OF EXPERIMENTAL MECHANICS TECHNIQUES FOR MULTIAXIAL FATIGUE TESTING *

David Backman[1], Hiroshi Nakamura[2], Min Liao[1], Tyler Musclow[1], Richard Desnoyers[1]
[1]NRC Aerospace; [2] IHI Corporation, Japan
* Paper being presented at ICAF2017

Performing multiaxial fatigue testing, whether tension-torsion or planar biaxial, is often significantly more complicated and expensive than a standard uniaxial fatigue test. The need for this type of testing is especially relevant when one is looking for accurate fatigue life assessments especially for rotating components or other fatigue sensitive components that are subjected to multiple loads, in multiple directions. Multiaxial fatigue testing using a planar biaxial test frame and precisely engineered test specimens has the potential to replicate very complex stress states and to take into account the effects of non-proportional loading, and/or negative biaxial ratios. The National Research Council Canada (NRC) has recently upgraded Canada's largest planar biaxial test frame, with a new control system and additional actuator supports, for both in-phase and out-of-phase, tension-compression fatigue testing. The upgraded testing system has been set up to take advantage of NRC's advanced experimental mechanics capabilities. Over the past years, NRC has developed expertise in the application of a suite of advanced experimental mechanics techniques, including Digital Image Correlation (DIC), automated photoelasticity, and Thermoelastic Stress Analysis (TSA). A test program currently underway at the NRC in partnership with IHI Corporation is looking at the fatigue life of complex titanium cruciform specimens under various loads and at various biaxial load ratios, as shown in Figure 12. To achieve these very specific local biaxial ratios, IHI developed cruciform specimens without notches and also with different notch geometries, and then validated the designs with the NRC experimental mechanics techniques.

The challenge with this particular test series was how to efficiently address various aspects of this program including validation of the coupon design, efficient early crack detection and automated crack growth measurement. Several optical based techniques were used to overcome these challenges. A single camera DIC system was used to capture the strain field during testing. Additional hardware and software were used to process the load signal and trigger camera operation only at the peak load. During the pilot phase of testing, the strain field results at peak load were crucial to validate the FEA model of the cruciform design. A comparison of between the FEA results and the DIC results is provided in Figure 13.

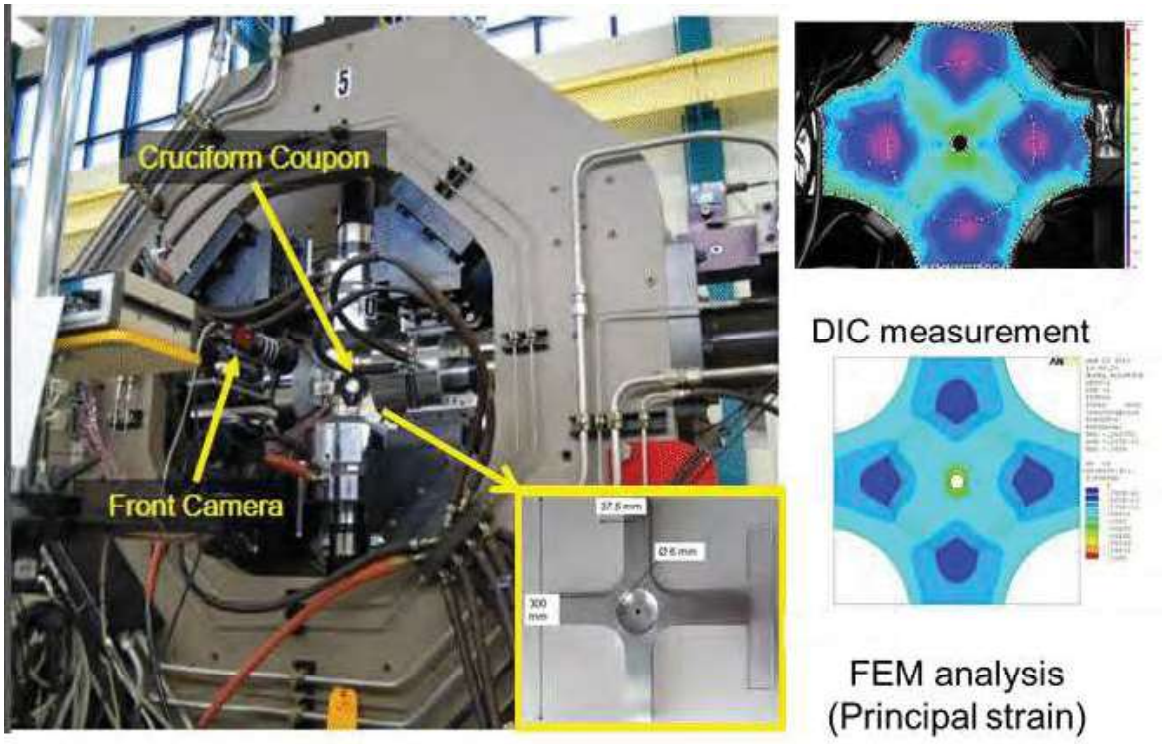

Figure 12 Biaxial fatigue testing on notched coupons

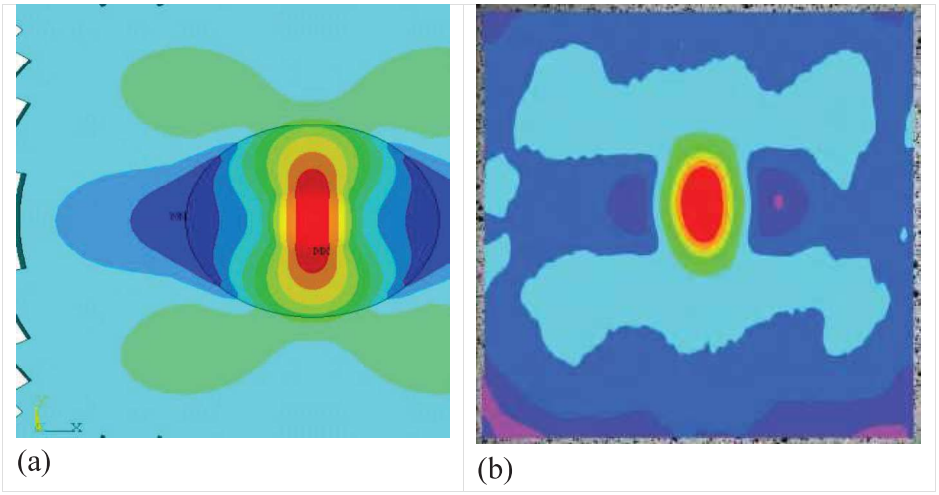

Figure 13 Comparison between (a) finite element analysis and (b) measurements of maximum principal strain of notch cruciform specimen using the same color and stress scale

On the opposite face of the cruciform, a highly sensitive infrared detector was used to measure the heat generated by the loads applied to the specimen. This technique, called thermoelastic

stress analysis (TSA), is able to produce a full field image that can be calibrated to represent the first stress invariant on the surface of the cruciform. For this test, the raw (uncalibrated) TSA image was used to provide an indication of an early, small crack formation, with the aid of additional image processing techniques. A comparison between the original image and the processed image is shown in Figure 14.

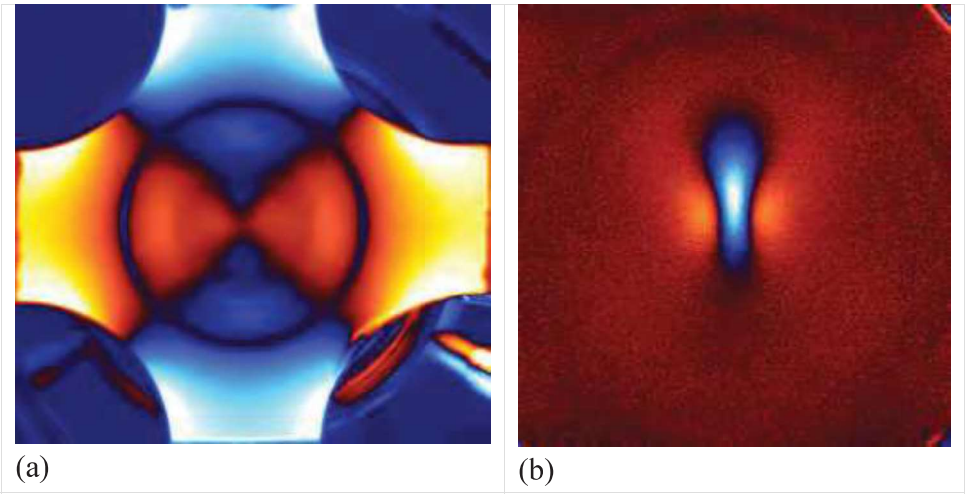

(a) (b)

Figure 14 Comparison between (a) raw TSA image on back face and (b) TSA image after image processing highlighting formation of a ~500 mm crack

A similar type of image processing was used on the raw, white light, camera images used for DIC. Once the crack was confirmed by visual measurement, the challenge was to determine how to best process these optical images to effectively measure crack length. A comparison between the raw, white light image and processed image is shown in Figure 15.

An optical microscope was used post-test to measure crack length from a silicon replica taken from the coupon surface. Fractography was also used to analyze the fracture surfaces after the crack had been excised and broken open. This analysis was used to determine the location of initial crack formation within the notch.

Overall, the combination of both white light and infrared optical techniques, in conjunction with low and high magnification analysis, allowed for rebuilding a complete history of crack formation and growth behaviour in these cruciform specimens, while maintaining very high test efficiency. The multiaxial fatigue testing has been successfully providing invaluable fatigue crack formation and growth data under various loading ratios, in order to support new component design and life cycle assessment.

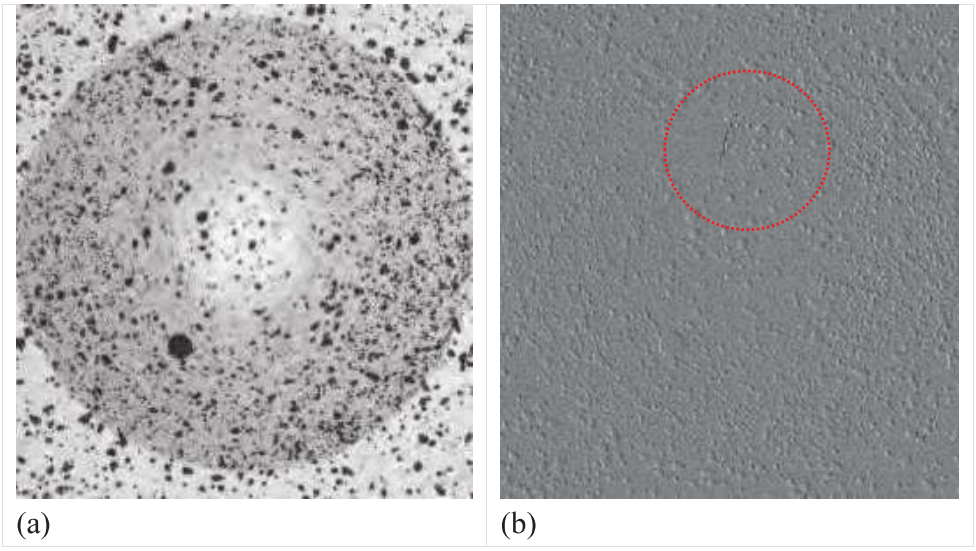

Figure 15 Comparison between (a) raw camera image on front face and (b) processed camera image with a crack (~800 mm) highlighted in red circle

2.6.1 REFERENCES

[3] David Backman , Min Liao , Simon Larose , Tyler Musclow and Richard Desnoyers , "Fatigue Testing of IHI Formal Smooth Specimens and Preliminary R-Notch Coupons", NRC Internal Report LTR-SMM-2016-0174

[4] David Backman and Daniel Dos Reis, "Scoping Study on Iodine-Stress Corrosion Cracking in Zirconium", NRC Internal Report LTR-SMM-2016-0034

[5] David Backman, Daniel Dos Reis and Min Liao, "Test Report: IHI Formal Notch Specimens", NRC Internal Report LTR-SMM-2016-0044

[6] David Backman, Min Liao, Tyler Musclow, Richard Desnoyer and Hiroshi Nakamura - IHI , "Application of Experimental Mechanics Techniques for Multiaxial Fatigue Testing", ICAF2017

[7] Hiroshi Nakamura - IHI, David Backman, Min Liao, Takuya Yoden - IHI and Tomoyuki Tanaka - IHI, "Multiaxial fatigue life assessment using cruciform specimen for Ti-6Al-4V", 29th ICAF Symposium

2.7 ADVANCED CONTROL TECHNOLOGIES FOR FULL-SCALE STRUCTURAL TESTS

C. Cheung, NRC Aerospace

NRC has a long and rich history of carrying out full-scale structural tests on fixed- and rotary-wing aircraft. These tests can be extremely complex from a control systems viewpoint due to the

large number of actuators and the many factors affecting the response of each actuator. In the past decade, the Structures, Materials and Manufacturing Laboratory (SMM) at NRC has undertaken several efforts to improve the manner in which full scale tests are conducted for our clients. This work ranges from developing reduced structural mass test loading systems to the development of cross-coupled compensation (CCC, or C^3 used by MTS as a utility of MTS AeroPro™ Control and Data Acquisition Software, http://www.mts.com/en/forceandmotion/aerospacetesting/MTS_4026296?article=1) technology to obtain higher performance and faster test speeds. Further efforts are on-going to continue to develop the NRC advanced control technologies to improve how full-scale structural tests are run.

The full-scale test lab at NRC-SMM had a helicopter tail boom test rig that was set up for experimental testing purposes, shown in Figure 16. This test set up was based on a client test to apply loads at the horizontal stabilizer and tail rotor (TR) gearbox (GB) attachment. To demonstrate some of the capabilities available within the MTS control system to further improve test speed and stability, degree of freedom (DOF) control was set up on this test in combination with CCC. Using DOF control for bending and torsion, the goal was to uncouple the actuators in the controller since bending and torsion stiffness of the test article were very different. Although DOF control adds complexity, advantages include increased stability, lower errors, and increased test speed.

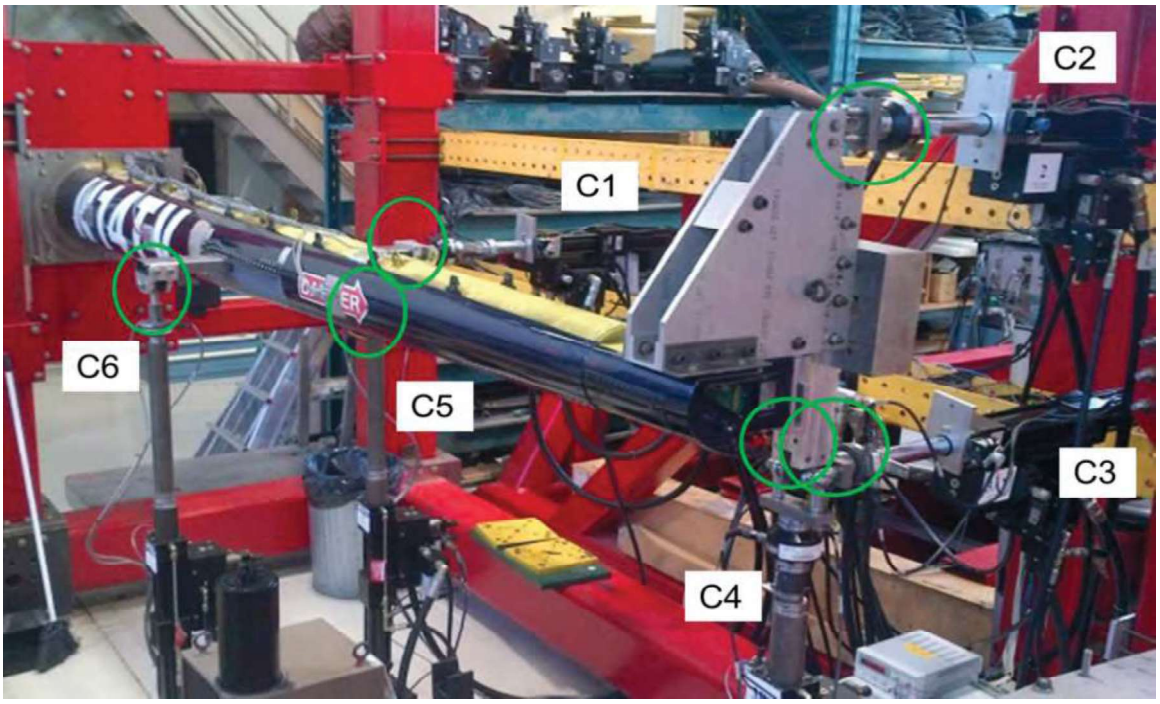

Figure 16 Helicopter tail boom test rig with 6 channels/actuators

3.0 FATIGUE LIFE ASSESSMENT AND MANAGEMENT

3.1 CF-18 AIRCRAFT STRUCTURAL INTEGRITY PROGRAM (ASIP) AND LIFE EXTENSION PROGRAM (ALEX)

L-3 Communications (Canada) Military Aircraft Services (MAS)

L-3 MAS conducts a full-fledged ASIP program on the CF-188 fleet on behalf of the RCAF. Above and beyond usage and structural condition monitoring activities mandated by MIL-STD-1530, the program has effectively extended the life of the aircraft by approximately 50% via the life extension program (ALEX). ALEX has been executed in three major phases, the last of which, CP3 is in production since 2012. Overall, the ALEX program is comprised of over 200 items, the majority being preventive modifications (50%), followed by inspections (25%) and various repair procedures (25%).

In 2015, L-3 MAS completed a detailed review of the completion of the certification status to ensure safe operation until fleet retirement, which is now planned for the 2025-2030 window. Whereby the ALEX program addresses known Life Limited Items (LLIs) that have been detected during certification tests conducted by the OEM, follow-on tests conducted by agencies such as the NRC, L-3 MAS and DSTG, or in-service, the certification effort is much broader and ensures that the basic structure is also certified to the latest standards and accounting for recent usage.

The so-called New Baseline Operational Spectrum (BOS) was developed in the late 2000's and it defers significantly from the original BOS that was developed in the early 1990's and used during the follow-on testing efforts. This is accounted for, as applicable, in the certification effort. In the early 2000's, the RCAF, with the collaboration of L-3 MAS, developed a unique and refined lifing policy and fatigue management approach for the CF-188. The fatigue life of the airframe is managed essentially via the main Individual Aircraft Tracking (IAT) fatigue index at the wing root, independently of airframe hours. Other areas are certified with higher scatter factors to account for other load influences that are not tracked by the wing root index and/or dynamic loading. The so-called Tracking Factor is embedded in the lifing in order to obtain a similar level of safety for all areas of the aircraft. In that context, the effect of any usage variation, i.e. the New BOS, is assessed in a relative manner, compared to the wing root index. What this means in practice, is that an area where fatigue is accrued at a rate that is within the wing root rate multiplied by the tracking factor is deemed acceptable even if loading influences are completely different. That effect can be assessed for the New BOS, as a fleet-wide average, but also for specific aircraft.

The approach described above poses some challenges for some areas of the aircraft that are managed by flight hours or ground-air-ground cycles because aircraft will retire at a different number of flight hours depending on the actual fatigue rates at which it is flying. In practice, this is resolved by making conservative (in this case, usually meaning low wing root rates allowing more flight hours) projections by aircraft type and squadrons. This subject will be further elaborated below for the Flight Control Surfaces.

FCS Life Extension

Up until the late 2000's, the Flight Control Surfaces (FCS) of the CF-188 had not been considered systematically and holistically as part of the Aircraft Structural Integrity Program (ASIP) effort. One of the key reasons is that FCSs are easily swapped from one aircraft to another and that, as a result, preventive modifications or refurbishment are not tied directly to the ALEX CP1-CP2-CP3 framework.

The RCAF has adopted an interim position to adopt OEM-recommended inspections at 6000 Cumulative Flight Hours (CFH) which provides an extension to 7000 CFH; however, even this effort is not adequate to meet RCAF fleet requirements. Supportability for the fleet until Estimated Life Expectancy (ELE) is a concern as the most up to date fleet logistic and supportability scenarios show that most FCSs need to be certified for up to 9000 CFH. This is slightly inferior to worst-case projections for the airframe (in the order of 10,000 hours) because the RCAF possesses sufficient spares (from aircraft that were retired in the mid-2000s) to backfill retired components.

Previously, a somewhat conservative assumption had been made that the FCS had to be certified to the original BOS. In reality, the New BOS, is less critical than the original BOS at the wing root and aircraft will be allowed to operate up to 9000 to 10000 CFH. As noted above, the overall fatigue management does not assume that all load influences vary the same way. Rather, this is verified and computed for every component type. In practice, what is seen, is that the fatigue accrual of most control surfaces is not tied to the wing root in terms of loading influences (exception being for leading edge surfaces on the wing), but is still somewhat in line with the wing root. Hence, the current plan is to certify FCSs to the New BOS instead. For most of the FCSs, the so-called Tracking Factor, discussed above, also applies.

The certification strategy is primarily based on full scale component testing of the horizontal stabilator, the aileron, the inboard leading edge flap and the trailing edge flap. L-3 MAS and the NRC, the test agency, are working in close collaboration on these programs. Further details are provided in the NRC portion of this summary.

Other Projects of Interest on the CF-18

As noted above, FCSs were intentionally left out of the ALEX CP1-CP2-CP3 framework and are being addressed at this point. A few other areas of the airframe are also being revisited because it is known that the certification fell short of the design standard, i.e. the lifing policy. All known LLIs have generally already been addressed via the ALEX program, so the associated risk is deemed manageable, but must be properly quantified and mitigated as necessary via special inspections, repairs or modifications. The so-called Structural Base Level Maintenance (SBLM), a mid-point between CP3 and retirement, is deemed a key opportunity for that work to take place. CP3, compared to CP1 and CP2, has fewer modifications and more inspections and the same trend is expected for SBLM. This is the natural outcome of the so-called logistic option analysis process, where the relative benefit of a preventive modification over recurring inspections is assessed based on access, number of inspection repeats, etc.

The areas that are requiring substantial efforts and/or are pausing the most significant risks at this point are the following:

- The horizontal stabilator back-up structure, namely the bootstrap which supports the actuator of that all-moving control surface and reacts torsion. None of the OEM and follow-on tests have properly covered that component. Various options are being looked into including full-scale testing.
- The wing root shear tie at Fuselage Station (FS) 508 which supports the back-end of the wing and transmits loads from the trailing edge flap. Flight tests revealed that the influence of dynamic loading from the trailing edge flap are not negligible. This coupled by the discovery of a small crack upon re-inspection of the OEM test article, Structural Test ST16, have triggered a detailed review. The area will likely necessitate an inspection, but the logistic risk associated with any finding in the areas is deemed very significant because repairability is very poor and requires removal of the wing. Component testing is envisaged as the best option to quantify that risk.
- Negative – G driven areas. The New BOS revealed that these manoeuvers are more frequent and more severe than originally anticipated in the original BOS. Overall, the situation can be assessed fairly easily because OEM tests were actually quite severe in that respect.
- Vertical tail attachments, also known as stubs. The RCAF have adopted a recurring inspection approach for those attachments and they are allowed to fly with some level of degradation, i.e. cracking due primarily to fretting. Over the last few years, repairs have been developed for the most susceptible areas based on the same concept as two repairs that had been installed on the FT46 fatigue test article at DSTG. The repairs in question are fairly complex to develop and certify because of severe access restrictions (tail remains in place) and because they are installed on significantly degraded structure. This implies designing for almost equivalent strength. Figure 17 shows one the vertical tail stub repairs.

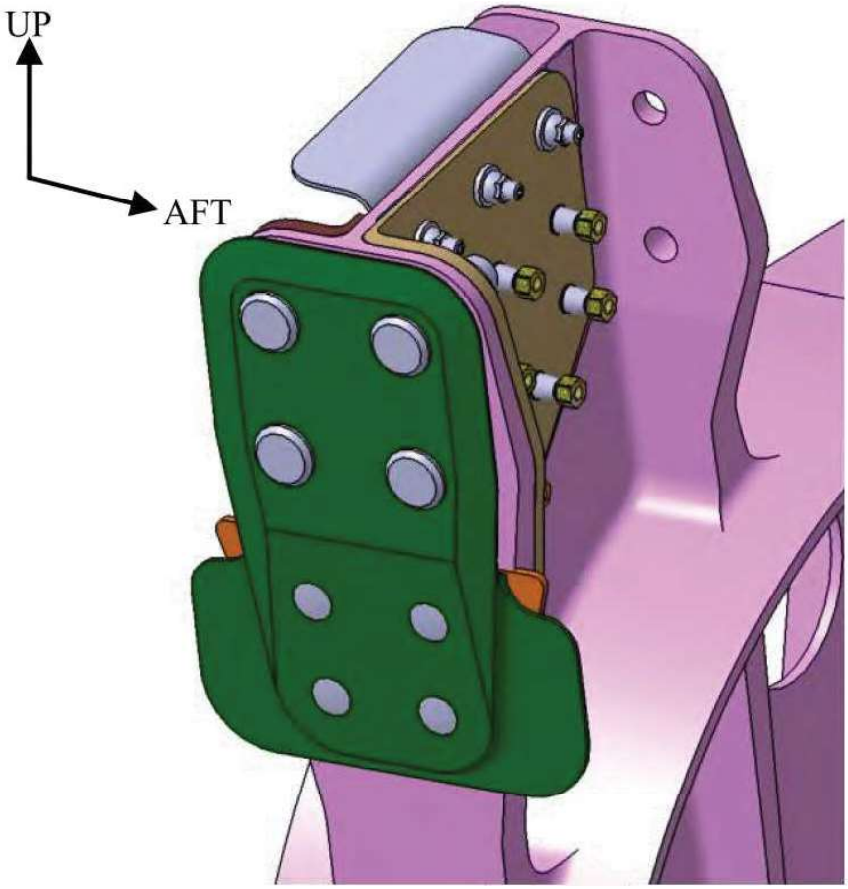

Figure 17 Repair of vertical tail attachment stubs

3.2 F-18 AIRCRAFT INTERNATIONAL SUPPORT

L-3 Communications (Canada) Military Aircraft Services (MAS)

Robotic Structural Modification Solutions

Over the past 15 years, L-3 MAS has invested considerably in its capacity to provide automated robotic solutions for component repair line and on-aircraft applications. The robot can be used to mill and to peen metallic part surfaces. Milling is a controlled form of machining, or blending, and peening bombards the surface with ceramic beads to provide added fatigue endurance to repeated loading. The use of a robot allows for greatly increased precision over manual operations, particularly for structures that are difficult to access or have complex geometries. L-3 MAS has performed thousands of robotic modifications and repairs on the F/A-18 of the Royal Canadian Air Force (RCAF) and Royal Australian Air Force (RAAF).

The United States Navy (USN) require life extension of their late-lot F/A-18C and D aircraft that did not receive CBR's (Center Barrel Replacements) through a series of discrete

modifications, which have been shown to be significantly more cost-effective than replacement of several major components. This is accomplished via the development of localized preventative modifications which utilize robotic shot-peening to provide the necessary life improvements to meet the desired service life of the aircraft. The use of robotic equipment is mandatory under USN regulations to ensure a repetitive peening quality for which a certified life improvement factor can be demonstrated.

In 2015, L-3 MAS was contracted to adapt several modifications for two European customers who operate F/A-18s: Patria is the prime contractor for the Finnish Defence Forces Logistics Command and RUAG for the Swiss Federal Office for Defence Procurement, or Armasuisse. Their F/A-18 models are a more recent version, and their respective Air Forces fly the aircraft in a very different manner than the RCAF. These aspects required very careful consideration in the adaptation of these modifications. More importantly, robotic technology has changed considerably in the last decade, including the physical equipment itself and the software used to program trajectories. In addition to offering its customers updated versions of these modifications using the latest technology, L-3 MAS also provided a single jig that can support the robot in 2 different positions to carry out 2 modifications with very limited manipulation and setup time between them. This application is shown in Figure 18 below.

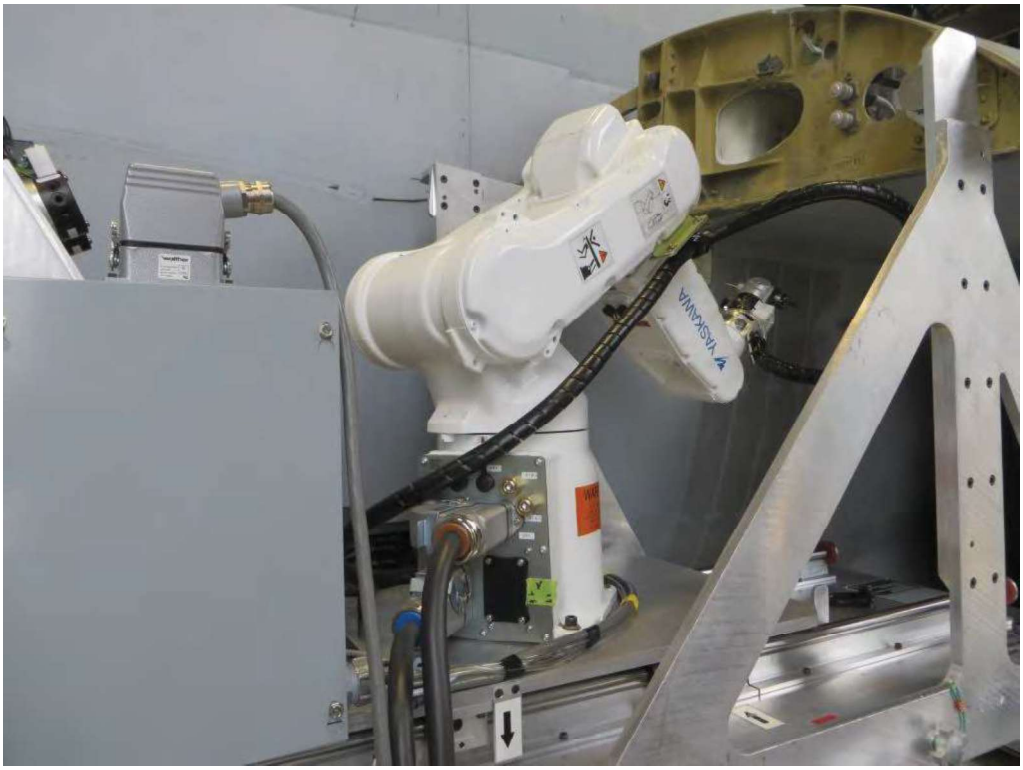

Figure 18 Robotic application

This is not the first time that L-3 MAS has supported Patria in developing a robotic solution. In 2010, L-3 MAS delivered a robotic/tooling solution to Finland that allowed them to start a modification (repair) line for their Inboard Leading Edge Flap hinges, which is still in operation in Finland today.

Other Work

L-3 MAS has also supported RUAG by developing a SF-18 (Swiss F/A-18) Baseline Operational Spectrum (BOS), an interface loads database for their aircraft and usage, and is continuing to support their rationalization of Strategic Reform Program SRP2 modification requirements via methodologies support, structural integrity analyses and modification development and implementation, when needed. Similar to the RUAG support noted above, L-3 MAS will likely also provide some of these services to Patria/FINAF in support of FN-18 aircraft and usage.

3.3 CT114 (TUTOR) AIRCRAFT STRUCTURAL INTEGRITY PROGRAM (ASIP)

L-3 Communications (Canada) Military Aircraft Services (MAS)

L-3 MAS conducts a full-fledged ASIP program on the CT114 Tutor fleet on behalf of the Canadian Forces. Aircraft usage monitoring is achieved by collecting, evaluating and processing the Operational Loads Monitoring (OLM) system data. Periodically, collected aircraft usage data is validated and accumulated fatigue damage is calculated for major aircraft components. In addition, remaining life for every major aircraft component is calculated based on predicted aircraft usage by using the software tool GIFTS. The monitoring program findings and L-3 MAS recommendations are reported to DND on a monthly basis.

L-3 MAS has recently been mandated to extend the service life of the Tutor fleet to 2025 or 2030. This involves a review of teardown inspection results, identification of additional SSI requiring inspection/rework, electrical / mechanical systems obsolescence and the development of a fleet strategy to manage the rotation of service aircraft with those in storage in order to meet the new planned retirement date. Follow-on work is planned to perform fatigue and damage tolerance analyses in order to address the new SSI created following the assessment of teardown inspection results. An example of the CT114's in their Snowbird role is shown in Figure 19.

Figure 19 CT114 Tutor

3.4 S-92 MARITIME HELICOPTER (CYCLONE)

L-3 Communications (Canada) Military Aircraft Services (MAS)

As part of the Maritime Helicopter Program, L-3 MAS is mandated to conduct an ASIP program on the S-92, designated as CH-148, shown in Figure 20, by the Royal Canadian Air Force (RCAF). As part of the Intermediate Support Readiness Validation (ISRV), L-3 MAS is currently validating the capabilities to perform structural condition monitoring and usage monitoring.

Usage monitoring will be enabled via the S-92 Health and Usage Monitoring System (HUMS). The HUMS has the capability to recognize regimes/manoeuvres via recorded flight parameters and sensor data. This data is processed by the Usage Comparison and Reporting Tool (UCART) that computes fatigue damage rates at selected locations for each individual aircraft and compares them to the design spectrum according to the requirements of MIL-STD-1530.

The other major component of the CH-148 ASIP Program is the Structurally Significant Item (SSI) database. The SSI database records all the relevant information about each SSI, also known as Primary Structural Element (PSE), from the design phase and into the in-service phase in order to enable ASIP analysts to monitor structural defects and, when needed, recommend changes to the maintenance program or modifications to the helicopter.

Figure 20 CH-148 Cyclone helicopter

3.5 CP140 SDRS FARS D/DTA METHODOLOGY VALIDATION

A.M. Brown, IMP Aerospace

The Canadian CP140 Aircraft Structural Integrity Program (ASIP) has recently completed a transition to recorded strain-based Individual Aircraft Tracking (IAT). The CP140 ASIP accomplishes structural usage monitoring through the use of a fleet-wide Structural Data Recording Set (SDRS) that records a variety of metrics on the aircraft including strains. Strain data are recorded at four locations on the CP140: three points along the lower portion of the right wing front spar and a single point on the upper forward spar cap of the horizontal stabilizer (H-Stab). Recorded strain histories are now used as the primary method for CP140 fatigue management following validation of the SDRS in 2009.

The SDRS validation initiated a transition from using analytically derived spectra to recorded strain-based spectra. Subsequently, the supporting analysis methodology for Durability and Damage Tolerance Analysis (DA/DTA) on the wings was updated and required validation. The updated methodology uses recorded strain histories at the three discrete points on the wing (H-Stab gauge is currently not used) and Transfer Functions (TF) for the generation of spectra at critical analysis locations. A Fleet Average Reference Spectrum (FARS) was developed using historical strain gauge data at each wing strain gauge location for use in predicting lives and

inspection intervals. Actual damage and crack growth is then predicted using IAT recorded strains. In both cases (using FARS or recorded individual aircraft spectra), TF are used to generate spectra at monitored critical locations.

Development of TF involves linear regression of the P-3C Service Life Assessment Program (SLAP) Full Scale Fatigue Test (FSFT) strain gauge data as well as minor modifications using detail Finite Element Models (FEM). This methodology is possible because the FSFT included SG installations at the same locations as the CP140 SDRS strain gauges. As depicted in Figure 21, strains recorded at the SDRS gauge location are transferred to an analysis location by applying a linear TF. The TF is derived by performing regression between the FSFT data at the SDRS location and the FSFT strain gauge closest to the analysis detail. If necessary, an additional FEM based factor may be applied to the TF.

Validation of the strain-based DTA methodology was performed through comparison to crack growth marker cycle data from the P-3C SLAP FSFT. FASTRAN v3.8 was used in all predictions and curves were adjusted to pass through the first marker cycle of a recorded test failure. Comparison was then made between the crack growth prediction curve and all subsequent marker cycles, shown in Figure 22. This methodology was adopted due to the difficult nature of identifying the initial flaw size from full scale test data. The goal of the validation was to show predictions that were conservative or within a 20% bound of the marker cycles.

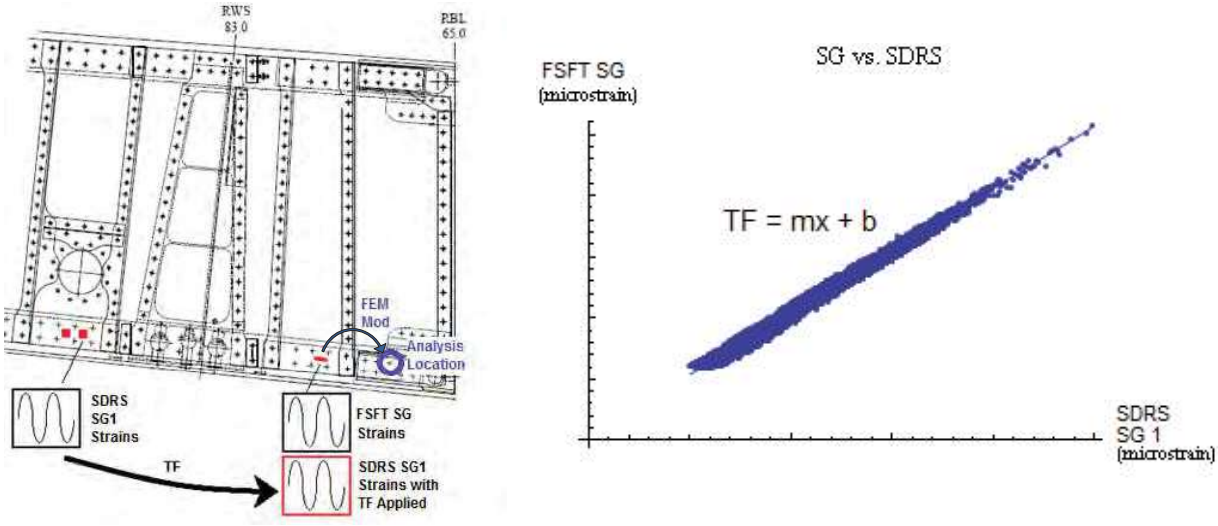

Figure 21 TF development

Validation of the durability methodology was achieved by performing comparisons of transferred P-3C SLAP FSFT spectra from SDRS gauge locations to locations of other FSFT strain gauges. This approach simulated the transfer of a recorded spectrum to a distant analysis

location and since the spectrum at the analysis location is known, a comparison of predicted fatigue lives using the two spectra could be made, as shown in Figure 23. The software jFAMS developed by TDA, Inc. was used for all fatigue predictions.

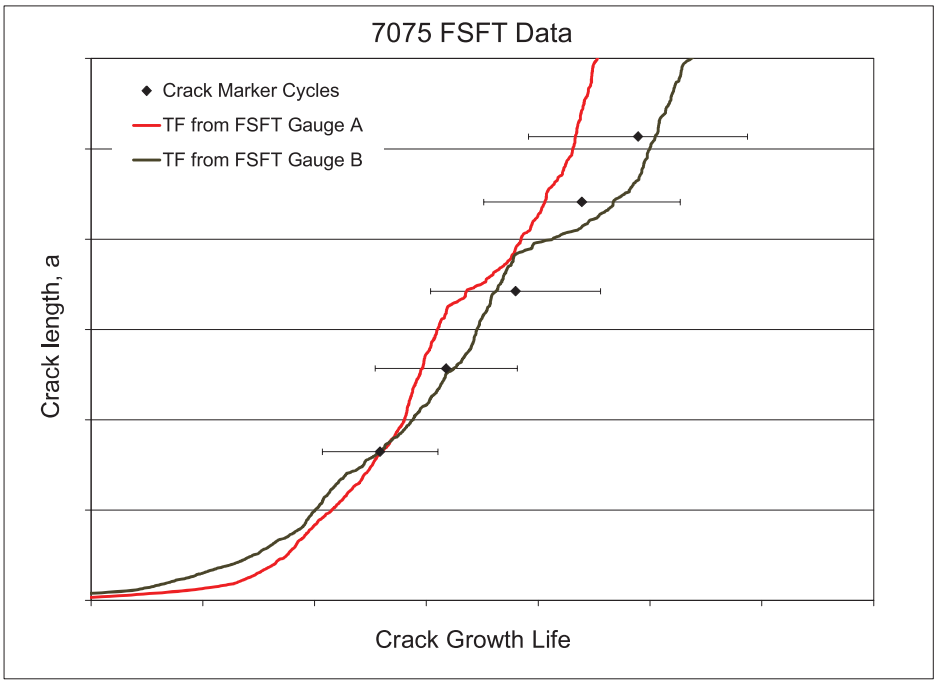

Figure 22 Transferred spectra crack growth predictions compared to marker cycles

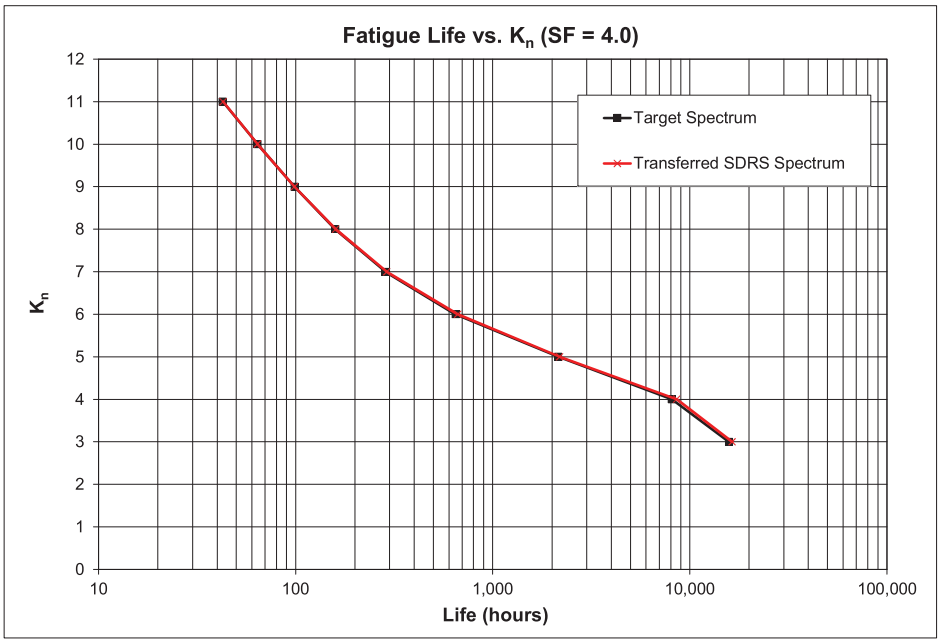

Figure 23 Transferred spectrum fatigue prediction compared to target spectrum

Overall, thirty locations spread over the CP140 wing were compared for the DTA portion of the validation and 22 locations were evaluated for the DA portion. Good agreement was found in all but one DTA case and in all DA cases; therefore, the methodology was considered validated based on the results of this study.

In one instance, crack growth did not agree for the final two marker cycles (of five) although this appears to be unique for this location, since Lockheed Martin Aeronautics (LMA) was unable to predict the final three marker cycles in a similar analysis. It is possible that the discrepancy is due to the inability of the analysis to handle the shear effects or due to the sequencing of the spectrum.

TF developed using different P-3C SLAP FSFT SG to the same analysis location provided very similar crack growth predictions supporting the robustness of the process.

3.6 NUMERICAL OPTIMIZATION OF FASTRAN MODEL PARAMETERS

Y. Bombardier, NRC Aerospace

Crack growth models are typically calibrated using experimental data prior to conducting damage tolerance analyses of aircraft structures. This process can be trivial for some crack growth models that only have few fitting parameters. However, other models, such as the FASTRAN equation with the analytical crack-closure model, include several model parameters that make the calibration challenging. To simplify the calibration process and improve the accuracy of crack growth simulations, an automated crack growth model optimization tool was developed, shown in Figure 24. This tool also aims at improving the robustness of crack growth models by reducing their dependency to the loading spectra and specimen geometries. Numerical optimization is used to minimize the discrepancy between experimental data and analytical crack growth. To demonstrate this approach, material model parameters were calibrated for P-3/CP-140 aircraft applications using the FASTRAN equation with the analytical crack-closure model. The optimization tool was found to be very effective at fitting crack growth simulation results to experimental data by changing the values of the parameters. It was observed that the automated calibration process can find multiple sets of FASTRAN parameter values that provide equivalent correlations with experimental data. In an attempt to develop a more robust material model, multiple test configurations with different geometries and loading spectra were used to determine an optimal trade-off model that maximizes the correlation for multiple test configurations. The conducted tests demonstrated that this approach is viable and could be used to improve the robustness of crack growth simulations.

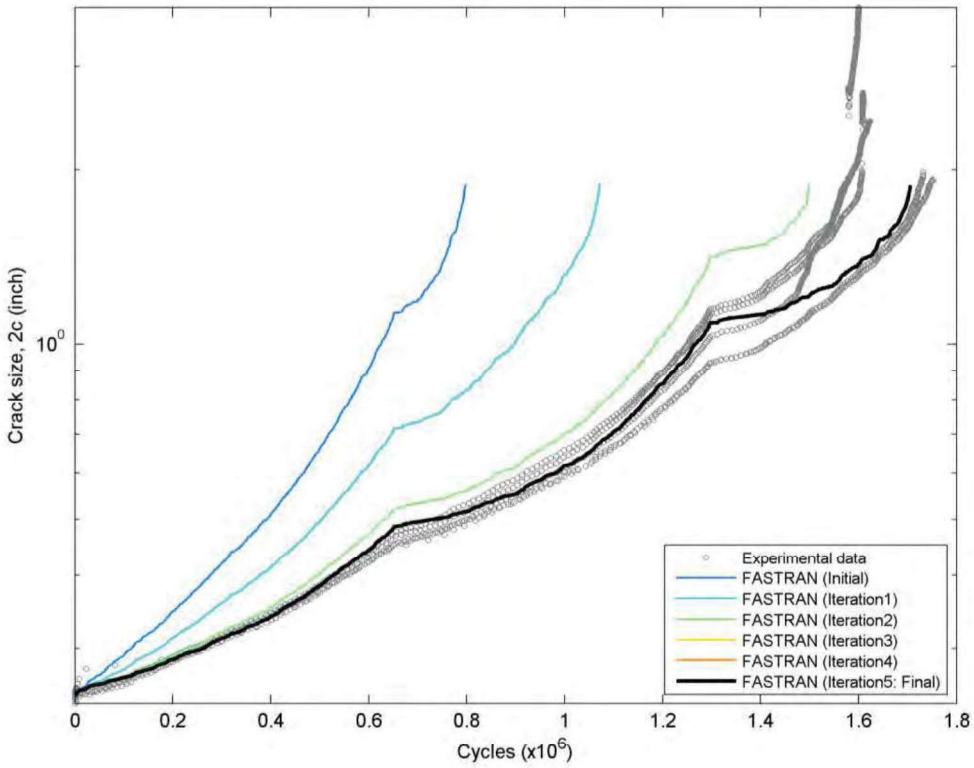

Figure 24 Evolution of the crack growth results during the optimization of 13 FASTRAN parameters

3.6.1 REFERENCES

[8] Bombardier, Y. and Renaud, G., "Numerical Optimization of FASTRAN Model Parameters," National Research Council Canada, LTR-SMM-2017-0025, Ottawa, 2017.

3.7 DETERMINATION OF INITIAL CRACK SIZE PROBABILITY WITH SPECIFIED CONFIDENCE

M. Oore, IMP Aerospace

Initial Crack Size is commonly used in damage tolerance analysis of aircraft structure. Studies regarding initial crack distribution are available including those of the USAF ASIP conference 2015. The objective of the present study is the determination of initial crack size probability, **with specified confidence,** of as manufactured aircraft structure. Two different procedures have been developed for this purpose and applied to teardown findings of cracked holes data of the P-3 full scale fatigue test and the Canadian CP140 special inspections. One procedure is probabilistic, based on hyper-geometric distribution, and the other employs statistical analysis using Log Normal distribution. The two methods gave very close results. A third method was

also applied by utilizing the non-central t-distribution. This method gave initial crack size values that are generally within 1% of the previous, as show in Table 3.

Table 3 Results of initial crack size at various probability levels

probability of	with 50% confidence that initial crack size smaller than	with 95% confidence that initial crack size smaller than
90 %	0.0048	0.0061
91 %	0.005	0.0064
92 %	0.0053	0.0067
93 %	0.0056	0.0072
94 %	0.0059	0.0077
95 %	0.0063	0.0083
96 %	0.0069	0.0091
97 %	0.0076	0.0103
98 %	0.0087	0.012
99 %	0.0108	0.0153

3.8 THE USE OF SAFETY CUTS IN FATIGUE DAMAGED FASTENER HOLE REPAIR

David DuQuesnay, Mechanical and Aerospace Engineering, Royal Military College of Canada

Safety cuts (or confidence cuts) are used in the repair of fatigue damaged fastener holes in aircraft structure to ensure that any residual crack is removed in the repair process, as shown in Figure 25. The necessity of using safety cuts was investigated by growing cracks in laboratory specimens and then “repairing” the specimens in the manner that would be done on in-service aircraft, both with and without safety cuts. The post-repair fatigue life for the safety-cut specimens showed a bimodal log normal distribution with the lower mode arising from machining flaws in the repair process, as shown in Figure 26. The results for the no safety-cut material, while having a similar mean life to the lower mode of the safety-cut coupons, showed nearly four times as much scatter in life. The results strongly suggest that residual cracks in no safety-cut coupons served as initiation sites for further crack growth, as shown in Figure 27. Consequently, despite the fact that safety cuts result in lower edge margins, they are a necessary part of the repair process.

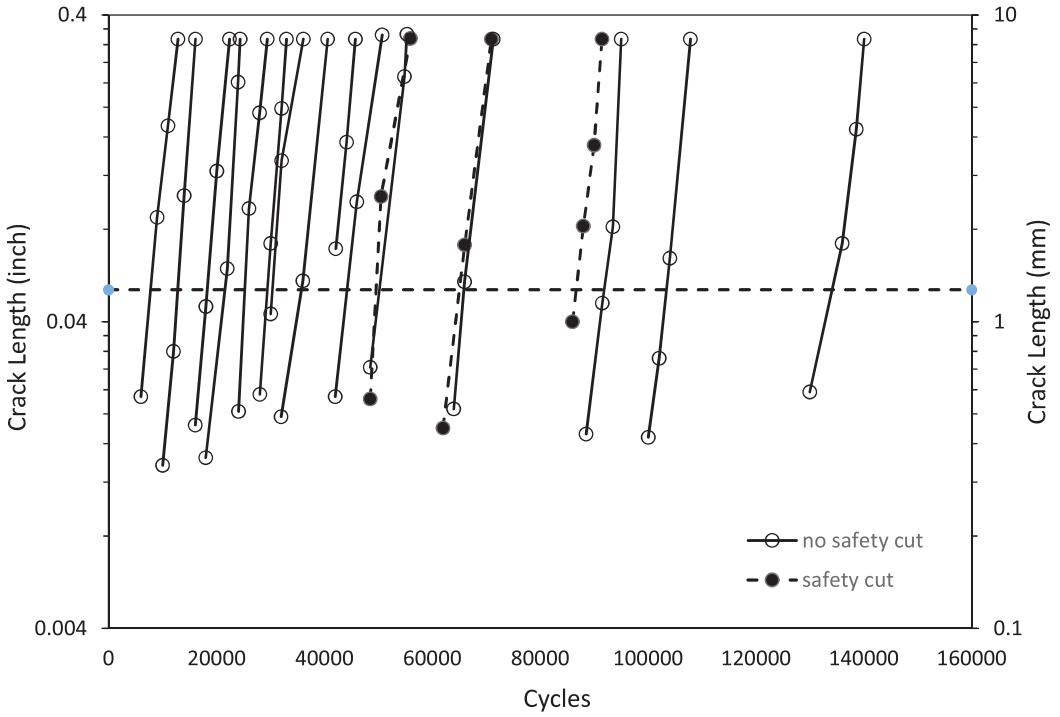

Figure 25 Crack growth curves for a number of specimens (both safety-cut and non-safety-cut). The dashed horizontal line marks 1.27 mm (0.050 inch), which is taken as the initiation size

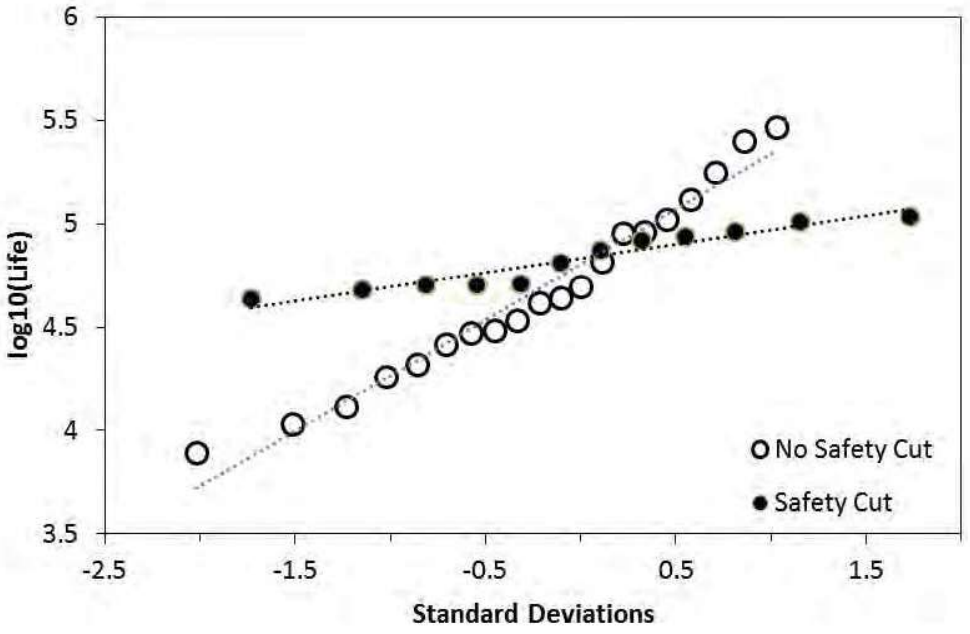

Figure 26 Normal probability plot of $\log_{10}$ (Initiation Life) for coupons with (solid) and without (open) safety cuts. The upper mode for the safety-cut coupons is not shown

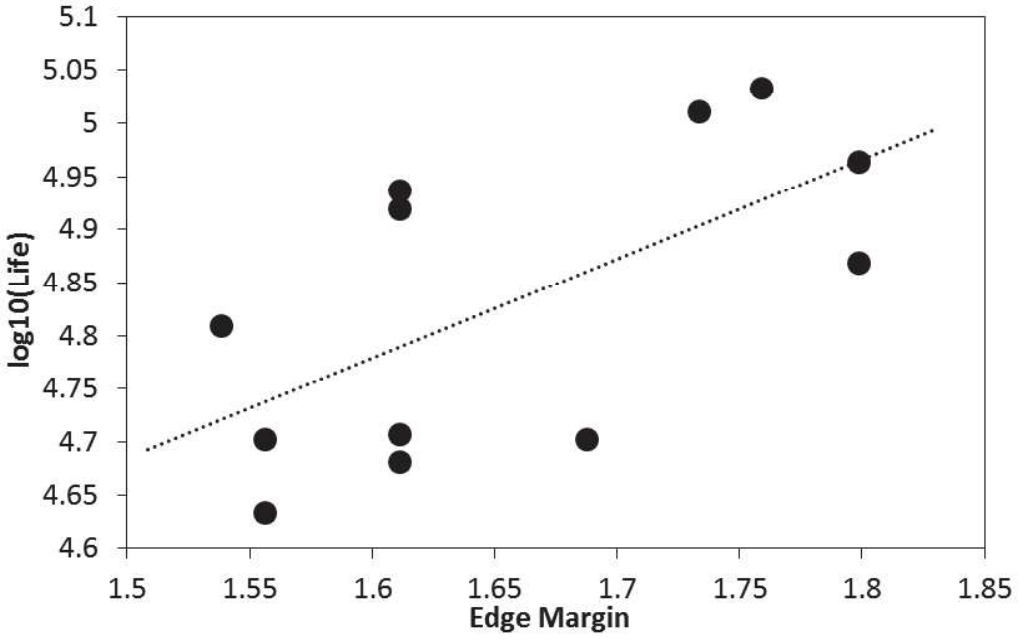

Figure 27 Plot of $\log_{10}$ (Initiation Life in cycles) vs. edge margin for safety-cut coupons from Figure 25

3.9 LOW CYCLE FATIGUE STUDY OF A CAST AUSTENITIC STEEL

X. Wu, NRC Aerospace

A mechanism-based approach—the integrated creep-fatigue theory (ICFT)—is used to model low cycle fatigue behaviour of 1.4848 cast austenitic steel over the temperature range from room temperature (RT) to 1173K (900°C) and the strain rate range from of 2×10^{-4} s^{-1} to 2×10^{-2} s^{-1}. The ICFT formulates the material's constitutive equation based on the physical strain decomposition into mechanism strains, and the associated damage accumulation consisting of crack nucleation and propagation in coalescence with internally distributed damage. At room temperature, the material behaviour is controlled by plasticity, resulting in a rate-independent and cyclically stable behaviour. The material exhibits significant cyclic hardening at intermediate temperatures, 673-873K (400-600°C), with negative strain rate sensitivity, due to dynamic strain aging (DSA), which occurs by slip dragging solute atoms. At high temperatures >1073K (800°C), time-dependent deformation is manifested with positive rate sensitivity as commonly seen in metallic materials at high temperature. The ICFT quantitatively delineates the contribution of each mechanism in damage accumulation, and predicts the fatigue life as a result of synergistic interaction of the above identified mechanisms. The model descriptions agree very well with the experimental and fractographic observations. The results of the work is partially reported at the ASTM Fatigue Symposium 2016, May 3-6, San Antonio, TX, and is compiled in ASTM STP 1598.

Thermomechanical fatigue tests were conducted on 1.4848 austenitic steel with constrain ratios from 50 to 100% in the temperature ranges from 473K (200°C) to 873K (600°C), 973K (700°C), 1073K (800°C), and 1173K (900°C). The material's cyclic and hysteresis behaviours were analysed in terms of the recognized deformation mechanisms, namely plasticity with dynamic strain aging, creep and oxidation. The effects of these mechanisms were quantitatively described by the integrated creep fatigue theory. The thermal mechanical fatigue (TMF) life prediction model is the same as that for low cycle fatigue, signifying the same physics underlying both LCF and TMF failures under different loading profiles and constraint conditions.

3.10 Research Advances on Aircraft Structural Integrity and Sustainment

Min Liao, Marko Yanishevsky, Prakash Patnaik, NRC Aerospace

A paper summarizes recent research advances conducted at NRC supporting aircraft structural integrity and sustainment. As a government R&TD agency, NRC carries out material and structural research for both military and civil aircraft. The efforts include innovative practical and researches in the areas of structural lifing, risk/reliability analysis; environmental effects; life extension and continuing airworthiness. Based on the lessons learned and the new challenges foreseen, NRC has been carrying out research on physics-based modelling, model-assisted non-destructive evaluation (NDE) and structural health monitoring (SHM), non-standard coupon testing and efficient structural testing, as well as integrated vehicle health management technology. Examples of best practices supporting the structural integrity and sustainment of Royal Canadian Air Force (RCAF) transport/patrol aircraft (CC-130, CP-140), fighter aircraft (CF-188), helicopters (CH-146, CH-149), and civil aircraft, such as the Harvard T-6, are presented. The presented research advances are featured with both fundamental and applied research progresses.

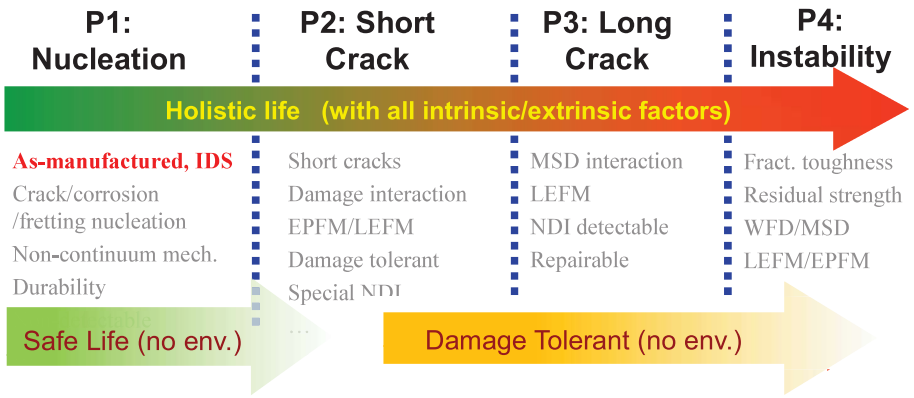

Figure 28 Holistic Structural Integrity Process (HOLSIP)

In conclusion, this paper presents some recent NRC research advances in the area of aircraft structural integrity and sustainment, which are aligned with the development of a new Holistic Structural Integrity Process (HOLSIP) framework. Some fundamental advances include: fatigue nucleation physics studies, practical small/short crack growth testing and modelling; development of multi-site damage/widespread fatigue damage evaluation tools; and development of risk analysis method/tools. The impact of environment on structural integrity was studied considering corrosion and fatigue interactions. Advanced NDE and SHM techniques continue to be developed to support structural integrity and sustainment. In addition, NRC has advanced experimental mechanics techniques including digital image correlation and thermal stress analysis. Novel loading fixtures and load control methodologies have been developed enabling faster component and/or full scale fatigue testing under both manoeuvre and dynamic loading. All these advances were presented through real life case studies, showing that the NRC advances, on both fundamental and applied research levels, have provided significant support to Canadian air fleet management with respect to maintain safety, increase availability, and reduce maintenance costs.

3.10.1 REFERENCE

[9] M. Liao, M. Yanishevsky, and P. Paknaik, "Research Advances on Aircraft Structural Integrity and Sustainment at NRC", The 30th Congress of the International Council of Aeronautical Sciences (ICAS), Daejeon/Republic of Korea, September 2016.

3.11 FROM SCIENCE TO ENGINEERING PRACTICE – EVOLVING A STRUCTURAL INTEGRITY FRAMEWORK

J. Komorowski (NRC), M. Liao (NRC), and D. W. Hoeppner (University of Utah)

In aeronautical engineering, the recognition of the importance of fatigue was only fully recognized after a series of de Havilland DH 106 Comet crashes with multiple fatalities. The time was the mid-20th century (1954). The engineering art of building structurally more efficient aircraft continued to evolve as the tools (engineering computational methods and mechanical tests) grew more complex. These tools, while largely based in experiment, often do not allow the capture of scientific knowledge of the phenomena that are behind the process of failure under progressive mechanical and environmental loading. Structural failure statistics show remarkable progress in aircraft safety. Unfortunately the tools used to ensure structural integrity continue to evolve particularly following an unexpected and often catastrophic failure with almost certain regularity. The common design approaches often lead to conflicting material choices (safe life vs. damage tolerance) and both ignore environmental effects (i.e. corrosion in metals). A small group of scientists, engineering researchers and aircraft structures engineers launched an effort at the beginning of this century to develop a holistic structural integrity process (HOLSIP). This process or framework allows to progressively integrate scientific knowledge of materials,

manufacturing processes and structural performance under intrinsic and extrinsic influences. Holistic here indicates that the framework emphasizes the importance of the whole and the interdependence of its parts. The approach has its origins in late 1960's and early development was encouraged by Rolls Royce, NRC, and a few others participating in Advisory Group for Aerospace Research and Development, an agency of NATO. Much of that effort was related to RB 211 engine development. The group started their collaboration in the 1990 period when problems symbolized by Aloha Airlines B737 multisite damage failure led the USAF and FAA to sponsor 'Aging Aircraft' programs. At the time teams from Lockheed, APES, University of Utah and NRC had effectively incorporated corrosion into structural integrity models. In turn USAF modified Mil-Std-1530 to incorporate corrosion in their Aircraft Structural Integrity Program (ASIP). HOLSIP will be introduced and some examples of current applications to aircraft design and sustainment will be described.

3.11.1 REFERENCES

[10] Jerzy Komorowski, Min Liao, and David W. Hoeppner, From Science to Engineering Practice - Evolving a Structural Integrity Framework, The ASTM JoDean Morrow Lecture on Fatigue, May 2016, San Antonio, USA. (https://www.astm.org/COMMIT/ASTM%202016%20Fatigue%20Lecture%20Komorowski.pdf)

4.0 FATIGUE LIFE ENHANCEMENT TECHNOLOGIES

4.1 SHOT PEENING TO EXTEND FATIGUE LIFE OF MILITARY AIRCRAFT

L-3 Communications (Canada) Military Aircraft Services (MAS)

The shot peening of aluminium parts as a retrofit to extend fatigue life of military aircraft has already been used for about two decades in Canadian aircraft industry. For the applications performed at L-3 MAS, the required Life Improvement Factor (LIF) was generally not higher than 1.5. Based on limited coupon testing performed in the late 1990's, engineers were satisfied that manual application of shot peening with a 200% coverage would provide this level of LIF. More recently, robotic systems were developed to perform shot peening in-situ as a Life Improvement Technique (retrofit) to extend the aircraft service life. In addition, for more recent applications, the LIF requested from shot peening went up to 3.0.

In that context, a new coupon test program was required to certify that higher LIF target using the robotic system. The application involves Al 7050-T7451 plate, 6" thick with a variable amplitude spectrum (maximum R-ratio of approximately -0.3). The geometries are generally radii at the bottom of machined pockets with Kts varying between 1.4 and 1.5 and stresses around yield point. Prior to the shot peening being applied at up to 80% of the baseline unfactored life of the critical hot spot, a light blend of 0.003" to 0.006" was carried out to remove some of the accumulated damage. Several test series were defined to address all bulkhead hot spot parameters that could affect the shot peening behaviour (ex. stress level, grain direction, geometry of the critical hot spot, etc.). The effect of performing this retrofit over a 0.015" deep crack was also verified. Besides this latter series, all test series showed LIF way above the requirement/expectations, as shown below in Figure 29.

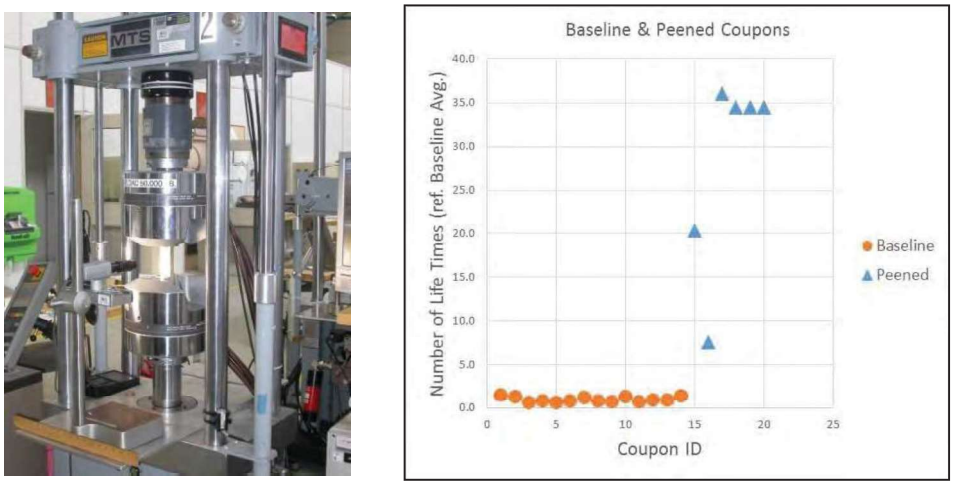

Figure 29 Recent test program on shot peening

4.2 CERTIFICATION TESTING OF A SHOT PEENING LIFE EXTENSION MODIFICATION

G. Renaud, NRC Aerospace

A robotic shot peening life extension modification developed by L-3 Communication MAS Canada was certified at National Research Council Canada (NRC). In total, 166 coupons were fatigue tested to determine the impact on the life improvement factor (LIF) of several parameters, including the stress level, the fatigue spectrum severity, the modification incorporation time, the location geometry, and the material grain orientation. Small crack detection was performed by a combination of Quantitative Fractography, shown in Figure 30 a), eddy current inspection, and reverse liquid penetrant inspections (Figure 30 b)). This technique was found to be more effective than regular liquid penetrant inspection to detect small cracks on a peened surface.

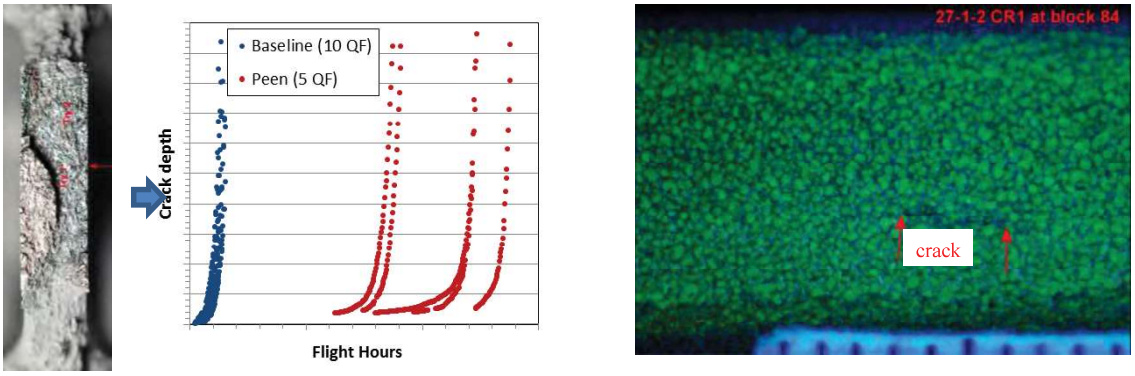

a) Qantitative Fractography b) Reverse Liquid Penetrant Inspection

Figure 30 Inspection methods

In some cases the effectiveness of the shot peening modification was significantly higher than expected, which caused a number of early fretting-induced failures under the grips. A method was developed to reduce fretting and was successful for preventing this type of failure, as shown in Figure 31.

Overall, all tested conditions exceeded the target LIF values, defined as the ratio of lives, at a certain probability reaching an “initiation” crack size, calculated from lognormal life distributions. This approach is illustrated in Figure 32.

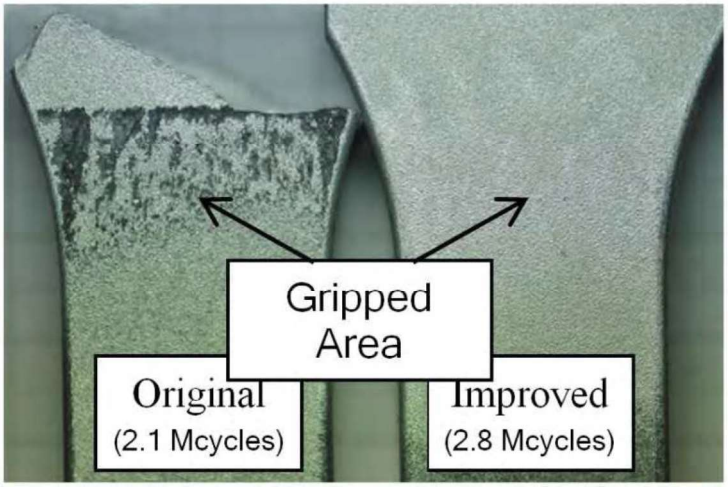

Figure 31 Early failure prevention

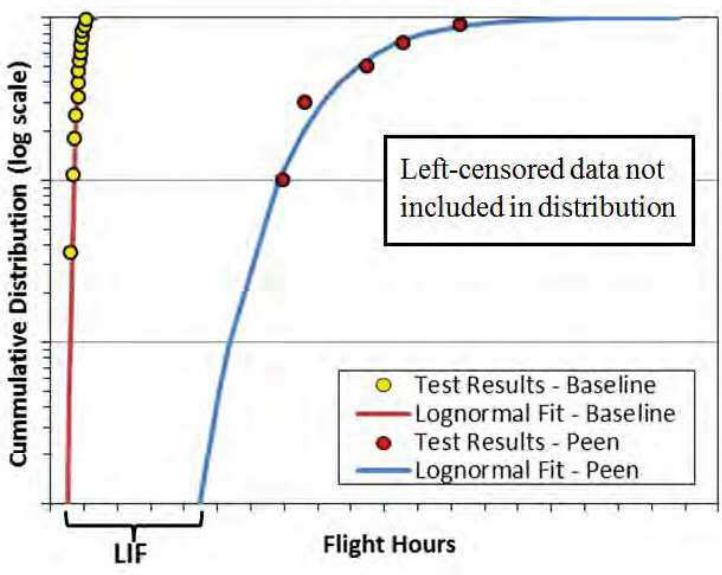

Figure 32 LIF calculation

4.2.1 REFERENCES

[11] Renaud, G., Martin, P., and Liao, M., "Experimental Life Improvement Quantification of a Robotized Shot Peening Modification", 2017 Aircraft Airworthiness & Sustainment Conference, May 22-25 2016, Phoenix, AZ, USA.

4.3 MODELING AND SIMULATION OF HOLE COLD EXPANSION LIFE EXTENSION *

G. Renaud, NRC Aerospace
* Paper being presented at ICAF2017

The split-sleeve cold expansion (CX) technique has been used for decades to delay crack nucleation and slow down propagation by inducing compressive stresses around fastener holes. However, the current damage tolerance analysis approach does not take into account the actual compressive stress distribution and its effect on the crack. By assuming that the life of a cold-expanded hole can be simulated using an artificially reduced initial flaw size, it generally results in life poor predictions that are overly conservative. Alternatively, life improvement factors (LIF) can be determined experimentally from specific costly coupon tests programs that are representative of the geometry and loading under consideration.

National Research Council Canada (NRC) is developing an approach to determine LIF values through modelling and simulation. First, a MSC Marc finite element (FE), developed to simulate the split-sleeve CX process, was validated using a database of residual stress distributions provided by the United States Air Force (USAF). From a given set of parameters, a Patran Command Language script automatically builds the parametric model, as shown in Figure 33, and determines the three-dimensional residual stress distribution around the cold-expanded hole.

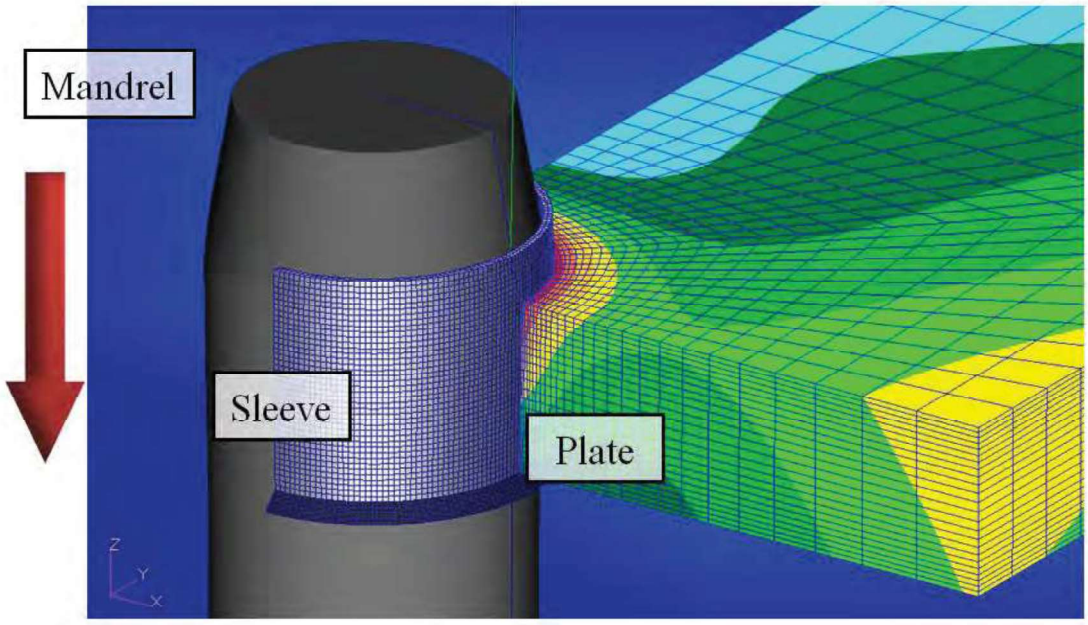

Figure 33 Split-sleeve cold expansion process finite element model

Results from the CX process simulation were exported to two crack growth tools, CPAT developed by ESRD, and BAMF developed by USAF, to perform crack growth simulation

within the FE-determined residual stress field. The crack fronts obtained from this purely analytical approach were in good agreement with shapes observed from fracture surfaces. An example of the evolution of a crack within a typical residual stress field is presented in Figure 34.

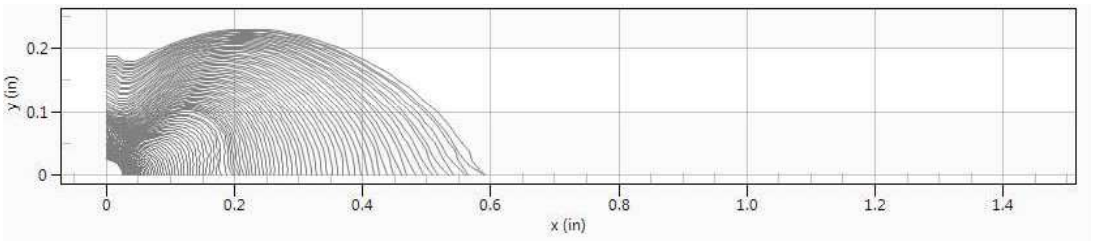

Figure 34 Typical crack growth within FE residual stress field using CPAT

The crack growth simulation in the above example assumed that the residual stress distribution is not affected by remote loading or by the presence of a crack. NRC is currently developing a fully integrated approach, shown in Figure 35, in which the crack can grow within a stress field that can be modified by these factors. An example of this coupling is the residual stress relaxation resulting from compressive overloads.

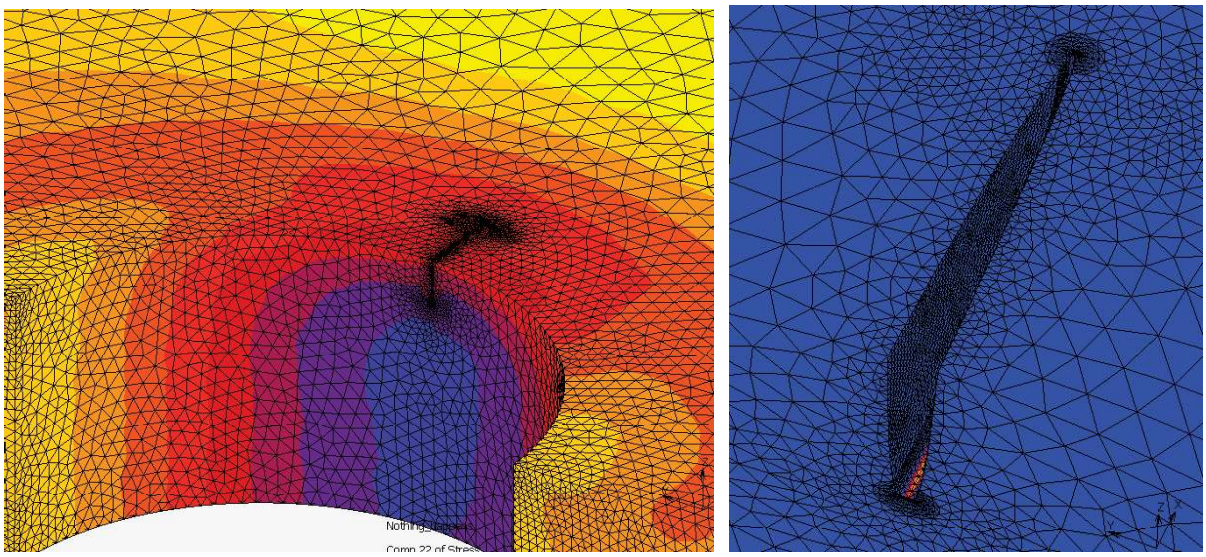

Corner crack in residual stress field | Stress Intensity Factor Calculation

Figure 35 Integrated CX process – crack growth simulation model

Future tasks have been established to improve the CX process simulation model by the use of anisotropic plasticity models calibrated from test results. Also, the integrated model will be coupled with a crack growth engine to allow calculation of improved analytical life improvement factors.

4.3.1 REFERENCES

[12] Renaud, G. and Liao, M., "Fatigue Crack Growth Simulation with Engineering Residual Stress Effects", 14th ICF Conference, June 18-23 2017, Rhodes, Greece

[13] Renaud, G., Liao, M., and Li, G., "Verification and Validation of Analytical Methods to Determine Life Improvement Factor Induced by Engineered Residual Stresses", ICAF2017, June 5-9 2017, Nagoya, Japan

[14] Renaud, G. and Liao, M., "Recent Development in Modeling of Cold Expanded Holes", AFGROW User Workshop 2016, September 13-14 2016, Layton, UT, USA.

[15] Renaud, G., Liao, M., Bombardier, Y., and Li, G., "Validation of Cold Expansion Modelling and Simulation", 2016 Aircraft Airworthiness & Sustainment Conference, March 21-24 2016, Grapevine, TX, USA.

[16] Renaud, G., Li, G., Bombardier, Y., and Liao, M., "Validation of Hole Cold Expansion Modeling", AFGROW User Workshop 2015, September 15-16 2015, Layton, UT, USA.

4.4 FATIGUE LIFE OF COLD EXPANDED FASTENER HOLES WITH INTERFERENCE-FIT FASTENERS AT SHORT EDGE MARGINS

D. DuQuesnay, Mechanical and Aerospace Engineering, Royal Military College of Canada

The fatigue life of 7075-T6 aluminium specimens with countersunk fastener holes with cold expansion and interference-fit fasteners with short edge margins was studied. The study was performed experimentally and through finite element analysis. The experiments measured the total fatigue life and crack growth, as shown in Figure 36. The results from the finite element analysis consisted of tangential residual stress profiles, which were combined with applied cyclic stresses for fatigue analysis. The experiments showed that the fatigue life improved with interference-fit fasteners and cold expansion at all edge margins. The fatigue life also increased with increasing edge margin. The finite element results were used to make fatigue life predictions that corresponded reasonably well with the experimental results, shown in Figure 37.

4.4.1 REFERENCES

[17] Vallieres, G. M. and DuQuesnay, D. L. (2015), Fatigue life of cold-expanded fastener holes with interference-fit fasteners at short edge margins. Fatigue Fract Engng Mater Struct, 38: 574–582. doi: 10.1111/ffe.12257.

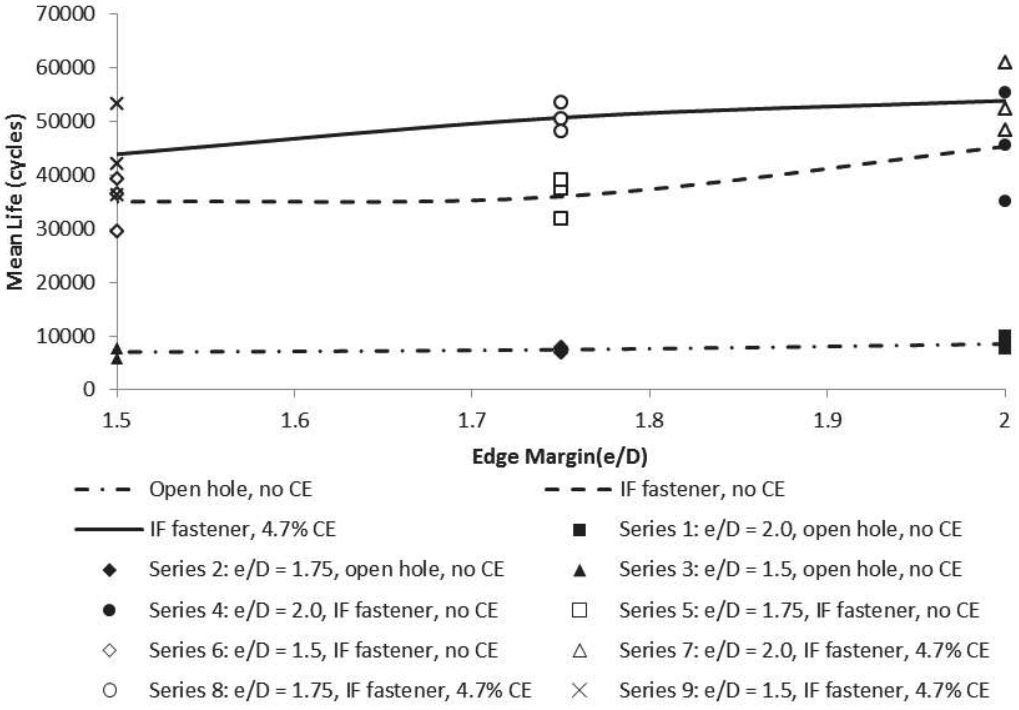

Figure 36 Effect of edge margin on life for cold expansion and interference-fit fasteners

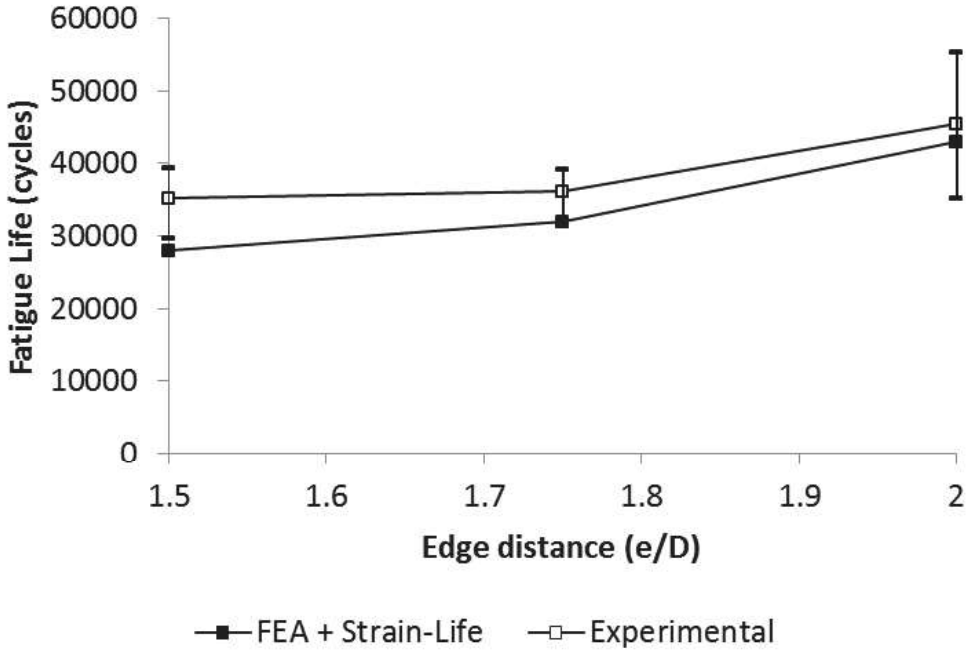

Figure 37 Fatigue lives of specimens with interference-fit fasteners

4.5 SURFACE DAMAGE EVALUATION OF AL HONEYCOMB SANDWICH PANELS

T. Reyno, D. Wowk - Royal Military College of Canada, C. Marsden - Concordia University

During maintenance inspections of honeycomb sandwich aircraft panels, measurement of dent depth and area are required for comparison with the damage limits specified in the standard repair manual. The measurement of surface damage is typically performed by hand and is subject to interpretation or variation based on the inspection personnel. It is also a costly process due to the time required to perform these assessments. Recent progress has revealed the potential for 3D scanning technology to be used as a more efficient and repeatable measurement tool for dented aircraft panels. This study examined the use of laser scanning for the inspection of flat honeycomb sandwich panels and evaluated its accuracy by comparing results to measurements taken using Vernier calipers and a coordinate measurement machine.

This method involves using a FARO® ScanArm laser scanning apparatus mounted to a lab workstation to generate a point cloud of 3D scan data representative of the entire damaged aircraft panel. The scanning is performed in conjunction with Geomagic Design X software, which supports handling of the data. A subset of the data is then considered for further analysis as illustrated in Figure 38. A 2D or 3D surface is then fit to manually selected regions of the point cloud data, which correspond to undamaged sections of the panel. This surface fit approximates the original, undented panel surface. Figure 39 shows five undamaged regions of the panel chosen in black, and the fit of the undamaged surface shown in yellow. Being able to recreate the undamaged panel surface is a key step in the process, as the original geometry of the panel is typically not available to the inspection personal.

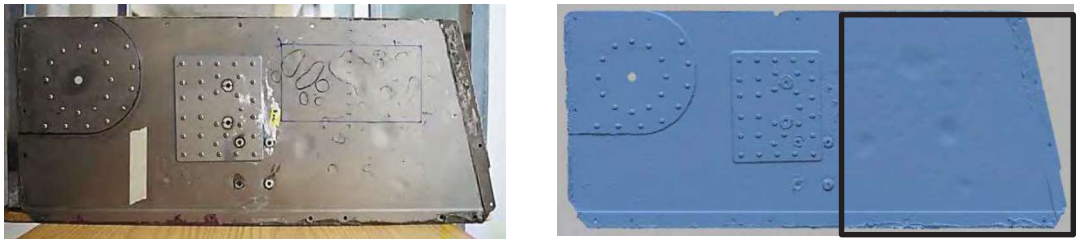

a) b)

Figure 38 a) the physical panel, b) a 3D point cloud of the entire panel, highlighting the region used for further analysis

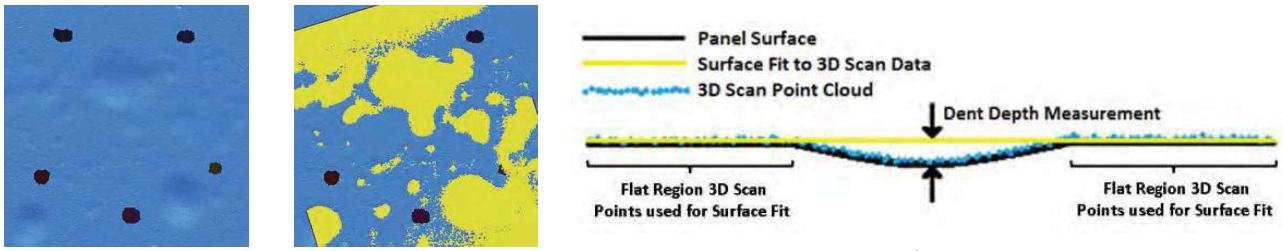

a) b) c)

Figure 39 a) selected undamaged regions are shown in black, b) the surface fit of the undamaged panel is shown in yellow, c) an illustration of the relationship between the point cloud, the panel surface and the undamaged surface fit

A deviation analysis is then performed automatically within Geomagic Design X, where the perpendicular distance between the surface fit and the 3D scan data is extracted in order to provide the dent depth. A dent was identified as having a depth greater than 0.1mm, and the maximum depth for each dent was noted. The image was then adjusted to reflect the 0.1mm threshold, as shown in Figure 40. The area of the dent was automatically extracted using the image processing software ImageJ by creating a black and white image.

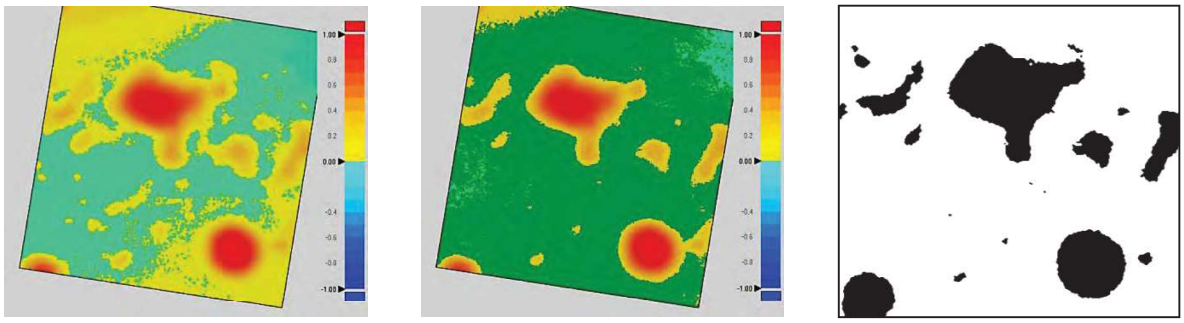

Figure 40 a) deviation analysis indicating the distance between the original panel surface and the scan data, b) dents are clearly indicated in yellow and red after application of the 0.1mm threshold, c) areas of the regions in black were extracted automatically

The accuracy of the 3D laser scanning method was evaluated by comparing the dent depth to measurements obtained using Vernier calipers and the "coordinate measuring machine" (CMM) capability of the FARO® ScanArm. The CMM method uses a touch probe to provide relative positions of points in 3D. The maximum difference in the measured dent depth was 0.03mm using the laser scanner when compared to both the calipers and the CMM method.

Laser scanning provides a very efficient, accurate and repeatable method for determining measurements of dent depth and area in the field. Work is presently underway to extend this method to both curved and corrugated sandwich panels.

4.6 CHARACTERIZATION OF SANDWICH PANELS SUBJECT TO LOW-VELOCITY IMPACT

S. Prior, D. Wowk - Royal Military College of Canada, C. Marsden - Concordia University
(Masters thesis. Captain Stephen Prior, The Royal Military College of Canada, April 2016)

Low-velocity impact on composite sandwich structures is a concern in the aerospace community, which has led to academic and industry investigation of failure modes, strength reduction and damage tolerance of structures with special attention to barely visible impact damage. Blunt impact as a result of tool drops or ground handling accidents may cause damage to the facesheet and core compromising the integrity of the panel while leaving minimal surface indication. This research characterizes damage as a result of out-of-plane impact of selected non-standard sandwich panels. Panels consist of carbon-fibre reinforced epoxy facesheets, and an aluminium alloy honeycomb core. The thicknesses of the facesheets, the thickness or the core, and density of core were varied for the panels, and the ability of various non-destructive inspection methods were evaluated in terms of their ability to detect and measure damage.

A test fixture, shown in Figure 41, was designed to allow for a drop-weight impact tower to contact panels perpendicular to their upper surface. The fixture was capable of swiveling to accommodate different panel thicknesses as well as a taper. A circular contact ring allowed for a simply supported boundary condition that enabled the panel to flex locally in the dent region. For impacts with the same kinetic energy, it was determined that impactors with larger radius tips produced fewer damage modes than smaller radius tips. The 12.7 mm radius tip produced delamination, fibre breakage, core crushing and adhesive cracking as shown in Figure 42, while the 79.8 mm tip only resulted in core crushing.

The surface dents were measured using laser topography, and the underlying panel damage was characterized with through-transmission ultrasound, radiography and an in-house damage detection method named the C-scan tap test, which detected changes in local stiffness similar to the computer-aided tap test. Three images of the damage region of one of the impacted panels are shown in Figure 43 through Figure 45. Both ultrasound (Figure 43) and the tap test (Figure 44) were able to detect damage in the core, with ultrasound having a higher resolution for determining the size and shape of the damage region. While radiography (Figure 45) could identify panel features such as cell walls and core splices, damage in either the core or facesheet was not visible. It was determined that laser topography is only able to detect damage if a surface dent is present. If there is significant springback, laser topography would not be able to detect the underlying core damage. None of the methods were able to identify whether or not fibre breakage or adhesive cracking occurred.

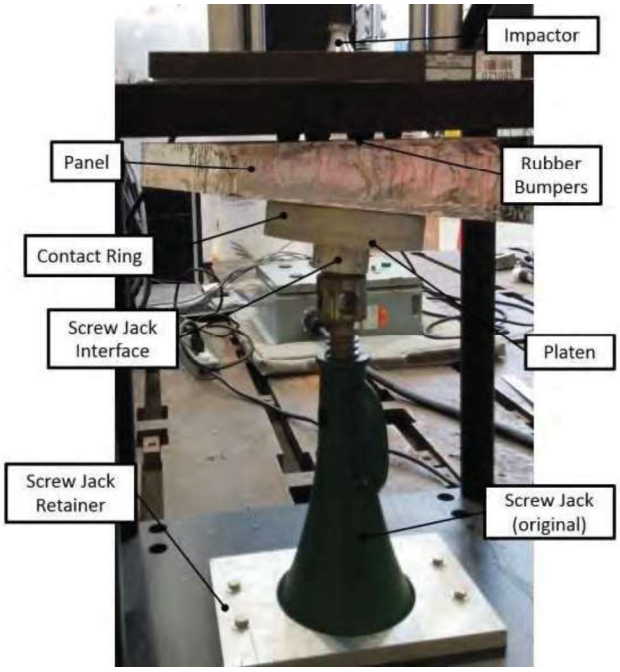

Figure 41 Drop test fixture for accommodating panels with tapers

Figure 42 Multi-mode panel damage using a 12.7mm radius impactor

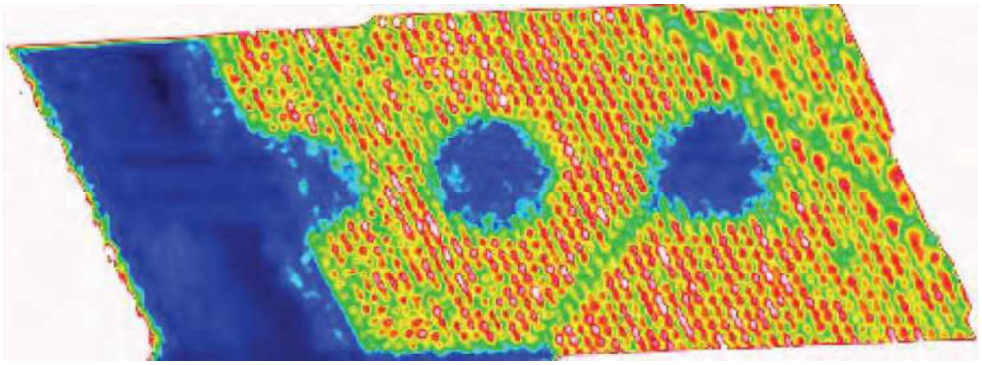

Figure 43 Through transmission ultrasound indicating 3 regions of damage

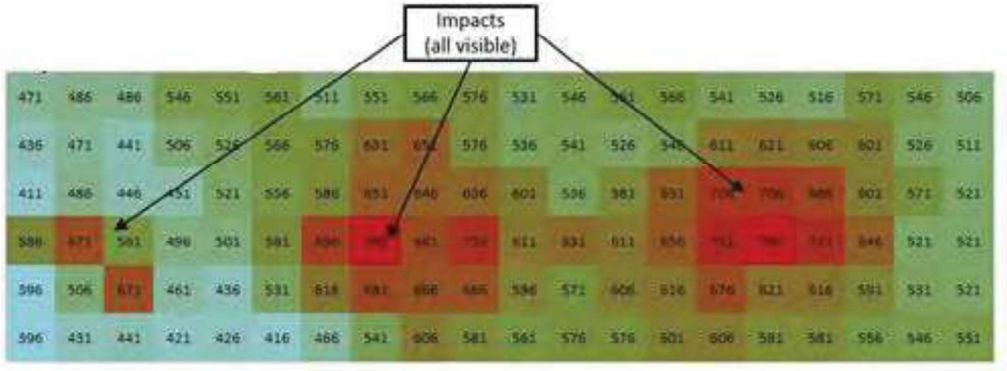

Figure 44 C-scan tap test indicating 3 regions of damage

Figure 45 Radiographic image with no visible damage regions

4.7 THE EFFECTS OF SKIN THICKNESS AND CORE DENSITY ON RESIDUAL DENT DEPTH IN AEROSPACE SANDWICH PANELS

D. Wowk, Royal Military College of Canada, C. Marsden, Concordia University

Sandwich panels are commonly used for aerospace structures that require a high bending stiffness, but the thin facesheets that are bonded to the core can be susceptible to impact damage. It is necessary to be able to identify and assess the severity of the damage, but this can be difficult when dents are not visible on the surface of the skin. This can occur when the dent elastically springs back immediately after impact, and can cause the skin to return close to its original position, leaving little indication that a damaged core exists. Identifying combinations of skin thickness and core density that are more susceptible to spring back can enable better decisions to be made with respect to inspection procedures.

Virtual testing of a spherical indenter impacting a 2.5”x2.5”x1” sandwich coupon with 7075-T6 skins and 5056-H39 aluminium core was performed using an explicit dynamic finite element code (AUTODYN). The three components included in the simulation are shown in Figure 46. Inertial effects, material plasticity, contact, large deformation and element failure strain were all incorporated, and the honeycomb core was represented at the cellular level. Each coupon was impacted to a prescribed depth and then allowed to elastically spring back to form a residual dent. Figure 47 shows a cross section of the deformed shape of the dent as well as the resulting core damage.

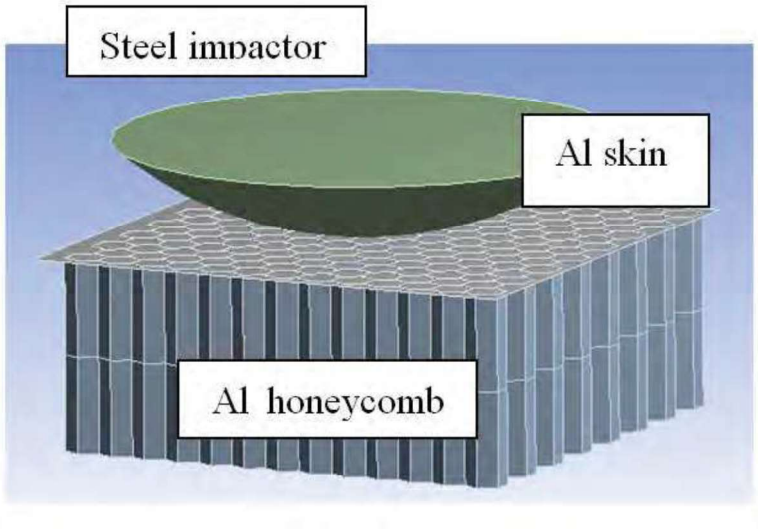

Figure 46 The three components of the sandwich panel impact models

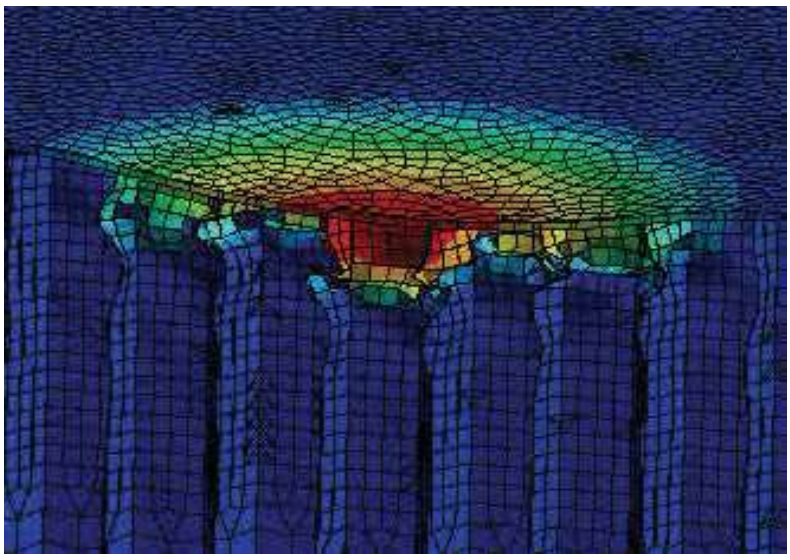

Figure 47 Cross-sectional view of the dented facesheet and crushed core. Red represents higher magnitudes of deformation

The baseline configuration of the sandwich panel had a skin thickness of 0.012", a cell wall thickness of 0.001", a cell size of 0.1875" and a maximum impact depth of 0.066". This impact depth was chosen to produce a damage mode consisting of core crush and plasticity in the skin. Simulations involving three different parameters were completed according to the specifications listed below. Each study started with the baseline case which is indicated in bold, and then parameters were varied independently from each other.

- Skin thickness (0.008", **0.012"**, 0.025", 0.032", 0.04", 0.05", 0.063", 0.071", 0.08");
- Cell size (0.125", 0.156", **0.1875"**, 0.25", 0.375"); and
- Cell wall thickness (**0.001"**, 0.0015", 0.0025", 0.0035", 0.004").

Predictions from this study show that the thickness of the skin has the largest effect on residual dent depth, with Figure 48 indicating that panels with thicker skins undergo more spring-back. The panel with a 0.08" thick skin springs back 54% from its maximum impact depth, and results in a residual dent depth that is 23% smaller than the 0.008" skin. The difference in residual dent depth occurs primarily because of the difference in the size of the damage region and the location of plasticity in the dent.

For a given maximum impact depth, cores with larger cell sizes and smaller wall thickness allowed more spring back to occur as seen in Figure 49 and Figure 50. The lower density core is more easily deformed, and therefore incurs less damage for a prescribed impact depth than the denser core. The less damaged core retains more elasticity and is therefore less able to resist spring back of the skin resulting in a shallower residual dent.

The results of these studies indicate that sandwich panels with a lower core density and thicker skins are the most susceptible to barely visible impact damage (BVID) due to the larger magnitude of spring-back that occurs. These trends could be used to help identify sandwich panels that should be inspected more closely, using techniques other than visual inspections.

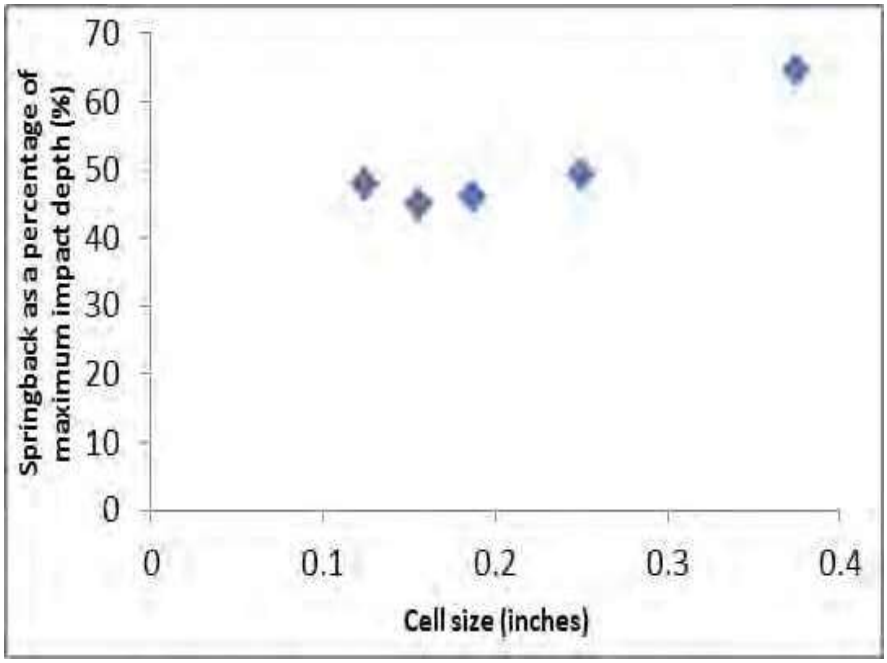

Figure 48 The magnitude of spring back for different skin thicknesses, measured as a percentage of the maximum impact depth.

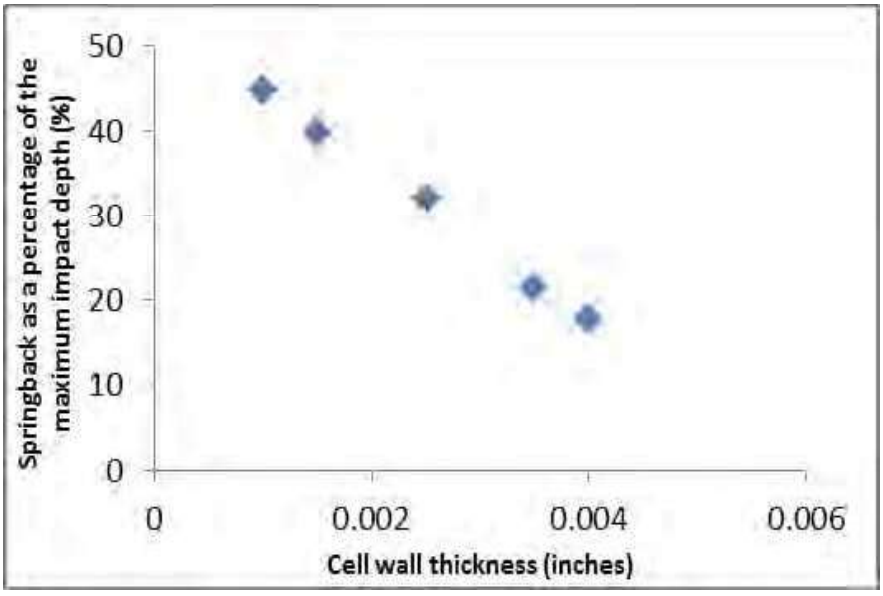

Figure 49 The magnitude of spring back decreases with increasing cell wall thickness.

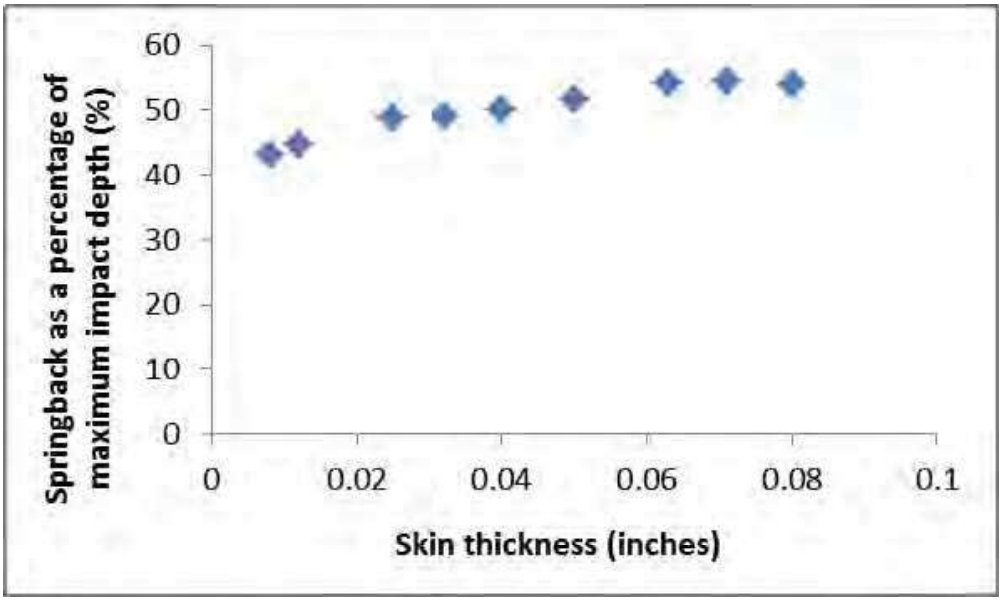

Figure 50 The magnitude of spring back increases with increasing cell size

4.7.1 REFERENCES

[18] D. Wowk, Royal Military College of Canada, C. Marsden, Concordia University, International Journal of Computational Methods and Experimental Measurements, Vol 4. No. 3, (2016) 336-344.

5.0 LOAD, USAGE, AND STRUCTURAL HEALTH MONITORING

5.1 HELICOPTER LOAD AND USAGE MONITORING RESEARCH IN 2015-2017*

C. Cheung, NRC Aerospace

* Paper being presented at ICAF2017

Helicopter load and fatigue life estimation

With changes to aircraft usage due to expanded roles, operators need to monitor the usage of the aircraft and component loads to ensure safe operation of the components within their fatigue lives. Although dynamic component loads can be measured and monitored directly, these measurement methods are not reliable and are costly and difficult to maintain. These challenges have inspired the implementation of computational intelligence and machine learning techniques to replace the need for costly sensor systems.

The National Research Council Canada (NRC) has developed a methodology, named Signal Approximation Method (SAM), which enables the estimation of helicopter loads and tracking load exceedances and fatigue damage for a targeted component using computational intelligence techniques as illustrated in Figure 51. The approach relies only on flight state and control system (FSCS) parameters, such as those recorded by a flight data recorder (FDR), and can also be applied to legacy aircraft or to those aircraft not equipped with HUMS. The methodology adapts to the input data available so is not constrained to one particular system or platform, and enables the estimation of loads through the duration of a manoeuvre instead of assuming a constant load for an entire manoeuvre. So far, SAM and its variant, extended SAM, have been tested on two different helicopter platforms, the S-70A-9 Australian Black Hawk (Sikorsky) and the CH-146 Griffon (Bell 412). Significant improvements are made over previous results for the S-70A-9 Black Hawk using SAM while using uniquely FSCS parameters obtained from a FDR to obtain full manoeuvre dynamic load signals in time. Furthermore, the application of the technology to a different platform and different original equipment manufacturer (OEM), namely the CH-146 Griffon, demonstrates the possibility of applying this methodology and its adaptability across different platforms.

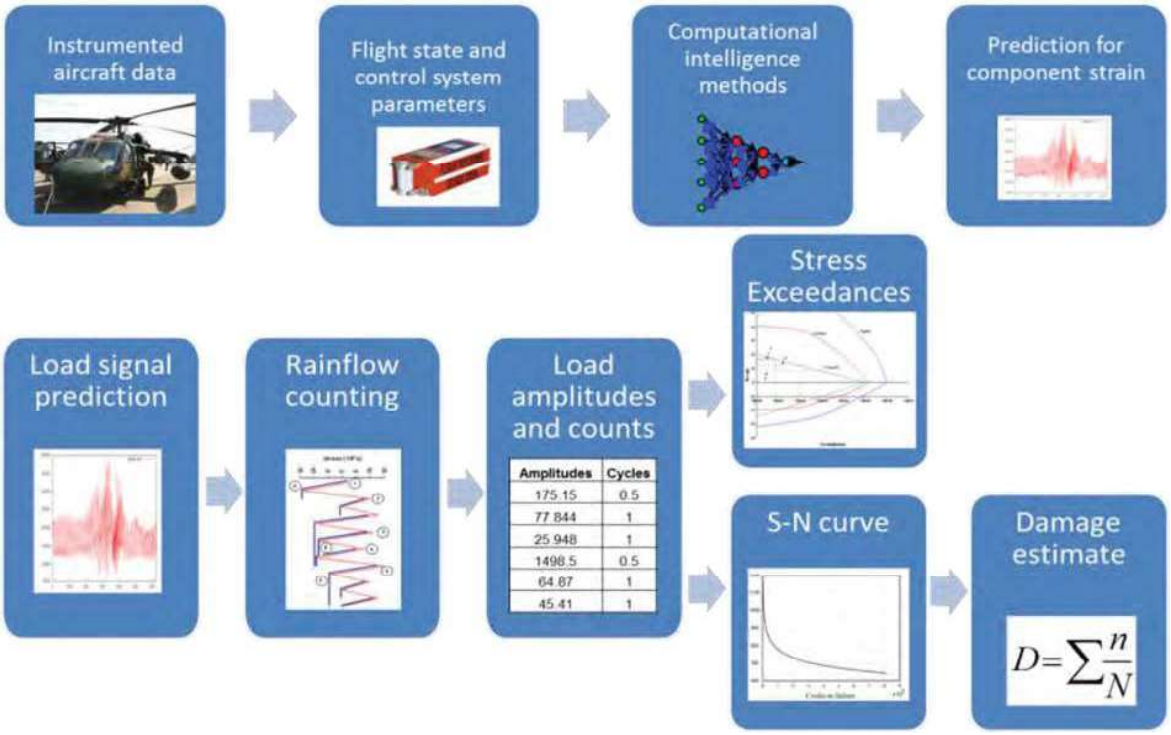

Figure 51 Load signal estimation methodology and fatigue life analysis

Continued research efforts in this area have been directed at reducing the number of dimensions of the input data using feature generation techniques in the load estimation methodology, beginning with intrinsic dimension analysis to determine the number of intrinsic dimensions in the data. The data set is then mapped using different implicit methods to a low-dimension representation of the original data, which is then used for load estimation and fatigue life analysis for comparison with the results of the original 26-dimension input data, shown in Figure 52. The resulting load signal and fatigue life estimates from the low-dimension representations are in most cases equal if not more accurate than those for the original input data. These promising results show that the low-dimension representations retain the relevant data from the original input data set and perhaps discard spurious data resulting in more accurate estimates.

Nonlinear transformations have been used for this purpose, but their computation via implicit methods becomes more complex, time consuming and impractical with data growth. Moreover, the relationships between the features of the original and the target spaces are more difficult to uncover. Extreme Learning Machines (ELM) are used as an explicit functional representation for implicit methods, in particular for the t-SNE mapping as seen in Figure 52. It was found that ELMs provided a good approximation to the implicit mapping, which preserves the appropriateness of the load prediction and damage estimation of critical helicopter components. In addition, the ELM model can be used for processing incoming streams of data, overcoming the limitation of the computation of the low dimensional mapping inherent to the use of implicit methods.

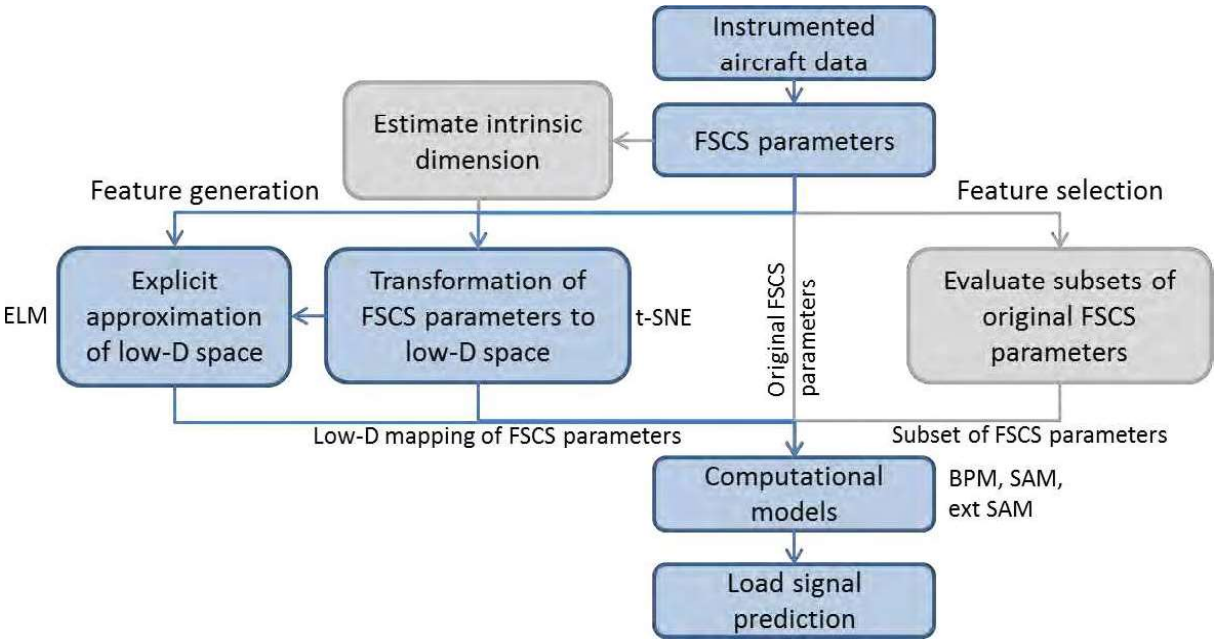

Figure 52 Flowchart of implicit and explicit approaches to generate low-dimension mappings of input data for load signal prediction

Usage monitoring using MEMS-IMU sensor system and FDR input data

With increasing demands on aircraft to fly expanded roles and missions, aircraft often operate differently than their manufacturers intended upon design. Monitoring aircraft usage is therefore an important task to track how the aircraft are flown and to ensure safety and effective usage of components. Many modern aircraft are now equipped with some type of health and usage monitoring system (HUMS) for usage monitoring activities; however, many older aircraft and even some modern aircraft fleets have minimal or no HUMS nor any other data capture systems installed. Still, these aircraft require usage monitoring activities to verify that the operational usage of the aircraft is consistent with the designed usage.

As an alternative to existing HUMS and data capture systems, the National Research Council Canada (NRC) developed a low-cost, standalone sensor system to record in-flight aircraft orientation rates of change, accelerations, and other flight measurements to detect flight manoeuvres, shown in Figure 53. This work was initiated as a temporary usage monitoring option for an older aircraft fleet where a standalone system was preferable.

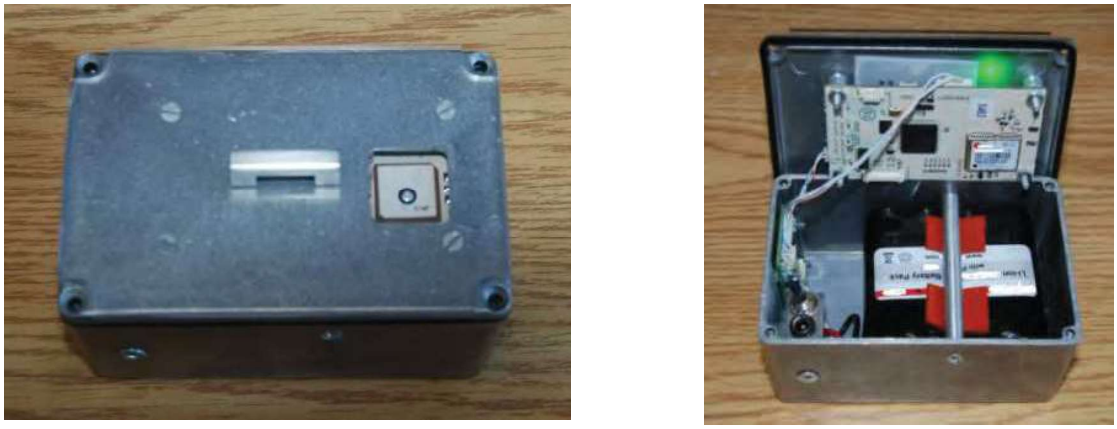

Figure 53 MEMS-IMU system for helicopter usage monitoring

An initial flight test of the sensor system was performed on a Bell 206 helicopter. The initial manoeuvre recognition results based on the sensor system measurements were very promising, though limited to only 7 general manoeuvres. More comprehensive in flight testing of the sensor system has recently been carried out on a Bell 412 CH-146 Griffon helicopter. A much broader range of 60 manoeuvres and regimes from the CH-146 usage spectrum were flown. Data was collected for several scripted flights from the MEMS-IMU sensor system as well as from the flight data recorder. Data-driven manoeuvre recognition models based on the recorded data from both data sources were developed and compared.

Although the collected flight data demonstrated considerable variability from flight to flight, as tested quantitatively using statistical tests, manoeuvre recognition models were developed using a pooled stratified sampling scheme combining data from the scripted flights. With both data sources, very high classification accuracy was achieved by these models overall as well as for the individual manoeuvres and regimes. Different input subsets to exclude GPS and/or magnetometer readings were attempted, still demonstrating very accurate classification results. These promising results demonstrate that the MEMS-IMU sensor system has the potential to serve as a simple low-cost standalone alternative for monitoring the flight data required for manoeuvre recognition. Since the system does not rely on aircraft power and is compact, it could serve as an option for any aircraft not equipped with FDR or HUMS.

5.1.1 REFERENCES

[19] C. Cheung, A. Lehman Rubio, J.J. Valdés, “Helicopter manoeuvre recognition: a data-driven approach using two different data sources”, Proceedings of International Committee on Aeronautical Fatigue and Structural Integrity (ICAF 2017), Nagoya, Japan, Jun 2017.

[20] C. Cheung, A. Lehman Rubio, J.J. Valdés, “Data-driven classification of CH-146 manoeuvres using MEMS-IMU sensor system”, Proceedings of the American Helicopter Society (AHS) 73rd Annual Forum, Fort Worth, TX, USA, May 2017.

[21] C. Cheung, J. Puthuparampil, J. J. Valdés, S. Pant, "Manoeuvre recognition using a low-cost standalone MEMS-IMU system", Proceedings of the AHS 72nd Annual Forum, West Palm Beach, FL, May 2016.

[22] C. Cheung, D. Backman, J. Puthuparampil, M. Kotwicz Herniczek, "Evaluation methodology for inertial measurement units (IMU) in structural health monitoring (SHM) applications", Proceedings of the 62nd CASI Aeronautics Conference Aero'15, Montreal, Quebec, May 2015.

5.2 STRUCTURAL HEALTH MONITORING (SHM)

L-3 Communications (Canada) Military Aircraft Services (MAS)

SHM has been a subject of great interest for L-3 MAS over the last decade. Recently, L-3 MAS has participated in a collaborative program called DPHM 501 - Characterization of Guided Wave Propagation in Aircraft Structures, as a member of the CRIAQ (Quebec Aeronautical Industrial Research Consortium). The project was aimed at developing a standard process to characterize guided wave propagation as well as a knowledge-base of guided wave interaction mechanisms with damages typically observed in aircraft structures. One of the key outcomes is a database containing experimental and numerical results for over 250 tests conducted.

Since September 2016, L-3 MAS and Paradigm Shift Technology are partnering in a technology demonstration project funded under the Build-in-Canada Innovation Program. The project evaluates the ability of the Prognostica™ technology to detect structural defects in different applications: Fatigue cracks in fastener holes and in fillet radii, disbonds and cracking in underlying structures (detected from the overlaying graphite epoxy skin). The final demonstration will be accomplished primarily via a coupon program conducted at the DND Quality Engineering test Establishment (QETE). The project is sponsored by the CF-188 Weapon System Management office and it will culminate in the installation of sensors on three operational aircraft at four chosen locations to assess the technology in the operational theatre. The sensor, coined Chameleon Skin Gauge (CSG^{TM}), is a passive, thin, isotropic film, which may be cut and formed in any shape. Once interrogated by the reader and processed though proprietary software, the sensor data provides direct information on the cumulative effect of host structure exposure to stress/strain loads and cracking.

5.3 DAMAGE DETECTION METHODS USING GUIDED AND BULK WAVES, PIEZOCERAMIC (PZT) TRANSDUCERS MODELING AND DESIGN, IMAGING TECHNIQUES FOR PHASED-ARRAY TRANSDUCERS,

Patrice Masson, Nicolas Quaegebeur, Philippe Micheau, Ahmed Maslouhi, Mechanical Engineering Dept., Université de Sherbrooke, QC

In collaboration with academic and partners from aerospace and manufacturing industries (Bombardier Aerospace, Defence Research and Development Canada, L-3 MAS, Olympus NDT, Pragma NDT, Ungava Tech, Abzac Canada, CRIAQ-Consortium for Research and Innovation in Aerospace in Québec), the Ultrasound team at Université de Sherbrooke (UdeS), led by Prof. Patrice Masson, has carried out various research projects on damage detection methods using guided and bulk waves, piezoceramic (PZT) transducers modeling and design, imaging techniques for phased-array transducers, Structural Health Monitoring (SHM) methodologies, and numerical methods such as Finite or Spectral Elements (FEM, SEM).

PZT transducers design and configuration

The discrimination of the guided wave modes propagating is critical in damage imaging, based on the measurement of Time-of-Flight (ToF), or on more advanced approaches, thus selective mode excitation is sought. This can be achieved by driving piezoceramics located on both sides of a plate in- or out-of-phase to select the mode (magnet-based clamp design shown in Figure 54 [1]). To further improve modal selectivity, multi-element PZTs have been designed and micro-machined [2].

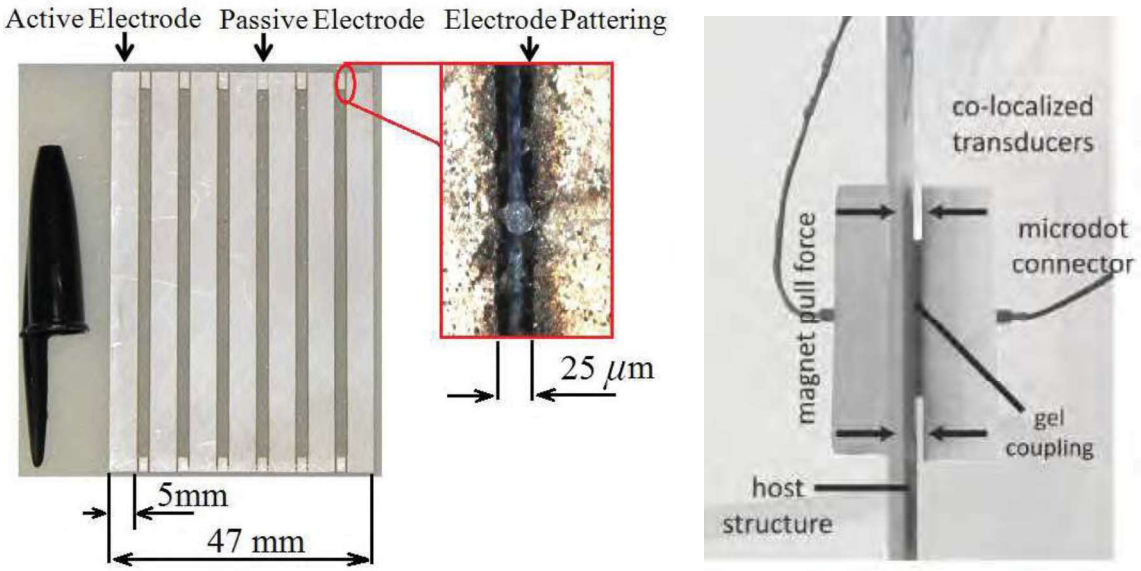

Figure 54 PZT array [23] and co-localized clamp [24]

The efficiency and robustness of PZT transducers have been studied, and metrics have been developed to evaluate the robustness under varying bonding and compensate for degradation [25].

Imaging algorithms for SHM and NDT

Significant improvement in resolution for source detection and localization has been demonstrated with respect to classical Delay-and-Sum, also referred as Total Focusing Method (TFM), using phased-array transducers by implementing Full-Matrix Capture (FMC) correlation-based damage imaging algorithms in multimode propagation, with demonstrated gain in computational load and damage discrimination, shown in Figure 55 [26]. The approach has been applied to composite structures [27].

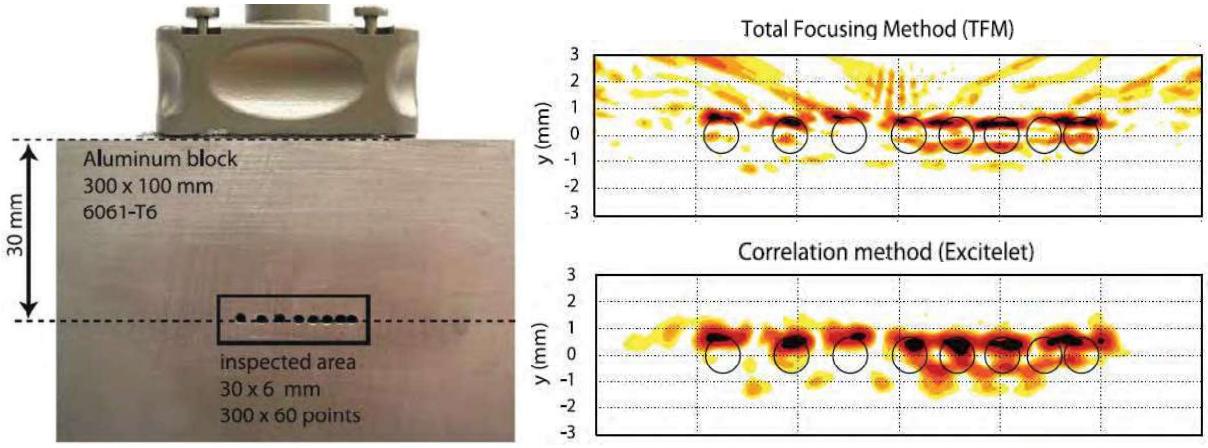

Figure 55 Correlation-based imaging [4]

Guided waves propagation models

Analytical and numerical tools have been developed, for better prediction of ultrasonic guided wave generation by PZT transducers [28], propagation in composite structures [29], and in-situ characterization of mechanical properties [30]. Modeling tools have also been developed to model the interaction of guided waves with damage features [31], shown in Figure 56.

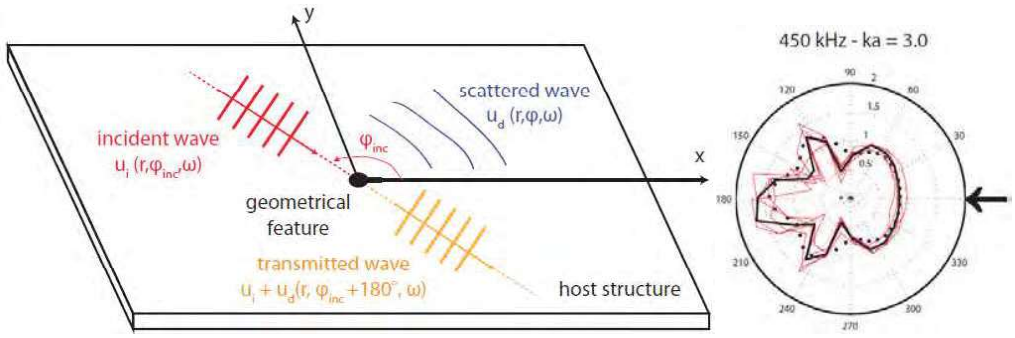

Figure 56 Guided wave interaction with a feature [31]

Design of Structural Health Monitoring systems

Design methodologies based on numerical and experimental studies have been conducted on various aerospace structures, such as composite joints [32] or metallic assemblies, as shown in Figure 57. Optimal configuration in terms of transducer localization, size, mode and frequency of interest has been derived as the result of a robust methodology. The efficiency of the system in terms of damage sensitivity, Probability of Detection (PoD) and Probability of Localization (PoL) have been derived successfully. Prognostic algorithms have also been derived and corrected on order to compensate for environmental changes affecting the system [25].

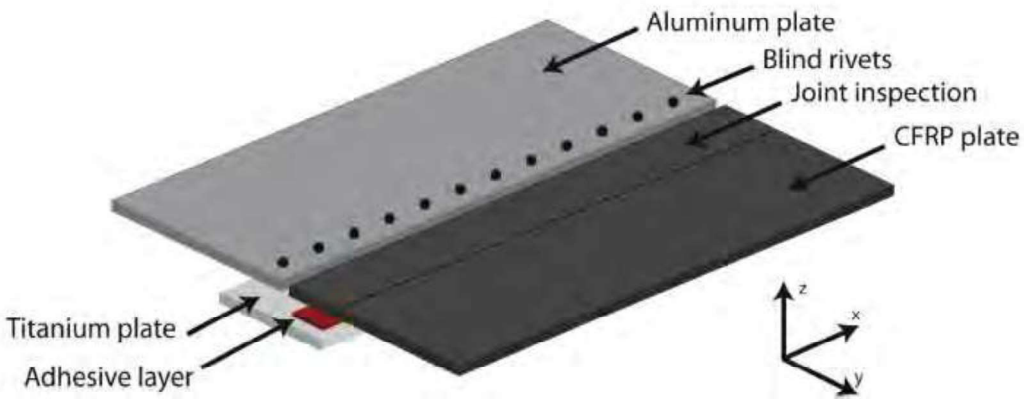

Figure 57 Design methodology [32]

5.3.1 REFERENCES

[23] R. Guitel, N. Quaegebeur, P.-C. Ostiguy, P. Micheau, P. Masson, “Clamped piezoelectric movable transducer for robust and selective guided wave mode generation”, CanSmart/SMN Workshop, Vancouver, BC, July 15-17, 2015.

[24] P.Y. Moghadam, N. Quaegebeur, P. Masson, “Design and optimization of a multi-element piezoelectric transducer for mode-selective generation of guided waves”, Smart Mater. Struct., 25, 075037, 2016.

[25] K.R. Mulligan, N. Quaegebeur, P. Masson, L.-P. Brault, C. Yang, "Compensation of piezoceramic bonding layer degradation for structural health monitoring", Structural Health Monitoring, 13(1), 68-81, 2014.

[26] N. Quaegebeur, P. Masson, "Correlation-based imaging technique using ultrasonic transmit-receive array for Non-Destructive Evaluation", Ultrasonics, 58(2), 1056-1064, 2012.

[27] P.-C. Ostiguy, N. Quaegebeur, P. Masson, "Comparison of model-based damage imaging techniques for transversely isotropic composites ", Structural Health Monitoring, 2016.

[28] N. Quaegebeur, P.-C. Ostiguy, P. Masson, "Hybrid empirical / analytical modeling of guided wave generation by circular piezoceramics", Smart Mater. Struct., 24(3), 035003, 2015.

[29] M. H. Sherafat, N. Quaegebeur, P. Hubert, L. Lessard, P. Masson, «Finite element modelling of Lamb wave propagation in composite stepped joints», J. Reinforced Plastics and Composites, 35(10), 796-806, 2016.

[30] P.-C. Ostiguy, A. Le Duff, N. Quaegebeur, L.-P. Brault, P. Masson, "In-situ characterization technique to increase robustness of imaging approaches in structural health monitoring using guided waves", Structural Health Monitoring, 13(5), 525-536, 2014.

[31] N. Quaegebeur, N. Bouslama, M. Bilodeau, R. Guitel, P. Masson, A. Maslouhi, P. Micheau, "Guided waves scattering by a geometrical feature: application to characterization of fatigue and machined cracks", Ultrasonics, 73, 187-195, 2017.

[32] N. Quaegebeur, P. Micheau, P. Masson, M. Castaings, "Methodology for optimal configuration in structural health monitoring of composite bonded joints", Smart Mater. Struct., 21(10), 105001, 2012.

5.4 PLATFORMS FOR ASSESSING AND VALIDATING STRUCTURAL HEALTH MONITORING AND LOAD MONITORING SYSTEMS TO IMPROVE THEIR TRLS

S. Pant, M. Yanishevsky, D. Backman, NRC Aerospace

Structural Health Monitoring (SHM) sensor and equipment developers most often demonstrate their system capability on simple coupons in a laboratory environment. However, before these SHM systems can be transitioned to service on aircraft, proper evaluation and validation is required to demonstrate their performance capabilities on representative platforms exposed to simulated service loading and environmental conditions. The National Research Council Canada (NRC) has developed several platforms of increasing complexity, shown in Figure 58, ranging from a simple wing plank (platform 1A) all the way to a complete outer wing from the CF-188 (platform 3).

Work this year was focused on the wing box platform (platform 2), which is designed to provide a realistic environmental spectrum with temperature, humidity and pressure extremes to determine the ability of SHM sensors to measure damage under these conditions. A redesign of the upper skin was undertaken on the wing box platform to facilitate entry into the test section of the wing box for both sensor installation and for inspection and measurement of crack growth.

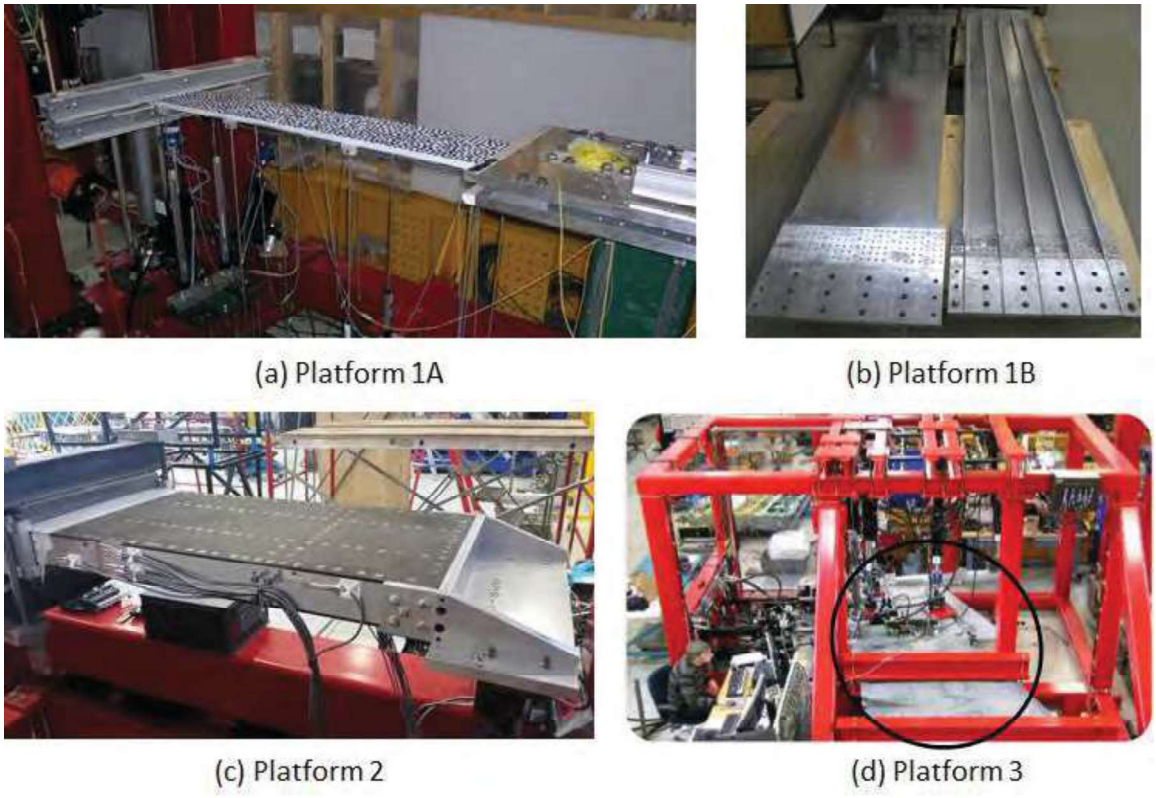

Figure 58 SHM platforms

Additional work was focused on developing algorithms that could be used with acoustic ultrasonic sensors to detect damage. A Damage Response Factor (DRF) was developed consisting of:

1. Correlation Coefficient (CC): scored between 0 and 1 and determining linear dependency, i.e. how close the waves acquired at different cycles were to the baseline.
2. Amplitude Ratio (AR): Absolute maximum amplitude of the current wave divided by the absolute maximum amplitude of the baseline wave. In this case changes are caused by wave attenuation and scattering due to the presence of a growing crack.
3. Energy Ratio (ER): defined as the Current wave energy / Baseline wave energy. The loss of wave energy is due to change in path around the crack.

The Damage Matrix considers all three of the previous outlined parameters in the form of a normalized Euclidean norm as:

$$DRF = \frac{\sqrt{CC^2+ER^2+AR^2}}{\sqrt{3}} \qquad \text{Eq. (1)}$$

Figure 59 shows exemplar data from the fatigue testing of the replaceable C-channel to be used within the wing box. The acoustic ultrasonic (AU) data was processed using the DRF algorithm. For the damage detection algorithm, the average DRF should be less than the threshold value, where 0.9 was selected based on a ~1 mm measured crack. This first criterion was met at 20,000 cycles and higher, where the average DRF was below the threshold value. The next step in analyzing the data was to determine where the lowest excitation frequency DRF was greater than the Upper bound (upper error bar) and the highest excitation frequency DRF was less than the Lower bound (lower error bar). This criterion was not met at 20,000 cycles, as the lower DRF corresponding to 50 kHz was still lower than the upper bound and the highest DRF corresponding to 200 kHz was still higher than the lower bound. The criterion was met at 43,000 cycles, where the lowest frequency DRF > upper bound and the highest frequency DRF < lower bound thus suggesting that crack propagation had commenced.

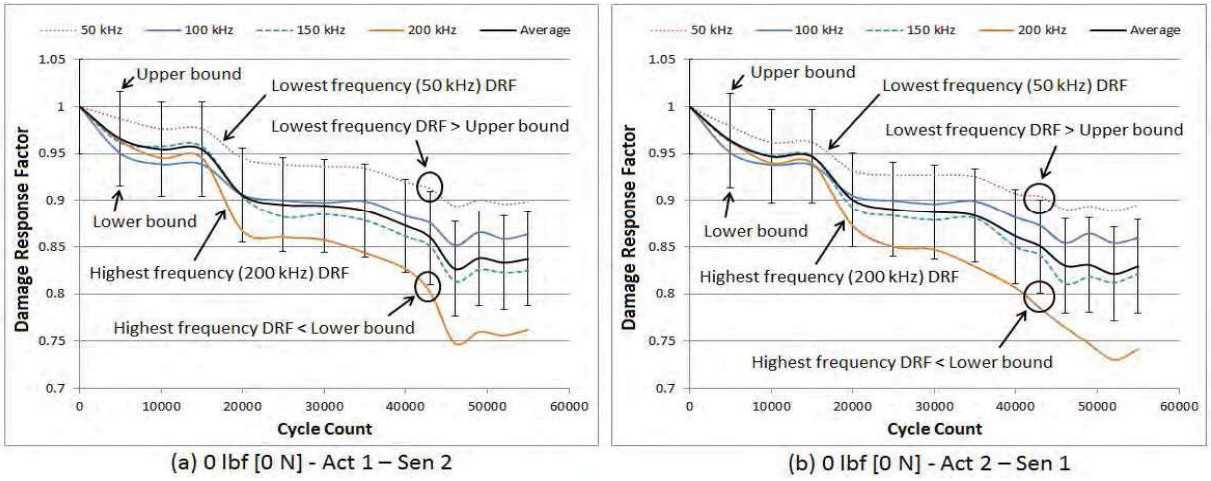

Figure 59 Sample analysis using the damage matrix algorithm

Additional work next year will be focused on verifying the effectiveness of the DRF algorithm to detect crack growth.

5.4.1 REFERENCES

[33] Shashank Pant, Marko Yanishevsky, Marcias Martinez and David Backman, "*Fatigue crack detection using load-enhanced multi-frequency guided wave technique*", Holistic Structural Integrity Process (HOLSIP) HOLSIP 16 Conference, Snowbird Utah.

[34] Shashank Pant and Robert S. Rutledge, "Potential Damage Location Indication Determined Using Acoustic Emission During CF-188 Aileron Fatigue Test", NRC Internal Report, LTR-SMM-2017-0002.

[35] Shashank Pant, Marko Yanishevsky and David Backman , "*Platforms for assessing and validating structural health monitoring and load monitoring systems to improve their TRLs*", 27th International Conference on Adaptive Structures and Technologies (ICAST).

5.5 NUMERICAL MODELLING FOR STRUCTURAL HEALTH MONITORING RESEARCH

Shashank Pant (NRC), Marko Yanishevsky (NRC), David Backman (NRC) and Marcias Martinez (Clarkson University)

Original Equipment Manufacturers (OEM), aircraft operators, and researchers are actively working on monitoring the health of aircraft structures utilizing Structural Health Monitoring (SHM) systems that make use of integrated/bonded sensors. These on-board sensors can be used to detect and identify damage evolution in structures, in order to assist structural engineers in their assessment of the structural integrity throughout the aircraft lifecycle. Before these SHM systems can be installed in an aircraft, the systems should be able to detect damage exceeding a prescribed threshold set by the established Probability of Detection (PoD) curves at a confidence level traditionally used by Non Destructive Evaluation (NDE) techniques. PoD methodologies for NDE techniques are well established, which is not the case for SHM. Some of the SHM techniques, for example, Acoustic Emission (AE) provide damage location but do not provide a damage size as a result of its analysis; hence, there is an inherent challenge in providing a PoD curve for a system that does not produce an estimate of damage size as an output. Other techniques, such as guided Lamb waves, infer the size of the damage as a function of change compared to a baseline signal; therefore, creating an opportunity for the development of PoD curves.

Lamb waves are ultrasonic guided waves that propagate between two parallel free surfaces. These waves co-exist in two modes - symmetric and anti-symmetric and propagate independently of each other. The use of guided Lamb waves for damage detection has been widely explored and demonstrated. It is well known that diffraction, scattering, and mode conversion of Lamb waves occurs due to the presence of damage. Damage in materials/structures can therefore be detected by analyzing the difference between the damaged versus the undamaged (baseline) state of the specimen, through a change in amplitude, energy, frequency, velocity, and phase shift of the wave signals.

Experimental assessment of SHM systems to generate a PoD curve can be extremely costly, requiring different structural components with varying damage sizes to be evaluated. To reduce this cost, Model Assisted PoD (MAPoD), has been proposed, which uses numerical models to minimize the need for experimental results. In order to apply the MAPoD approach, first a simple yet robust numerical model needs to be developed by minimizing the error between the numerical and the experimental models tested in laboratory coupons. Once proven in a simple structure, the numerical model can then be incrementally tested on structure with increasing complexity and can be used to simulate a wide range of damage, which cannot all be experimentally evaluated. The model can then be used to observe the sensitivity of the signal received with respect to the sensor position and varying damage sizes for evaluating sensor

placement, as well as selecting proper excitation frequencies. The numerical model can also be included as part of the Digital Twin framework being developed, which requires the development of modelling techniques that mimic the state and presence of damage as it is found in an aircraft. The overall goal of this research was to determine if the numerical simulations can match those of the experimental guided Lamb wave behaviour in a C-Channel type structure with the presence of a fatigue crack.

A C-channel type structure, shown in Figure 60, was analyzed both experimentally and numerically to observe how the presence of a 2.1 mm fatigue crack emanating from a 3.2 mm diameter hole with a 0.4 mm saw-cut starter notch affects guided wave propagation behaviour. Piezoelectric sensors, examples of which are shown in Figure 61, were utilized to generate and capture a series of 50 kHz and 200 kHz Hanning windowed signals to evaluate the presence of damage along each sensor path.

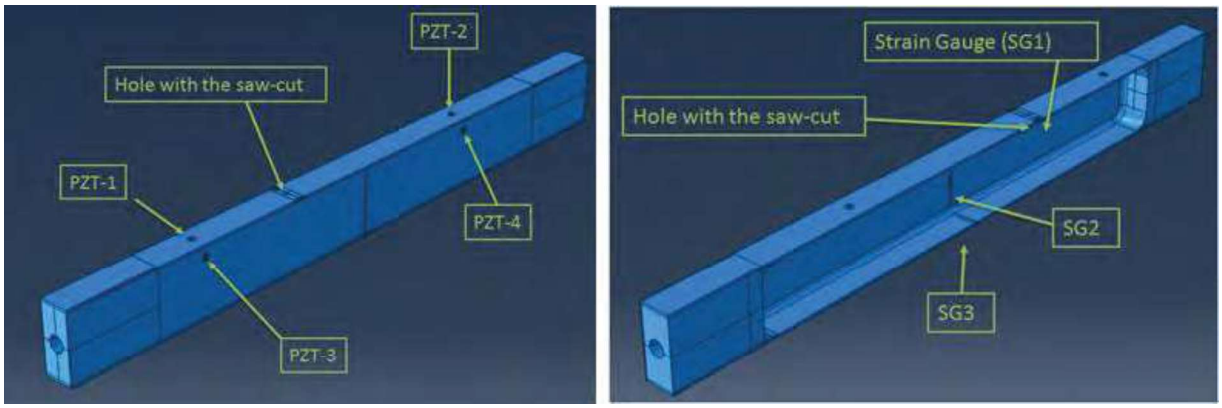

Figure 60 Numerical model of the C-Channel

The numerical data was initially compared against the experimental data for the 0.4 mm saw-cut at zero cycles; where the arrival of the So and the Ao waves were captured by both. The time of arrival of these wave packets (group velocity) were extracted by fitting a Morlet Wavelet at a central frequency of 50 kHz and 200 kHz. For the arrival of the Ao wave, the error was found to be 0.01 milliseconds for waves captured for the 50 kHz wave, and less than 0.005 ms for the 200 kHz wave. However, using the Morlet Wavlet, the arrival time of the So wave could not be extracted for the 50 kHz wave and an error of 0.004 ms was found for the 200 kHz wave. A similar trend was also found when the numerical data was compared against the experimental data for 2.1 mm crack at 55306 cycles. This proves that the numerical model was able to accurately model the time of arrival of both the Ao and So waves excited at 50 kHz and 200 kHz, as shown in Figure 62.

Overall, it was concluded that the numerical model developed in this work was able to reproduce the reduction in the wave amplitude in the presence of a 2.1 mm crack for 200 kHz. The model needs to be further refined by analyzing the effect of residual stresses around the crack-tip and its

effect on the propagating waves. It was also found that there was a shift in the wave depending on which PZT node was chosen for comparison. In this work, only the average of these PZT nodes were taken; however, the actual charge distribution and how it affects the signal from the PZT sensor needs further attention to improve this model.

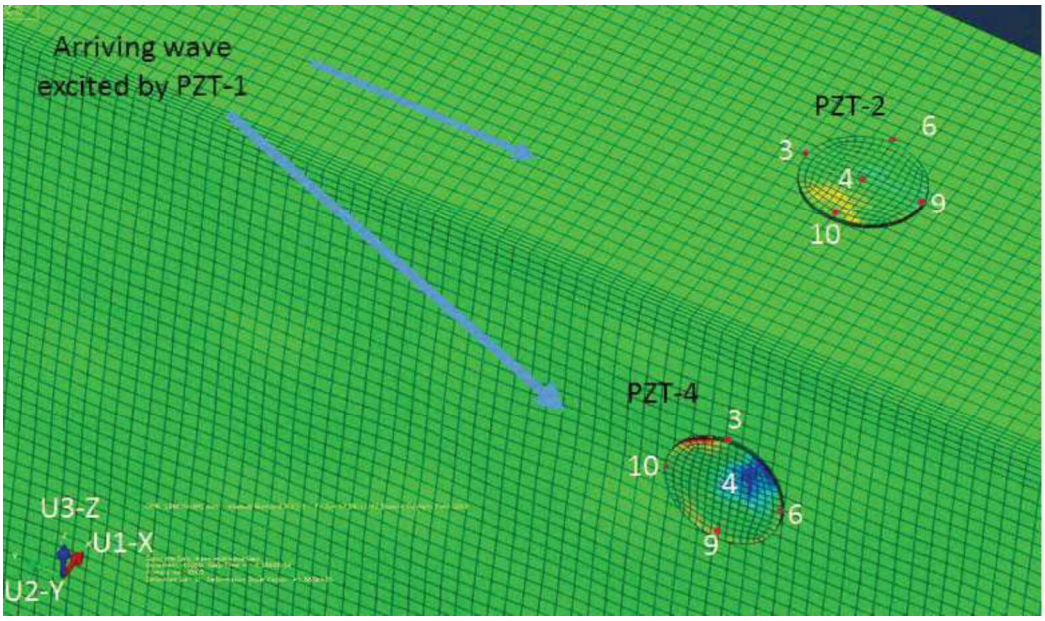

Figure 61 Arriving wave from PZT-1 along with the node numbering of PZT-2 and PZT-4

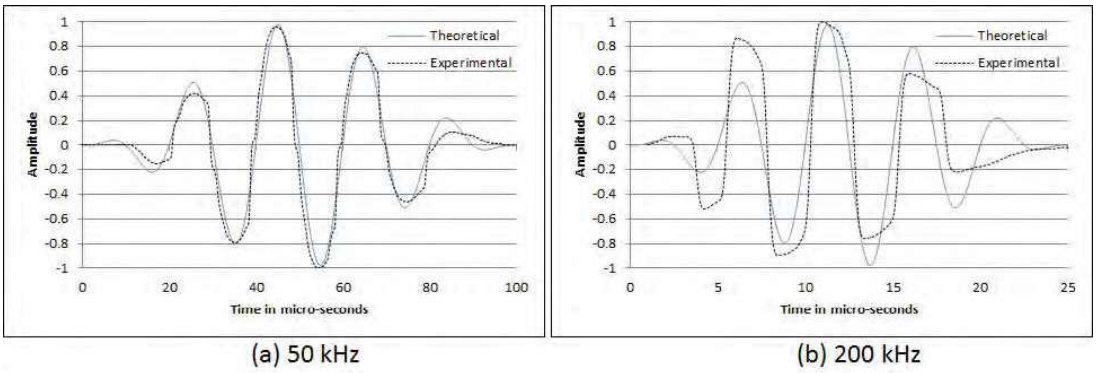

Figure 62 Comparison of theoretical versus experimental wave propagation results

5.5.1 REFERENCES

[36] M. Martinez, S. Pant, J. Ocampo, M. Yanishevsky and D. Backman, "Effects of Residual Stress Fields of a Closed Crack on Lamb Wave Propagation", Holistic Structural Integrity Process (HOLSIP) HOLSIP 16 Conference, Snowbird Utah.

[37] M. B. Romero, D. Gagar, S. Pant and M. Martinez Clarkson, USA, "Study of complex geometrical effects on acoustic emission based SHM system for improvement in time-of-arrival extraction technique", The 27th International Conference on Adaptive Structures, Bolton, NY. October 2016.

[38] S. Pant, M. Martinez, M. Yanishevsky, D. Backman, Finite Element Modelling and Analysis of Guided Wave Propagation in a C-Channel type Aerospace Structure with Fatigue Crack Damage, NRC Internal Report LTR-SMM-2017-0053.

5.6 EXPERIMENTING CAPACITIVE SENSING TECHNIQUE FOR STRUCTURAL INTEGRITY ASSESSMENT

Zheng Liu, School of Engineering, Faculty of Applied Science, University of British Columbia, Okanagan, Kelowna, British Columbia, Canada

This paper presents the experimental results of capacitive imaging sensors for structural integrity assessment. The capacitive sensor is based on the measurement of capacitance change due to the anomaly or discontinuity in structures and materials. A number of sensor prototypes, shown in Figure 63, are investigated in the study. The observation of the scanned image of an aluminium plate, shown in Figure 64 and Figure 65, a carbon fiber plate, shown in Figure 66, and ductile iron pipe segments, is summarized in this paper. The use of capacitive imaging technique for structure integrity assessment is explored in this study. The preliminary results demonstrate the effectiveness of this technique for different materials and structures, as shown in Figure 67. Because the capacitive imaging technology has the potential to be used in the field, further research and development is to enhance its effectiveness. The next phase will focus on improving the sensor design, identifying optimal operational parameters, and automating the signal processing to enable rapid in-situ detection and quantification of anomaly or discontinuity, such as the pitting corrosion on buried pipes, without the need for cleaning and sandblasting. Future research will consider applying signal/image processing techniques to quantitatively characterize the anomaly or discontinuity for a more comprehensive assessment of structural integrity in varied applications.

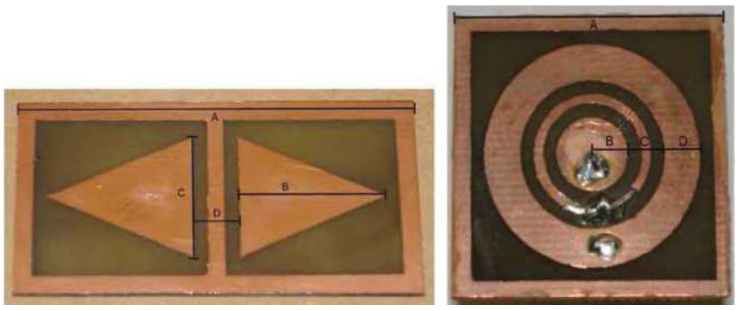

Figure 63 Two different types of configurations of capacitive sensor

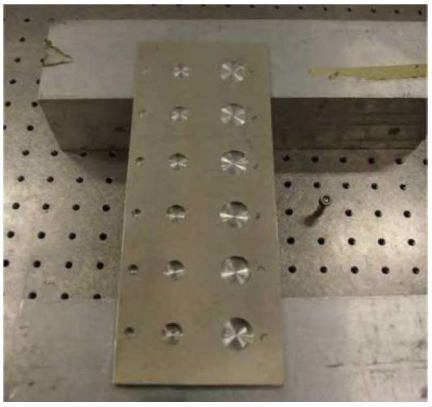

Figure 64 Aluminium plate (7075-T6) used in the experiments

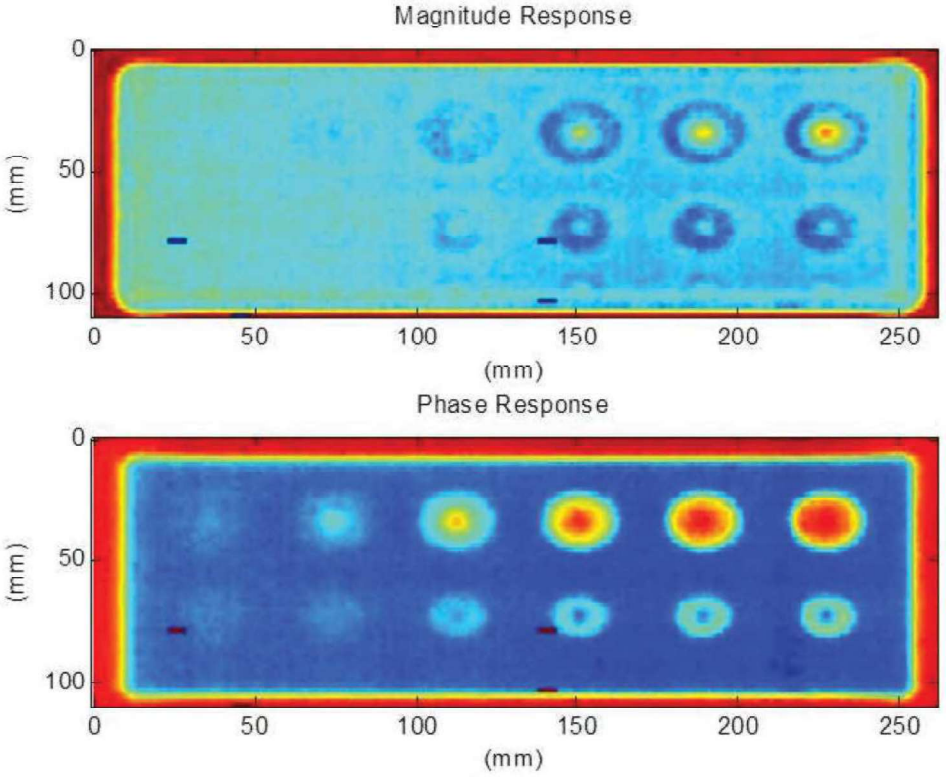

Figure 65 Aluminium plate inspection result with sensor 6

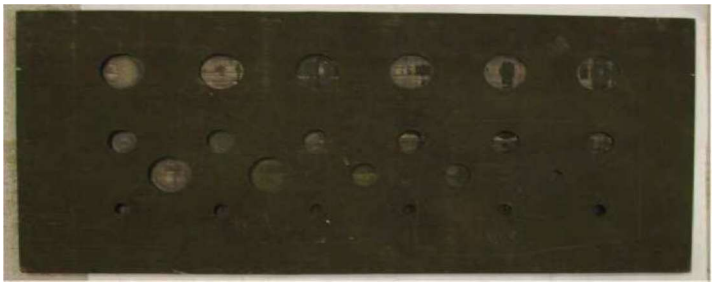

Figure 66 The carbon fiber plate.

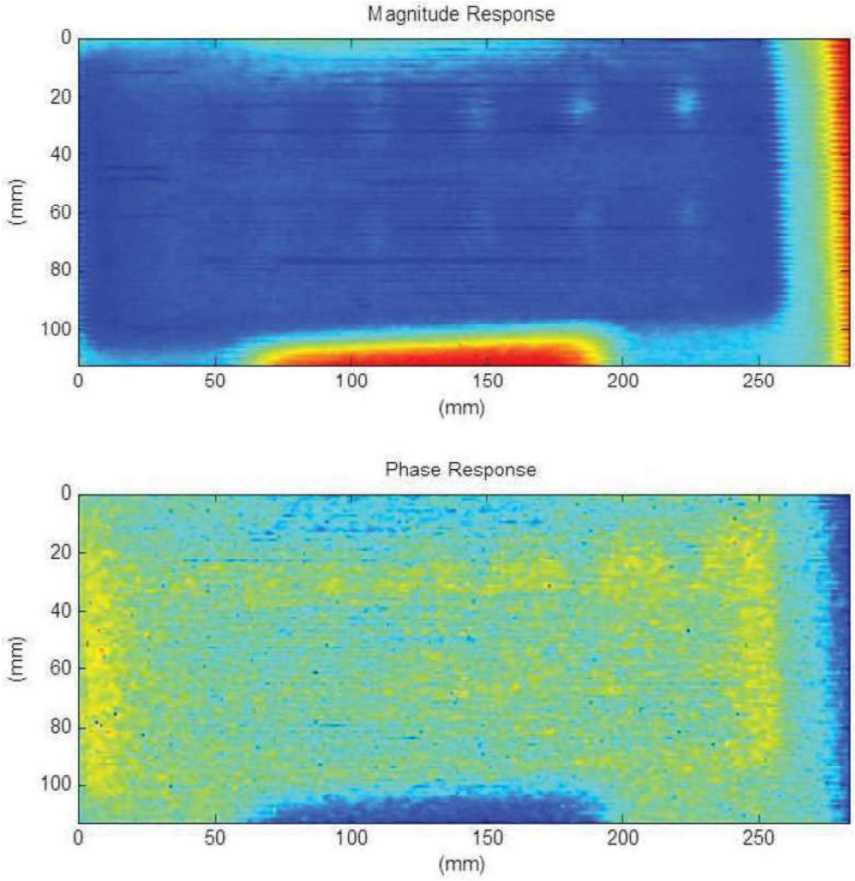

Figure 67 Result with sensor 7 at frequency 20 kHz

5.6.1 REFERENCES

[39] Zheng Li and Huang Liu Experimenting Capacitive Sensing Technique for Structural Integrity Assessment, 18th Annual International Conference on Industrial Technology, March 22-25, 2017, Toronto, Canada.

6.0 NON-DESTRUCTIVE EVALUATION

6.1 QUALIFICATION OF COMPUTED RADIOGRAPHY FOR AEROSPACE APPLICATIONS

Muzibur Khan, NRC Aerospace

Industrial radiography is a very mature non-destructive testing (NDT) technique for volumetric investigation. Radiography is based on the differential absorption of penetrating electromagnetic radiation of very short wavelength. Aircraft structures tend to be light and less dense, which favour radiation penetration and provide high throughput in inspection and insensitivity to variations existent in composite and metal structure. Therefore radiography is one of the most important tools for aircraft maintenance, which can effectively detect different kind of defects and anomalies such as: water ingress in honeycomb structure, core damage, foreign object damage (FOD), defects in weld and casting, as well as cracks and corrosion in aircraft windows, wings and fuselage.

Currently used film-based radiography requires consumables (films, toxic chemicals and proper disposal of chemical waste), darkroom facilities and manual processing. The process which is not only time consuming, but also generates more radiation than digital systems. Use of film for NDT applications is therefore gradually diminishing primarily because of reduced time and long term cost and the potential benefits from digital radiography. Industrial radiographic inspection is making an intense effort to replace the conventional film technique with digital technologies (Digital Radiography or Computed Radiography (CR)). CR uses a reusable phosphor imaging plate (IP) instead of a film and therefore, allows faster/easier image acquisition digitally. Despite numerous benefits when compared to conventional film, its widespread application still poses significant challenges (e.g. acquisition cost, steep learning curve, lack of procedures to choose parameters, lack of demonstrated system performance, imaging artifacts, etc.). Before replacing film-based inspection procedures with CR, detailed assessment of the reliability of the new technology, including qualification and validation of CR systems are required to determine if whether they effectively provide equal or better performance than existing film based technology and to ensure that the inspection system performance would still be capable of meeting the inspection requirements under all possible variations of identified parameters. The National Research Council Canada (NRC) has been tasked by the Royal Canadian Air Force (RCAF) to develop documentation and protocols for the qualification of Computed Radiography.

The major CR system quality parameters such as spatial resolution, contrast sensitivity, contrast-to-noise ratio (CNR), signal-to-noise ratio (SNR), Equivalent Penetrameter Sensitivity (EPS) as well as other system quality parameters were being measured as part of qualification processes and assessing suitability of CR for aerospace applications. These are shown in Figure 68. Spatial resolution is one of the key parameters required to measure for initial qualification, subsequent monitoring and being measured by Duplex Wire Image Quality Indicator (IQI) as well as using

the Line Pair Gauge method. Signal-to-noise ratio (SNR) is interpreted as a ratio of the mean value of the signal intensity and depends on the radiation exposure dose, X-ray photon fluctuation, analog/digital conversion and system hardware properties.


CR System at NRC

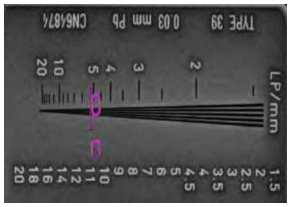

Resolution (Line Pair Gauge)

Resolution (Line Pair Gauge)

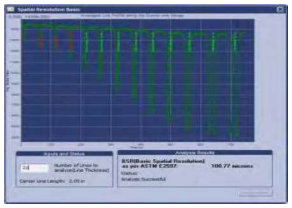
Spatial Resolution (Duplex Wire)

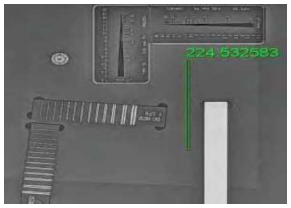
Signal-to-Noise Ratio (SNR)

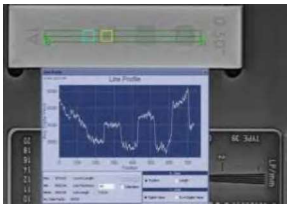
Contrast Sensitivity


Contrast-to-Noise Ratio (CNR)

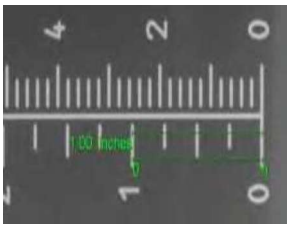
Geometric Distortion

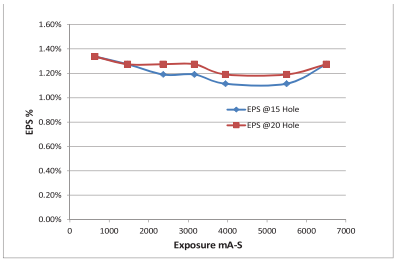

EPS

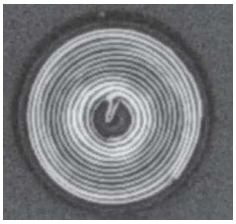
Central Beam Alignment

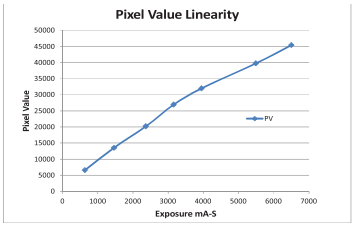

PV Linearity

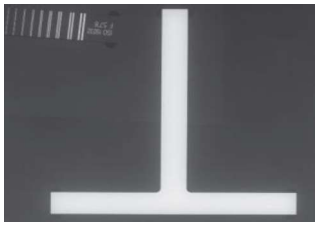
Blooming or Flare

Figure 68 CR system performance evaluation at NRC

Contrast sensitivity measures the system ability to detect variations in image intensity caused by very small changes in object thickness/density due to anomalies such as cracks, substructure features, entrapped water, FOD, voids, etc. Contrast-to-noise (CNR) is defined as the ratio of the difference of signal intensities of two regions of interest to the background noise. The Equivalent Penetrameter Sensitivity (EPS) defined the value that allows relating a discernible hole size of the IQI thickness with the specimen thickness being radiographed and this information is useful for establishing the overall image quality equivalency of a system and developing an optimized exposure range.

There are several other parameters that were also evaluated as part of qualification process. Shading or pixel uniformity testing consists of non-uniform pixel values perpendicular to the IP transport direction, which may also be caused by improper alignment of the light guide or photomultiplier tube assembly. Central Beam Alignment Testing verifies that the radiation beam aligned perpendicular to the quality indicator (BAM-Snail) and resulted in image consists of a regularly spaced spiral. Scanner slippage is the slipping of an IP in a scanner transport system, resulting in the fluctuation of intensity of horizontal image lines. The laser jitter test evaluates the horizontal and vertical performance (scan line integrity and scan line drop out) of the laser optics and transport systems of the CR reader, and determines whether the mechanical motion of the image plate, laser, and optics are consistent.

The next steps of the on-going qualification process are to develop process control and standard operating procedures to ensure a high degree of repeatability of CR-based radiographic inspection results.

6.2 TECHNICAL JUSTIFICATION OF ULTRASONIC INSPECTION PROCEDURE FOR HELICOPTER COMPONENTS

Muzibur Khan, NRC Aerospace

Damage tolerance analysis of aircraft components and structures requires the information of detectable discontinuity size (a_{NDI}) for a non-destructive inspection (NDI) technique to determine safe inspection intervals. In some cases these values are assumed based on engineering judgement, in other cases there are opportunities to quantify the minimum detectable discontinuity size, which would lead to increasing inspection intervals and increasing margins for repair. However, the required a_{NDI} data for all NDI procedures are often neither available nor is there the required time or resources to carry out full POD studies. For a helicopter component, driven by the needs for an alternative approach of establishing minimum detectable discontinuity sizes using an ultrasonic pulse-echo inspection procedure, a project was undertaken to meet such objectives. Inspection qualification through technical justification (TJ), appeared to be the promising approach and therefore selected for demonstrating reliability of the selected ultrasonic NDI procedure.

The performance of the inspection system is necessary to assure that it is capable of achieving the expected results under real examination conditions and that the proposed inspection will achieve what is required. This process is named *inspection qualification* and also known as NDT performance demonstration, a systematic process by which the application of an NDT procedure is shown to meet the requirements of the objectives stated in the inspection specification.

Qualification of inspections is intended to provide confidence, by direct demonstration, that the specific non-destructive test is capable of attaining its objectives.

The two major elements of inspection qualification are the technical justification and practical assessment. TJ plays an important role in the qualification of non-destructive evaluations recommend by European Network for Inspection and Qualification (ENIQ). The primary focus of this study is to provide a basis for justification and demonstrate that the selected ultrasonic inspection procedure and associated equipment is adequate for reducing the minimum detectable discontinuity size of helicopter components without compromising the current level of confidence.

The processes involved in the TJ processes are shown in Figure 69. Influential parameters provide information, which can potentially influence the performance and outcome of the inspection system. The component to be inspected, inspection equipment and ultrasonic probe were the three factors that influence the selected ultrasonic procedure. The essential parameters are a subset of influential parameters, whose change in value would actually affect a particular inspection in such a way, that the inspection can no longer meet its defined objectives. The essential parameters and their tolerances or ranges were identified for this study.

While physical reasoning can be used to justify the choice of some ultrasonic inspection parameters (e.g. transducer frequency, equipment, transducer angle, wave mode etc.), model and experimental can provide more quantitative information. Simulations were used to determine the parameters influence on ultrasonic examination. Modelling in this study demonstrated that the skew of the discontinuity, sample thickness and variation of probe positioning are essential parameters.

In this work, experimental evidence relevant to angle beam ultrasonic inspection is provided. The achievement of inspection objectives using the given procedure is confirmed, and weakness identified. This work also discussed limitation in performance and of objectives of inspection using the given procedure, and then presented recommendations to improve the inspection procedure/system, design of test pieces, personnel qualification etc.

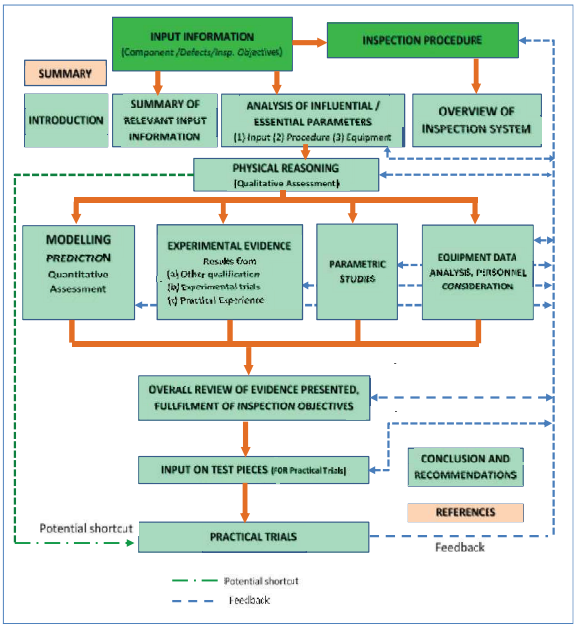

Technical justification framework and their inter-relationship

Inspection Geometry of UT Procedure

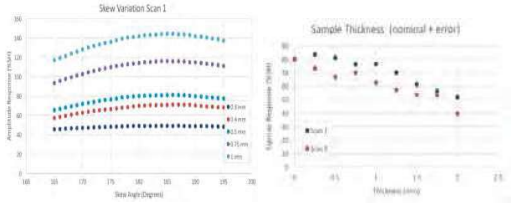

CIVA Modelling Result

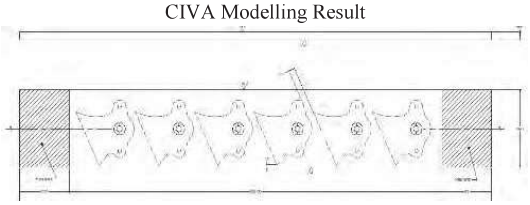

Test Trial Specimen Design

Figure 69 Technical justification of ultrasonic inspection

6.2.1 REFERENCES

[40] Khan, M., "Review of Approaches for Cost-effective Estimation of Reliability of Nondestructive Inspection Procedures, NRC Technical Report, LTR-SMM-2015-0398, February 2015.

[41] Khan, M, "Technical Justification of Ultrasonic Inspection Procedure for Upper Tail-cone Assembly (Interim Report), NRC Technical Report, LTR-SMM-2016-0040, November 2016.

6.3 NUMERICAL SIMULATION OF INDUCTION THERMOGRAPHY ON A LAMINATED COMPOSITE PANEL

Gang Li, M. Genest, NRC Aerospace

The thermography technique is less sensitive to crack orientation or part geometry than typical eddy current inspections, and has potential to improve the inspection speed and ease the flaw detection in complex geometries with the aid of infrared cameras. A 3D finite element (FE) model was developed using the COMSOL multiphysics software version 5.1 for simulating induction heating of an anisotropic laminated composite panel. The FE model, consisting of: air, laminated panel, coil, and water, is shown in Figure 70. The equivalent electrical and thermal

conductivities are determined based on the layup condition of the laminated composite panels. Comparisons of the test and numerical results for a pristine panel and a specific flawed panel are shown in Figure 71 and Figure 72. The shape of the heated area obtained from simulation was slightly different from the test results, which was due to the fact that the first loop of the experimental coil was almost parallel to the panel surface, whereas the loops of the numerical model were parallel to each other (constant angle) with a fixed axial pitch and hence, a nearly identical distance to the panel surface could not be ensured. The model was applied to analyze the temperature distribution in a flawed panel under different scenarios. Several representative flaw scenarios in the composite panel were studied; a case is shown in Figure 72. The developed numerical capability supports the development of new inspection techniques for practical damage detection in aircraft structures using induction thermography.

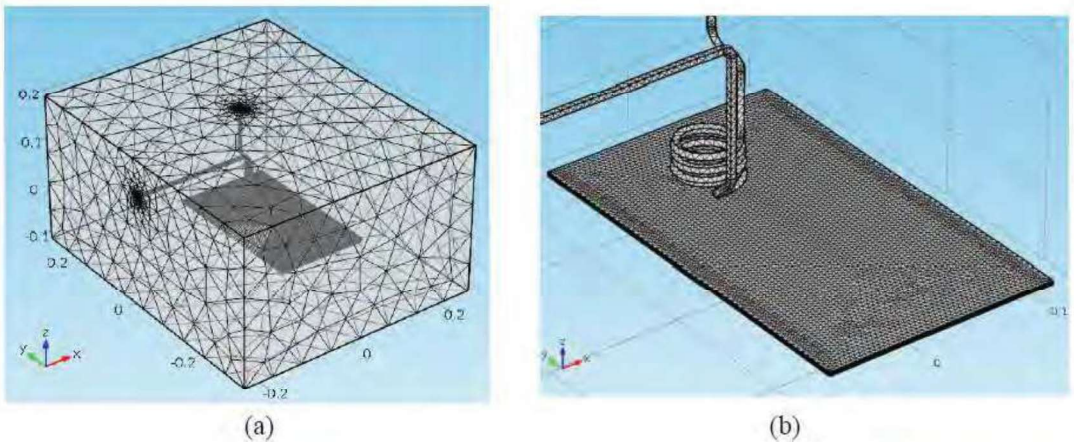

Figure 70 The three-dimensional FE model for induction heating of a laminated composite panel, where (a) is the meshed model with 280425 elements and (b) is for a close-view of the composite panel and coil.

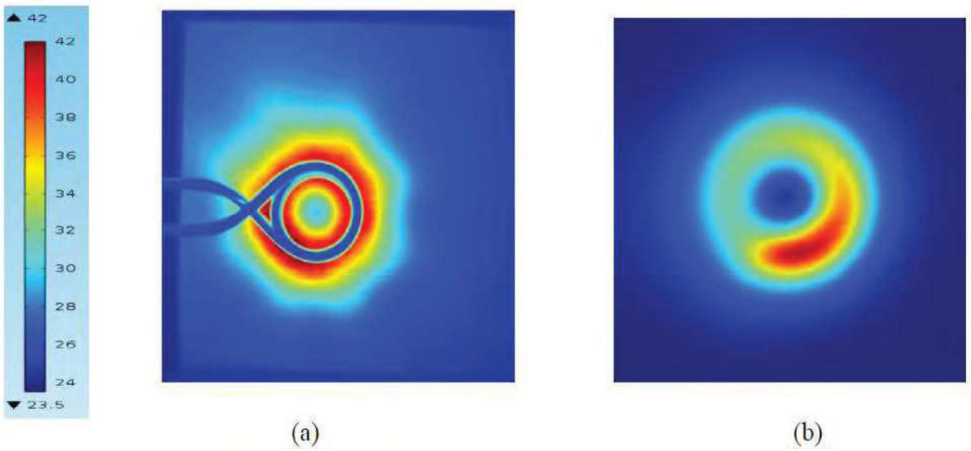

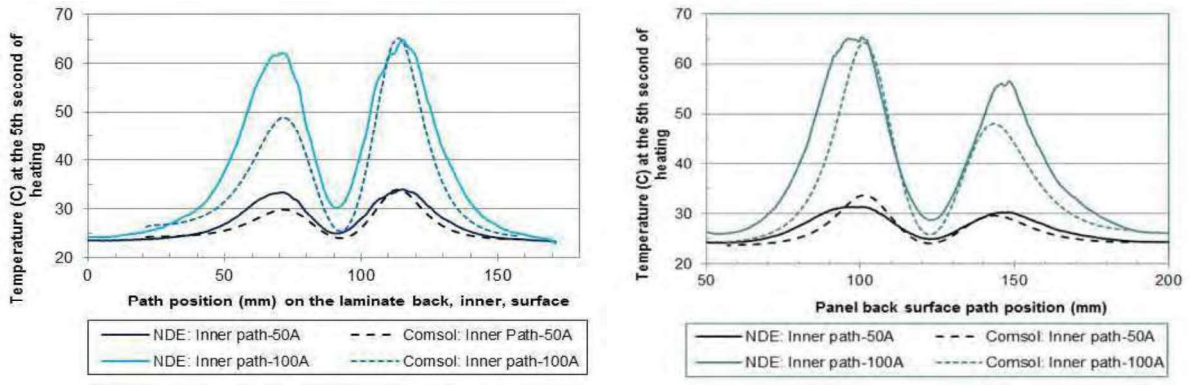

(c) A pristine panel (d) A flawed panel

Figure 71 Full-field temperature contours on the panel outer surface obtained from: (a) experimental, and (b) numerical methods; and path temperature comparisons of a pristine (c) and a flawed panel, and (d) using a 50 A current after 5 second heating

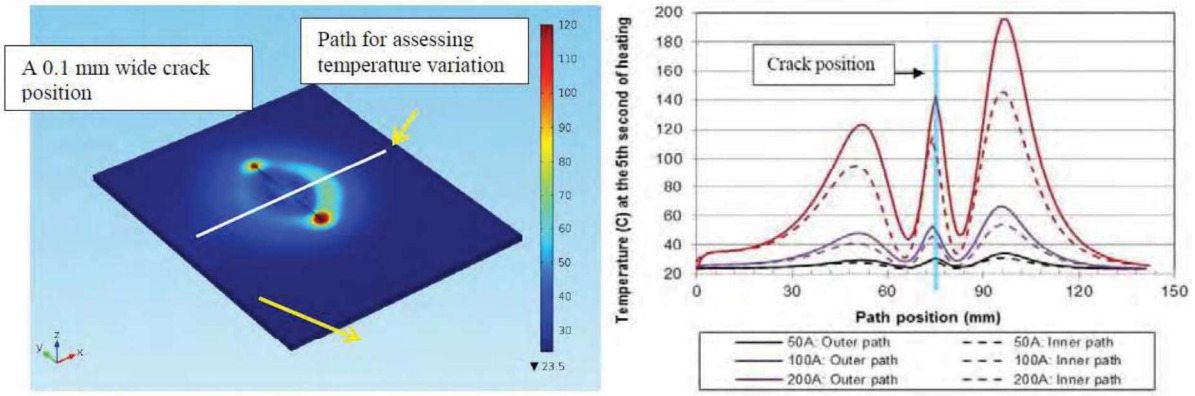

(a) (b)

Figure 72 Numerical results (a) the full-field temperature contours and (b) temperature profiles along the surface path at the 5th heating second obtained from the coil positioned 4 mm from the outer surface, and supplied with 50 A, 100 A, and 200 A currents at 300 kHz

6.3.1 REFERENCES

[42] Li G, Genest M, Numerical simulation of induction thermography on a laminated composite Panel, American Society for Composites 31st Technical Conference, Williamsburg, USA, 2016

6.4 THREE-DIMENSIONAL NUMERICAL MODELLING OF INDUCTION THERMOGRAPHY ON METALLIC PANELS

Gang Li, M. Genest, NRC Aerospace

Three-dimensional (3D) finite element models were developed to simulate induction heating of aluminium material, shown in Figure 73. An induction heating system with a 3-turn circular and a straight hollow coil system positioned in front of an aluminium alloy panel surface was modelled. As can be seen in Figure 74, good agreement in temperature profile and distribution was achieved between the experimental and numerical results for both pristine and EDM notched panels. Results show that the coil should be positioned no further than 10 mm away from the aluminium workpiece surface to obtain meaningful heating capability. The numerical model shows that as the crack width reduces, the amount of heat generated at the crack tip is also reduced, and thus could explain why experimental results did not show any temperature increase at the crack tip. Temperature increases generated by the looped coil are higher than those of a straight coil for similar crack/notch width. From the experiments and model, the 4mm width EDM notches using a straight coil generated a temperature increase around 0.1°C, which is likely close to the detection capability of the infrared camera used. The numerical methodology was used to further study the effect of flaws on the generated temperature profile. It was found that: (i) identical temperature variations are found at panel coil side and back surface of pristine panel; and (ii) the temperature variation on the panel coil side surface can be considerably increased by the presence of damage, which is not seen from the back panel. The study suggests that the temperature variation for potential flaw detection is better measured from the coil side surface. The analysis provides a reference for supporting practical NDE thermography applications in the damage detection and confirms that the experiments should be performed in reflection mode, i.e. with the infrared camera located on the same side as the induction coil. The modelling of various metallic materials suggests that further study on induction thermography should focus on Inconel and Titanium components, as it should be more sensitive to flaws in those materials, as shown in Figure 75.

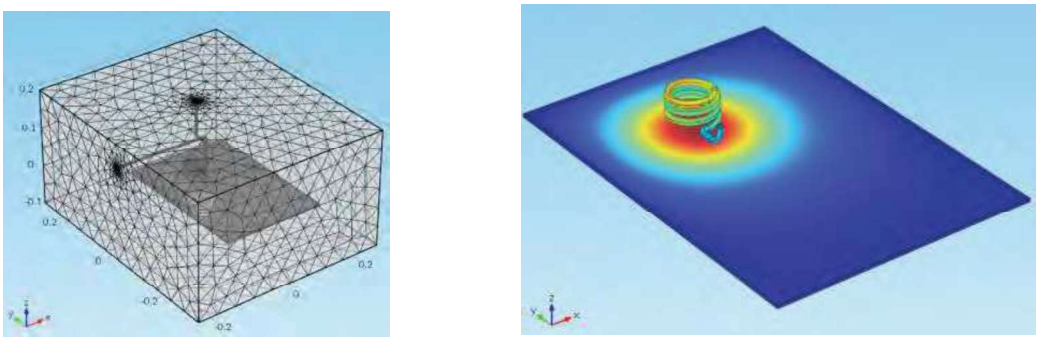

(a) (b)

Figure 73 Three-dimensional multiphysics modelling information for (a) a 3D model , (b) full-field temperatuture contours induced for an aluminium panel

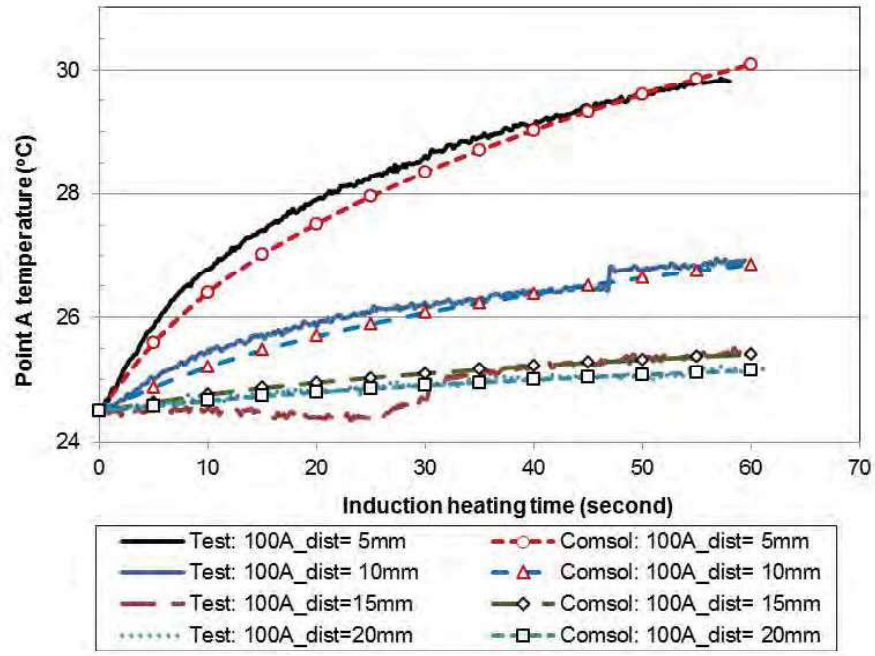

Figure 74 Comparison of temperature variations at a point on the panel inner surface

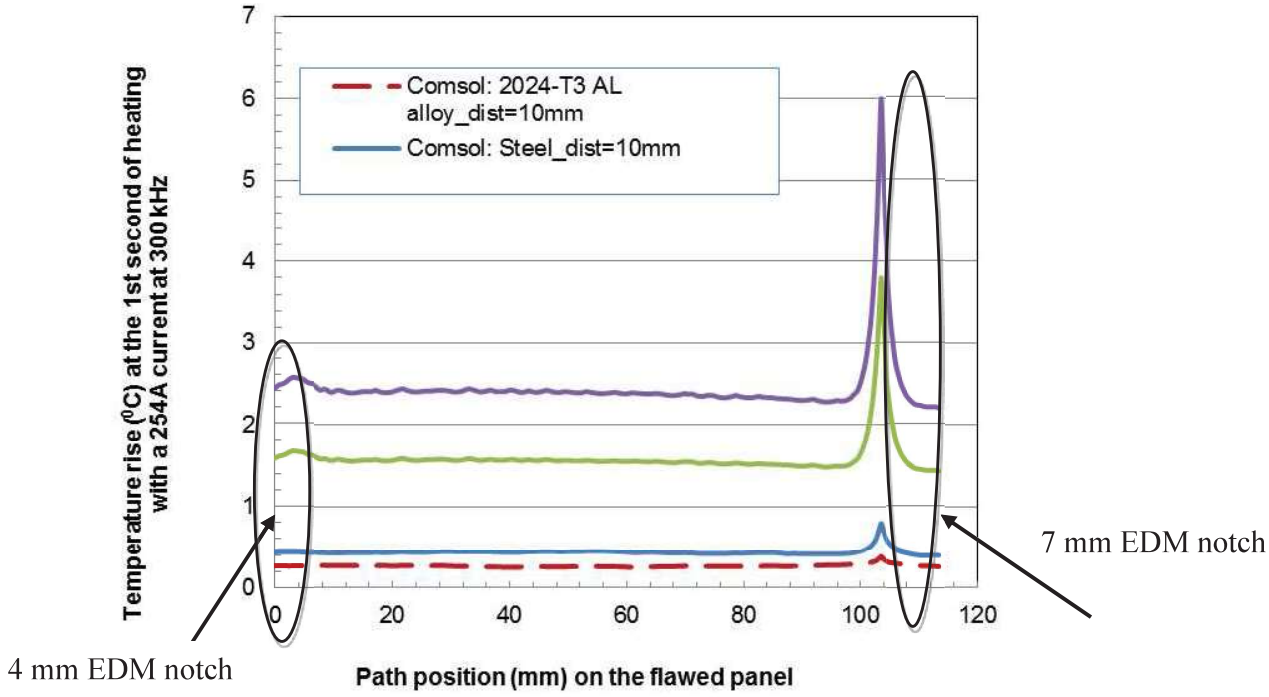

Figure 75 Temperature comparison obtained from model with the straight coil placed 10 mm above the panel surface for various metallic materials

6.4.1 REFERENCES

[43] G. Li, M. Genest, "Two-Dimensional Finite Element Simulation of Induction Thermography of an Aluminium Alloy Panel", Canadian Aeronautics and Space Institute AERO'15 Conference 23rd CASI Aerospace Structures and Materials Symposium, May 19-21, 2015, Montreal, QC.

[44] M. Genest, G. Li, "Inspection of Aircraft Parts by Induction Thermography", NDT in Canada 2015, June 15-17, Edmonton, AB.

[45] Gang Li and Marc Genest, "Numerical Simulation of Induction Thermography on a Laminated Composite Panel", American Society for Composites 31 Technical Conference and ASTM Committee D30, September 19-22, 2016. Williamsburg, VA.

[46] Gang Li, Marc Genest, "Three-Dimensional Numerical Modelling of Induction Thermography on Metallic Panels", CPR-SMM-2016-0059, NDT in Canada, Nov 15-18, Burlington, ON.

6.5 MODEL-ASSISTED PROBABILITY OF DETECTION ASSESSMENT FOR AIRCRAFT ENGINE COMPONENTS

Muzibur Khan, NRC Aerospace

Most military and civilian aircraft engines are currently designed and operated under the "safe life" philosophy for their critical components, which mostly rely on deterministic fracture mechanics. The reliability and integrity of the engine designed in this way have been achieved through analytical modelling and experience from engine and components rig tests. However, experience demonstrates that there is a very low probability (1/1000) of component failure due to fatigue. It has been estimated that some engine components (ex. engine discs) lifetime determined using the safe life philosophy still have some useful remaining life at retirement. Damage tolerance-based maintenance is an alternative supplemental promising life management philosophy. Damage tolerant design provides second line of defence against premature fracture. Damage Tolerance (DT) implies "the ability of the engine to resist failure due to the presence of flaws, cracks, or other damage, for a specified period of unrepaired usage". Also known as safety-by-inspection (SBI), recognizes the potential for the existence of a defect in all critical components, but ensures the ability of the engine to resist failure for a specified period of time until the defect is detected during routine non-destructive inspection.

Damage tolerant design and non-destructive inspection are key tasks for ensuring aircraft airworthiness. Damage tolerance is the ability to resist fracture from pre-existent damage for a given period of time and is an essential attribute of components whose failure could result in catastrophic loss of life or property. Non-destructive inspection (NDI) results need to be reliable and quantifiable in terms of Probability of Detection (PoD), in order to apply damage tolerance to the engine components. The PoD curve determined based on empirical non-destructive investigations of parts is time, energy and cost demanding. Model- assisted PoD (MAPoD) is an

emerging concept whose purpose is to reduce, but not eliminate the need for empirical inspections. In this way, significant time and capital resources necessary for empirical POD are considerably reduced. In the absence of fatigue cracks, MAPoD uses either simulated damage, such as electrically discharged machining (EDM) notches instead of fatigue cracks, or numerically-simulated signals.

A project on MAPoD was undertaken aimed to demonstrate the MAPoD concepts for estimating the PoD for aircraft engine components. The goal of the project was the potential transition of the life management of engine components from the current safe-life to a damage tolerant approach. The targeted component was the second stage turbine disc of the Rolls-Royce T56 engine. Set of EDM and end thermal fatigue cracks coupons were manufactured with a flaw located at the middle and the edge of a grove simulating the geometry of a disc fir tree slot, as shown in Figure 76.

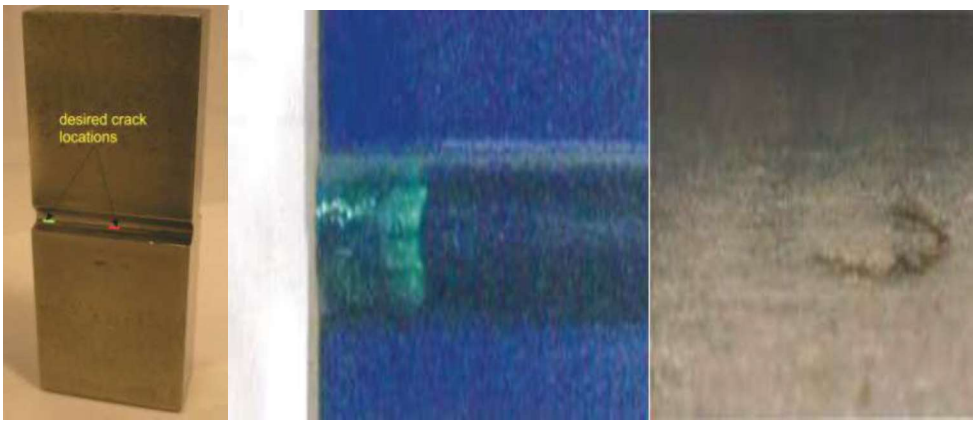

Specimen

Thermal Fatigue Crack
(Penetrant & Microscopic Image)

Figure 76 Manufacture of the cracked coupons

Crack often occurs in high stressed regions near the slot edges of turbine disc. However, during eddy current inspection contribution of nearby edge signals mask the crack contribution. The influence of the edge is more prominent when probe is closer to the edge and at some point the crack signal is fully replaced by edge effects. In addition, the curvature of the edges vary from slot to slot and thus produces different lift off signals for different slots for any given disk and add further challenges to the eddy current inspection. No commercially available EC probe was found to be capable to inspect and detect small corner cracks in the samples.

In order to design and develop an appropriate custom design eddy current probe aimed to detect crack at the edge of the coupons, physics-based numerical models of possible probe designs were performed in three different probe configurations. Transmit-Receive and Split-D Reflection configurations showed that edge noise is almost the same as the crack and unable to distinguish

crack signal from edge signal. However, a Transmit/Receive (Sliding) probe configuration using ferrites core, showed promise to distinguish between edge noise and the crack and thus mitigate the existing challenge of eddy current inspection, as shown in Figure 77. Although project was unsuccessful to generate a POD curve, a new EC probe design was developed, and samples required for PoD study were manufactured, which may be useful for future study.

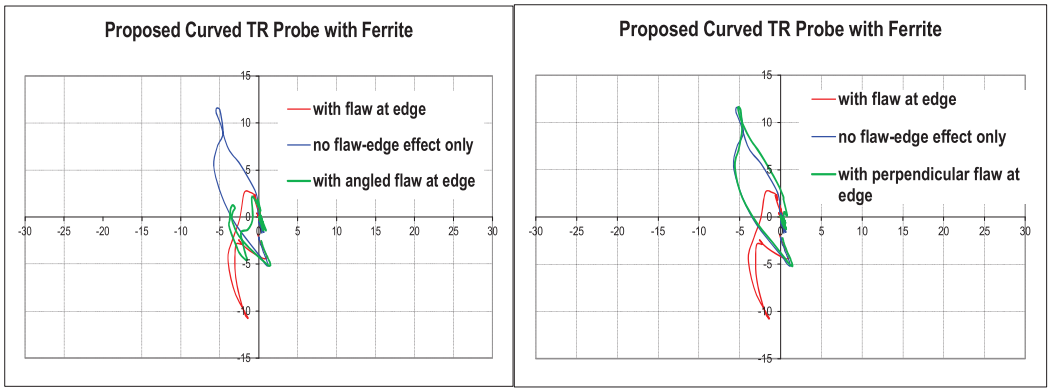

Figure 77 Modelling of Transmit/Receive (Sliding) EC Probe

6.5.1 REFERENCES

[47] Khan, M, "Model-Assisted Probability of Detection Assessment for Engine Components: Status Report (March 2015), LTR-SMM-2015-0419, March 2015.

7.0 ENVIRONMENTAL EFFECTS ON FATIGUE AND STRUCTURAL INTEGRITY

7.1 MULTI-PURPOSE ATMOSPHERIC PLASMA FOR PAINT STRIPPING AND ENHANCED LPI

Marko Yanishevsky, Ali Merati, and Lucy Li, NRC Aerospace

Paint stripping and subsequent non-destructive inspection using Liquid Penetrant Inspection (LPI) has been routinely used by the Canadian Forces (CF) to assist in aircraft maintenance and repair. Studies have found that conventional methods such as chemical paint stripping and media blasting present not only environmental and safety issues, but they also mask the indications of surface cracks due to entrapped media or residues from the strippers. Other routine methods such as hand sanding remove partial surface indications of cracks along with the paint, compromising the ability to reliably assess the damage and aircraft structural integrity.

Atmospheric plasma, a multi-purpose next generation technology for aircraft repair and maintenance, has demonstrated good potential for paint/coating removal, surface preparation for non-destructive inspection (NDI), as well as surface preparation for bonding. This non-contact, media-free technology allows for removal of paints and sealants from aircraft structures in an exceptionally controlled manner. Recent results from United States Air Force (USAF) trials showed that atmospheric plasma led to significantly improved detection rates of surface cracks using LPI indications, with 100% detection of cracks as compared to less than 50% from conventional paint stripping methods [48]. Atmospheric plasma technology requires only standard electrical power and a dry compressed air source, making it portable and field deployable. Another advantage of this novel technology is its inherent scalability. The United States Navy (USN) is currently looking into its application for paint stripping of large naval platforms [49].

As part of a DND green initiative for aircraft repair and maintenance, NRC had been tasked to investigate the potential of this novel technology. The primary purpose of the proposed work was to evaluate priorities for the application of atmospheric plasma technology by the Department of National Defence (DND), to conduct research to determine and optimize atmospheric plasma process parameters for the studied applications and to determine the impact of the process on the environment and the performance of materials of interest.

Since 2015, the NRC study compared current paint stripping methods to a novel atmospheric plasma (AP). Aluminium and steel coupons were prepared with military aircraft quality topcoat and primer paint schemes. Hardness and conductivity measurements as well as metallographic sectioning and microscopy, were used to characterize the stripped samples. Among different

plasma suppliers, the APS PlasmaFlux^{TM} system was selected and acquired by NRC for further trials on different paint and coupon schemes to optimize and validate the process for paint and primer removal [50]-[56].

The effectiveness of the novel APS system was compared to the Chemical Solution and Type VII starch-acrylic media blasting stripping processes. The effectiveness was assessed mainly by four criteria: i) extent of paint removal, ii) extent of deformation, iii) effect on temper/ property in particular damage fatigue property, and iv) effect on crack detectability during Liquid Penetrant Inspection.

Paint Removal Efficiency

Initial indications revealed that the Atmospheric Plasma process was quite sensitive to several parameter settings that need to be investigated further and optimized, for it to be considered as an accepted industrial paint removal process. A working envelope of process parameters for the APS PlasmaFlux paint removal system was established by plasma stripping painted test panels at various plasma pen heights, speeds and number of passes per stripe. The working parameters as well as the boundary of potential damaging and ineffective parameters were identified.

From the results it has been concluded that the APS PlasmaFlux system is capable of providing a multitude of combinations of parameters for removing paints. The system allows for a selective operation that can remove each layer of coating at a time. Also as a general conclusion, the presence of primer did not appear to affect LPI detectability.

Warping/deformation on thin sheet

None of the studied paint stripping processes appeared to induce permanent deformation and warping; although the media blasting and plasma stripping were used for partial de-painting (a selected area of the panel section was stripped).

Of the three processes, chemical stripping did manage to completely remove the paint and primer with no induced warping or damage to the substrate. Induced deformation can be prevented or minimized by selecting optimum process for the other two processes.

Effect on fatigue properties / heat treatment

The objective here was to determine whether paint stripping using Atmospheric Plasma was beneficial, detrimental or neutral with respect to the fatigue properties of aluminium substrates. Conductivity measurements indicated no change in conductivity to any portion of the aluminium test panels; including the most severely paint stripped locations. There was no considerable

effect from any of the three processes on heat treatment and consequently, the mechanical properties of the aluminium panels. This observation demonstrates that the duration of local heat exposure from the plasma torch within the determined operational working space window appeared to not change the precipitation condition (temper) of the alloys.

Fatigue testing and plotting the results of the crack length measurements revealed that the AP paint stripping process, similar to the traditional processes, was neither detrimental nor beneficial to the fatigue properties of the aluminium substrates. Therefore it was concluded that there was no considerable effect from any of the three processes on heat treatment and, consequently, mechanical properties of the aluminium panels.

Effect on LPI crack detectability

Post-strip macroscopic and microscopic examinations revealed varying amounts of paint and debris residue in most of the cracks, whether the processing was done by chemical, starch-acrylic media blast, or Atmospheric Plasma. There were indications of residual paint entrapped in all three methods (although less from the AP process). More importantly, the residues did not appear to affect the LPI crack detection process.

Table 4 below summarizes the degree of paint removal, level of damage incurred to the substrate, changes to fatigue properties, and the potential negative influence of the paint removal process on LPI crack detectability for each de-painting method.

Table 4 Summary of paint stripping results

Removal Process	Surface damage	Effect on temper and properties	Removal Rate - Cleanliness (debris in cracks)	Effect on LPI (crack masking)	Effect on fatigue property
Atmospheric Plasma	No	No	Negligible	No	No
Type VII Starch-acrylic	No	No	Minimal	No	No
Chemical Solution	No	No	Minimal	No	No

This limited paint removal study has determined that the AP process has the potential to replace current hazardous and less environmentally friendly paint removal methods; though a full systematic qualification and evaluation process is still required for it to be considered as an accepted industrial paint removal process. For this to occur, the range of process conditions corresponding to the minimum and maximum severity of paint removal process has to be

established for each particular combination of paint scheme and substrate. The system allows for a selective operation that can remove each layer of coating at a time.

In summary, the results in this study are encouraging for the Atmospheric Plasma paint stripping process and support further development for the technology's emergence into industrial applications for paint stripping.

7.1.1 REFERENCES

[48] N. Tracy, Nondestructive Evaluations (NDE) Exploratory Development for Air Force Systems, AFRL-RX-WP-TR-2010-4200, Dec 2009.

[49] P. Yancey, "Media Free Coating Removal Technology for Navy Platforms using Atmospheric Plasma", Sol NO. Navy SBIR FY2009.1, 2009.

[50] M. Yanishevsky and V. Pankov, "NRC Operating Procedure for APS PlasmaFlux Paint Removal System", LTR-SMPL-2015-0144," NRC, Ottawa, 2015.

[51] A. Merati, M. Yanishevsky, T. Despinic and P. Lo, "Metallographic Analysis of Paint Stripping Techniques - Atmospheric Plasma", LTR-SMM-2016-0015," NRC, Ottawa, 2016.

[52] A. Merati, P. Lo, T. Despinic, M. Yanishevsky and M. Genest, "Effect of Paint Removal Techniques on Crack Detectability - Liquid Penetrant Inspection", LTR-SMM-2016-0062, NRC, Ottawa, 2016.

[53] A. Merati, T. Despinic, P. Lo, and M. Yanishevsky, M. Genest, "Effect of Atmospheric Plasma Paint Stripping on Fatigue Properties of Aluminium Substrates", LTR-SMM-2016-0098, September 2016

[54] A. Merati, T. Despinic, P. Lo, and M. Yanishevsky, "Atmospheric Plasma – An alternative paint stripping process for aircraft structures", International Conference & Exhibition on Advanced & Nano Materials (ICANM2016) Proceedings, August 2016, Montreal, pp. 61-72

[55] A. Merati, P. Lo, T. Despinic, and M. Yanishevsky, "Effect of Paint Removal Process on Crack Detectability using Liquid Penetration Inspection Method", International Conference & Exhibition on Advanced & Nano Materials (ICANM2016) Proceedings, August 2016, Montreal, pp. 48-59.

[56] A. Merati, T. Despinic, P. Lo, V. Pankov, M. Yanishevsky, "Preliminary Investigation for Effective Atmospheric Plasma De-painting Process Parameters", LTR-SMM-2016-0129, December 2016 .

8.0 FATIGUE AND STRUCTRUAL INTEGRITY OF COMPOSITES

8.1 PREDICTING THE RELATIVE MAGNITUDE OF INTERLAMINAR STRESSES DUE TO EDGE EFFECTS IN THIN ANGLE-PLY LAMINATES USING MACROSCOPIC FINITE ELEMENT MODELING

D. Wowk, D. Thibaudeau - Royal Military College of Canada, C. Marsden - Concordia University

Carbon-epoxy and other composite materials are widely used in the design of aircraft and other structural components, and the Classical Laminate Theory (CLT) is most often used to establish the ply layup, thickness and stacking sequence of these components. The CLT does not account for out-of-plane or through-the-thickness stresses, which can be important initiators for certain failure modes, particularly at the edges of laminated sheets. For this reason, finite element modeling (FEM) is used to predict the magnitude and location of edge stresses that may become critical during the life cycle of the component. However, the FEM methodologies and resulting predictions vary considerably due to the stress singularity that exists at free edges between plies simulated with a perfect interface. The main purpose of the present study was to compare interlaminar stress predictions between perfect interface models and resin interface models to determine if the much simpler, perfect interface finite element models can be reliably used to compare the relative magnitude of interlaminar stresses for different ply layups in the context of laminate design.

The comparison between the two macroscopic finite element approaches was performed for a thin, rectangular, laminated angle-ply coupon in tension. The coupon measured 100 x 15.88mm with an overall thickness of t = 2.36mm. Six different $[+\theta/-\theta]_s$ layups with θ ranging from 0° to 60° were studied along with four quasi-isotropic layups. The perfect interface model consisted of laminate plies directly connected to each other, as shown in Figure 78 a). The resin interface models included an isotropic material layer representing the resin between each laminate ply as shown in Figure 78 b). The thickness of the resin layer was 10% of the overall ply thickness. With the inclusion of the resin layer, the resin interface models predict a finite value of the interlaminar stress at the free edge as opposed to the mesh dependent values predicted using the perfect interface model.

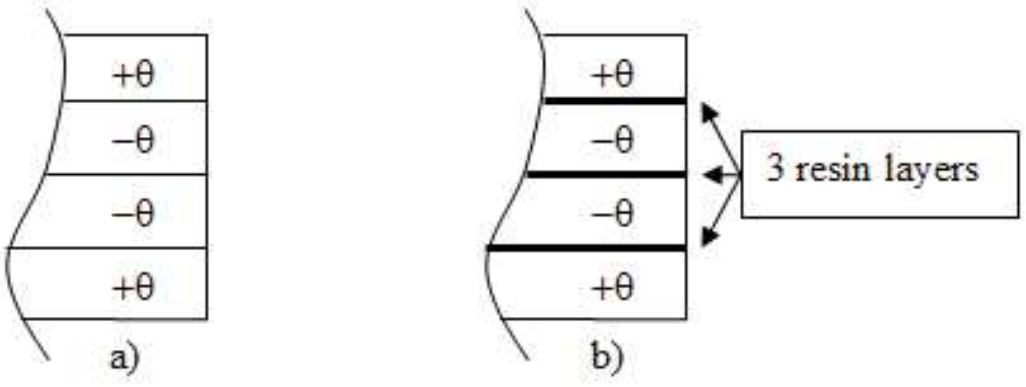

Figure 78 a) simulated layers in the perfect interface model, b) simulated layers in the resin interface model

As seen in Figure 79, the resin interface models produced a distribution of the interlaminar shear stress, $\tau_{xz,}$ across the width of the coupon that is zero at y/b = 0 (centre of the coupon) and increases towards the maximum value at y/b = 1 (free edge). τ_{xz} is contained to a region within a distance *t* (coupon thickness) from the free edge. The interlaminar normal stress, $\sigma_{z,}$ displays a similar overall shape, but is contained to a region within t/20 from the free edge. The magnitude, shape and sign of the σ_z distribution vary slightly depending on the thickness of the resin layer, and was tensile for all layups except for $[60/-60]_s$.

The relative magnitude of the interlaminar stresses was determined by dividing the peak stress for each layup by the maximum stress of all the layups being compared (τ_{xz}/τ_{xz}max and (σ_z/ $\sigma_z$max). Figure 80 shows that for τ_{xz}, the perfect interface and the resin interface models predict the same relative magnitude of the maximum interlaminar stress for all ply interfaces of the $[+\theta/-\theta]_s$ and quasi-isotropic layups. It is important to note that for the perfect interface models, the results were extracted in the region of singularity, but because of the similar shape of the τ_{xz} stress distribution, the relative magnitude of stress could be predicted even though a finite maximum stress value could not be determined. It is shown in Figure 81; however, that perfect interface models cannot be used to predict the relative magnitude of σ_z due to the influence of the thickness of the resin layer on the maximum values of $\sigma_{z.}$

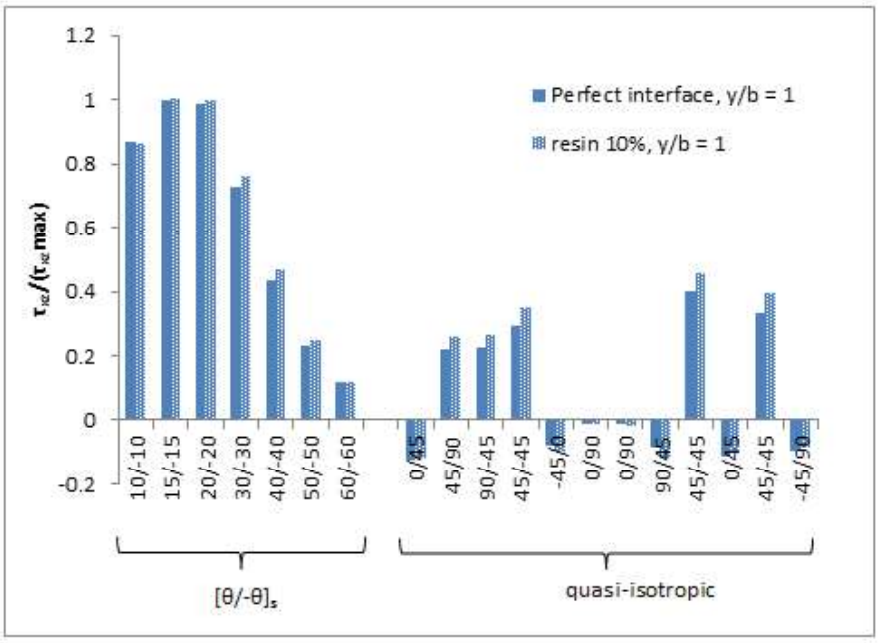

Figure 79 Overall distribution of τ_{xz} near the free edge, for $[\theta /- \theta]_s$ layups. Values were extracted along the +/- interface of the laminate

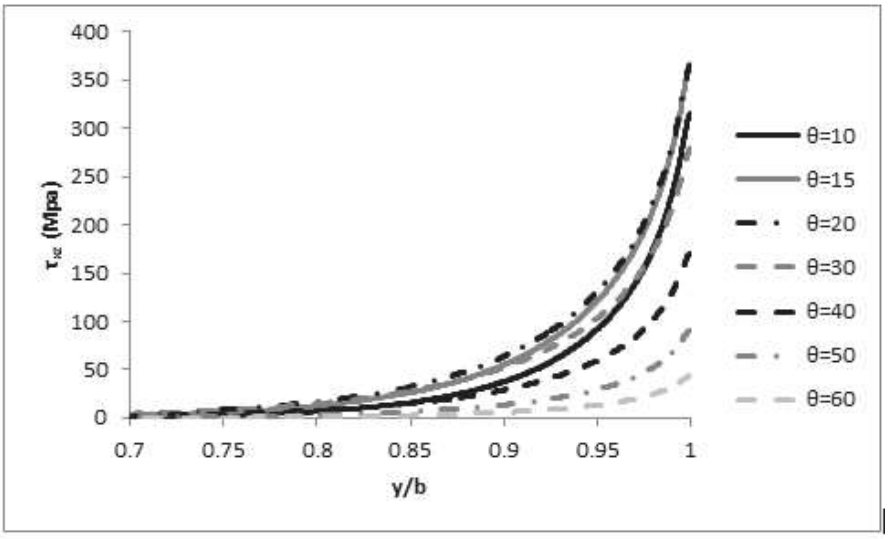

Figure 80 A comparison between the relative magnitudes of the maximum τ_{xz} for quasi-isotropic and $[\theta/-\theta]_s$ layups as predicted by the perfect interface model and the resin interface model

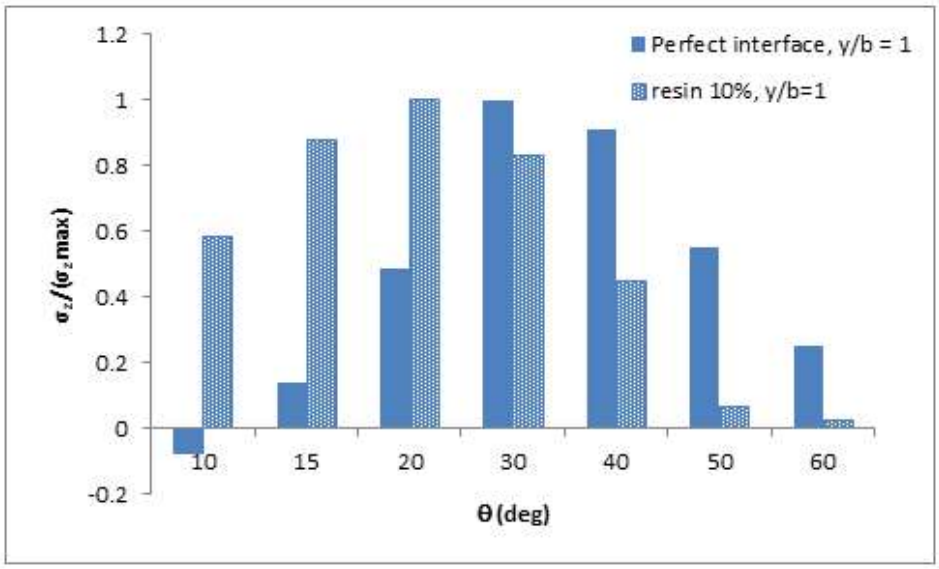

Figure 81 A comparison between the normalized magnitudes for the maximum normal interlaminar stress σ_z predicted by the perfect interface model and the resin interface model

It was shown that the simpler and computationally more efficient perfect interface models were able to effectively predict the relative magnitude of the interlaminar shear stress, τ_{xz} between different layups, but resin interface models should be used for predicting the relative magnitude of the interlaminar normal stress, σ_z.

8.2 PROGRESSIVE FAILURE MODELLING OF COMPOSITE STRUCTURES

Lucy Li and Gang Li, NRC Aerospace

Progressive failure modelling of composite structures has continued to be a primary focus of composite material research. Progress has been made on damage onset and progression of woven fabric under Mode I peel loading [57]. The effect of several architectural factors on G_I were investigated, such as fibre orientation, yarn width, yarn thickness and stacking configurations of weaves. Results showed that for weaves, G_I was mostly affected by the bifurcation of the delamination front around yarns and by subsequent yarn bridging. The framework for empirical models was proposed for describing fibre bridging and the effects of weaves on G_I. This work contributes to a better understanding of damage tolerance of woven composites.

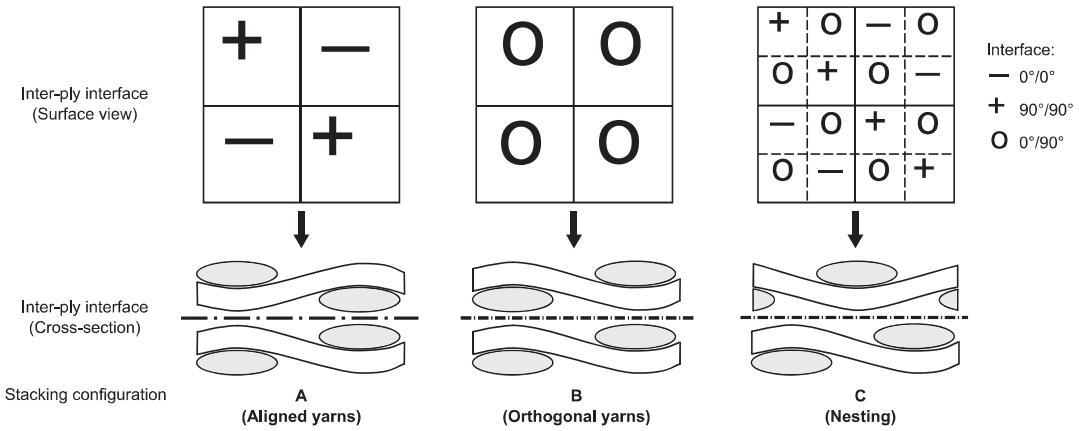

Figure 82 Unit cell of the weave stacking configurations

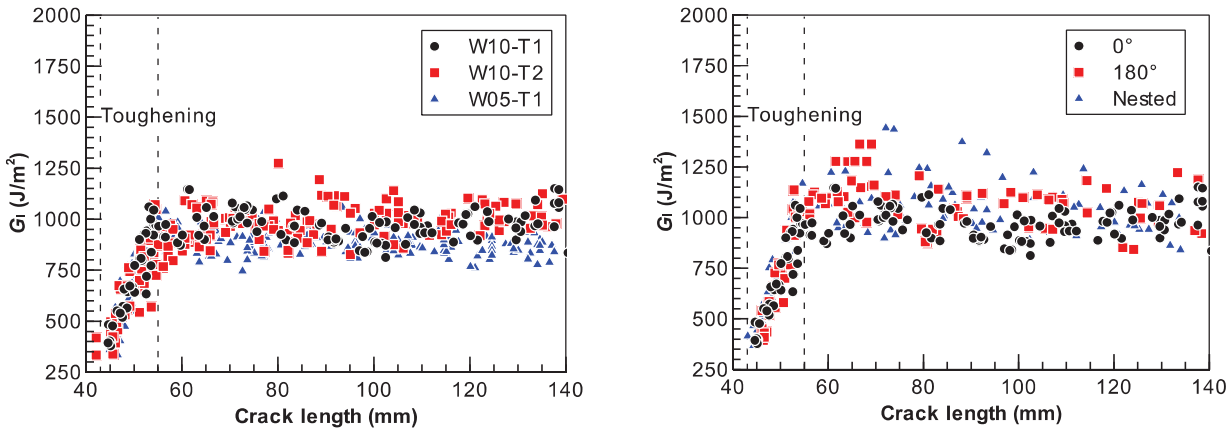

Figure 83 Instantaneous G_I values of woven specimens: a) effect of yarn width and thickness, and b) effect on stacking configuration

Progress have also been made to develop an ASTM standard test method for Mode I fatigue delamination propagation of unidirectional fibre-reinforced polymer matrix composites by analysing round robin test data generated from multi-nation effort under ASTM D30 group [58]. This test method determines the delamination growth per fatigue cycle, da/dN based on the Opening mode I cyclic strain energy release rate, G_{Imax}, using the Double Cantilever Beam (DCB) specimen. This test method applies to constant amplitude, tension-tension fatigue loading of continuous fiber-reinforced composite materials. The results may be shown as a da/dN versus G_{Imax} curve.

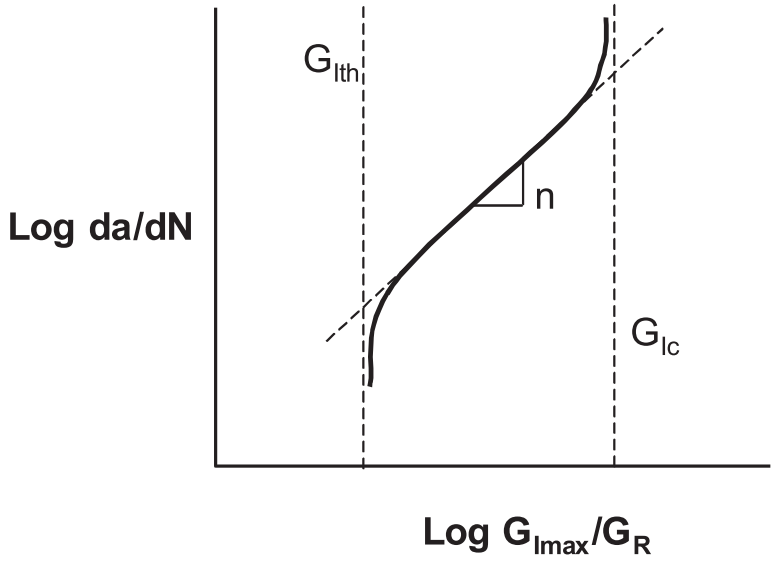

Figure 84 Modified power law for Mode I fatigue

8.2.1 REFERENCES

[57] Simon Baril-Gosselin and Chun Li, Characterizing and predicting the effects of weave geometry on Mode I fracture toughness of composites, American Society for Composites 31st Technical Conference, Williamsburg, USA, 2016.

[58] Chun Li, Development of ASTM standard test method for Mode I fatigue delamination propagation of unidirectional fibre-reinforced polymer matrix composites, HOLSIP 2017, Utah, 2017.

8.3 MODELLING DYNAMIC RESPONSE OF KEVLAR PANELS

Gang Li, NRC Aerospace

Impact damage is a major threat for new generation of aircraft made with a considerable amount of composite materials. Low-velocity impact and high-velocity ballistic perforation simulations were conducted for Kevlar panels, as shown in Figure 85. A low-velocity impact FE model and the comparison between impact forces obtained via testing and simulation are shown in Figure 85 (a). A perforation FE model and the predicted damage after impact are shown in Figure 85 (b) for a bonded Kevlar fabric structure. The 3D composite Hashin damage criteria were employed for simulating the failure in this model. The effects of modified Kevlar material

parameters, adhesive thickness, and adhesive material parameters on the panel impact response were investigated numerically using the developed model.

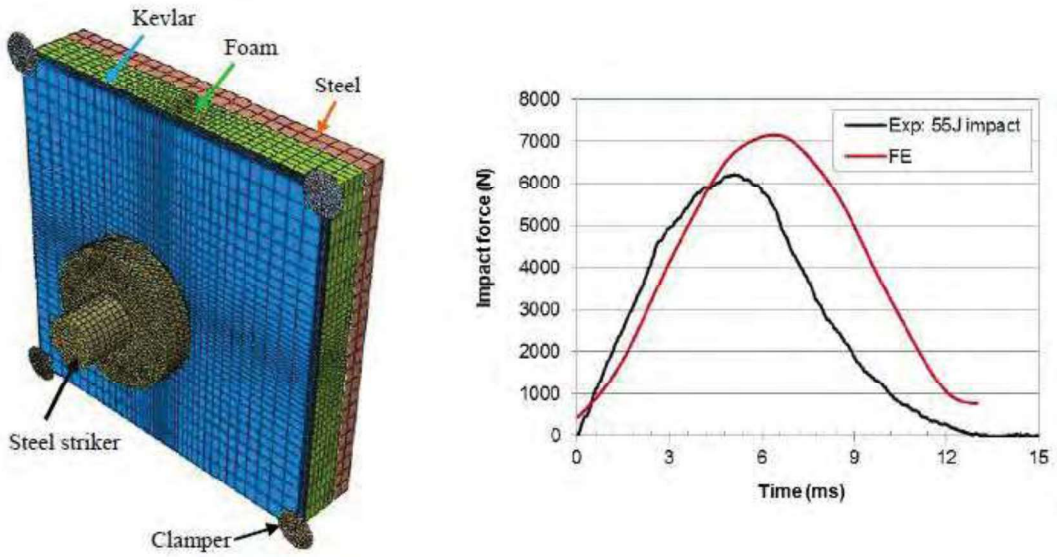

(a) Low-velocity impact of a Kevlar fabric panel supported by a foam/steel backup assembly

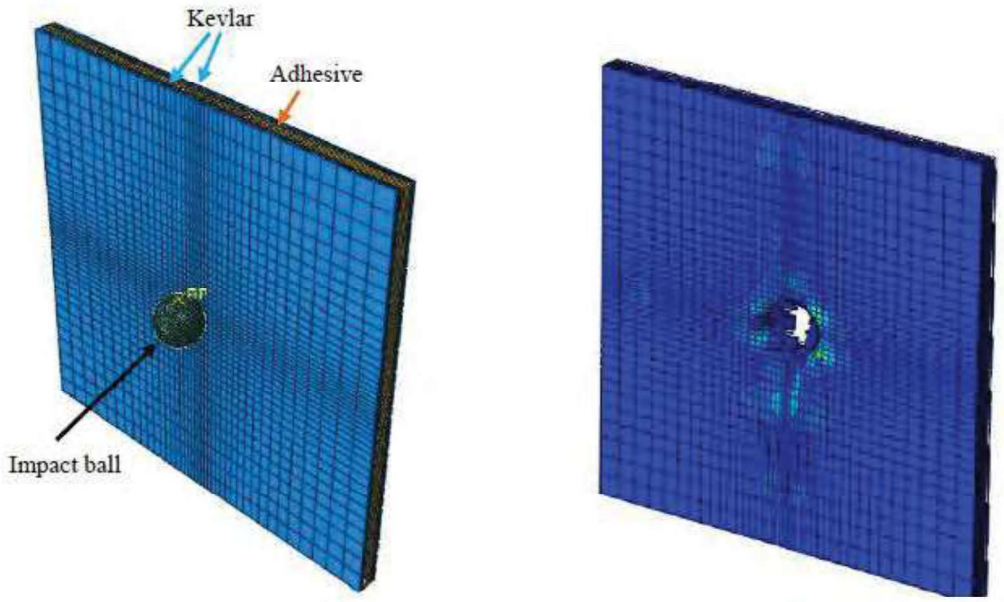

(b) Perforation of a "Kevlar/adhesive/Kevlar" structure

Figure 85 Three-dimensional FE models for simulating two impact cases: (a) low-velocity impact of a Kevlar fabric panel and (b) perforation of a layered Kevlar fabric structure

8.3.1 REFERENCES

[59] G. Li, M. Genest, "Two-Dimensional Finite Element Simulation of Induction Thermography of an Aluminum Alloy Panel", Canadian Aeronautics and Space Institute AERO'15 Conference 23rd CASI Aerospace Structures and Materials Symposium, May 19-21, 2015, Montreal, QC.

[60] M. Genest, G. Li, "Inspection of Aircraft Parts by Induction Thermography", NDT in Canada 2015, June 15-17, Edmonton, AB.

[61] Gang Li and Marc Genest, "Numerical Simulation of Induction Thermography on a Laminated Composite Panel", American Society for Composites 31 Technical Conference and ASTM Committee D30, September 19-22, 2016. Williamsburg, VA.

[62] Gang Li, Marc Genest, "Three-Dimensional Numerical Modelling of Induction Thermography on Metallic Panels", CPR-SMM-2016-0059, NDT in Canada, Nov 15-18, Burlington, ON.

9.0 FATIGUE AND STRUCTURAL INTEGRITY OF NEW MATERIAL AND MANUFACTURING

9.1 MEASUREMENT OF THE RESISTANCE TO FRACTURE OF 7249-T76511 ALUMINIUM EXTRUSION

Y. Bombardier, NRC Aerospace

During the course of the P-3C/CP-140 Service Life Assessment Program (SLAP), Lockheed Martin Aeronautics (LMA) and the United States Navy (USN) undertook a program to identify a newer aluminium (Al) alloy capable of reducing the susceptibility of the P-3C fleet to corrosion and stress corrosion cracking. This development program led to the selection of Al 7249-T76511 extrusion (Al 7249) as the material of choice to replace the original Al 7075-T6511 (Al 7075) for all new wings. The initial Al 7249 test results showed that the material properties of Al 7249 where equal or superior to Al 7075 in every instance that was tested. To reduce material testing costs, it was assumed that the overall fatigue performance of Al 7249 was similar to Al 7075, enabling the P-3C operators to employ the extensive data set previously generated for Al 7075. Subsequent testing has shown that this assumption was optimistic and that further material evaluation was required. The current test results indicate that the fatigue crack growth threshold of Al 7249 is significantly lower than that of Al 7075, allowing cracks to develop and grow more rapidly at very low stress intensity factor ranges. It was also found that Al 7249 does not exhibit the same level of crack growth retardation as Al 7075 for structures subjected to loading spectra with loads producing high stresses, resulting in shorter crack growth lives and reduced inspection intervals.

In an attempt to extend the current inspection intervals, the National Research Council Canada (NRC) was tasked to measure the crack growth resistance (K_R) of Al 7249 as a function of material thickness to accurately establish the residual strength capability of the CP-140 structures instead of relying on the unsubstantiated assumption that Al 7249-T76511 has equivalent or better crack growth resistance than the original material, Al 7075-T6511.

The fracture toughness of 7249-T76511 aluminium (Al 7249) was tested according to ASTM E561 using middle-cracked tension specimens. Four specimen thicknesses were tested: 0.090, 0.110, 0.270, and 0.400 inch. For the tested thicknesses, it was observed that the fracture toughness of Al 7249 unexpectedly increased as a function of thickness. This unexpected trend can be explained by the fact that the fracture toughness can gradually decrease as thickness decreases when plane stress conditions prevail because the volume of material available for plastic deformation energy absorption decreases. Despite this unexpected trend where there was a reduction in fracture toughness for thinner specimens, the results show that Al 7249 has higher fracture toughness than the original alloy used for the P-3C/CP-140 wing (7075-T6511) along

the L-T direction. By comparison, the fracture toughness of Al 7249 aluminium extrusion is equal to or better than 7075-T76511 aluminium extrusion.

9.1.1 REFERENCES

[63] Bombardier, Y., "Measurement of the resistance to fracture of 7249-T76511 aluminium extrusion," National Research Council Canada, LTR-SMM-2017-0056, Ottawa, 2017.

9.2 FATIGUE TESTING OF NEGATIVE POISSON RATIO MATERIALS

David Backman[1], Scott Yandt[1], Tyler Musclow[1], Minh Quan Pham[2], Ali Shanian[2], Megan Schaenzer[2], Christopher Booth-Morrison[2], Genevieve Bourgeois[2] Miklos Gerendas[4], Katia Bertoldi[3], Farhad Javid[3]

[1]NRC Aerospace; [2]Siemens Canada, [3]Harvard University, Faculty of Engineering; [4] Rolls-Royce Deutschland

A collaborative project between Siemens Canada, Harvard University and the National Research Council Canada has focused on the design, fabrication and testing of structures that exhibit Negative Poisson Ratio [NPR] behaviour (Figure 86). Combines periodic slits of varying complexity induces rotation and expansion [i.e., negative Poisson behaviour] under the effect of a tensile load. This geometry has been designed to focus on strain controlled applications, specifically temperature induced thermal strain. This paper reviews the finite element (FE) modelling performed during the design process of the strain controlled NPR material, as well as the static tensile tests that were performed to both validate the FE model as well as to calibrate the peak strain to be applied during fatigue loading. Two basic coupon geometries were tested, shown in Figure 87, a flat sheet coupon and a more complex cylindrical coupon. In both cases strain results were compared against the control coupons with non-NPR geometry. The overall results showed a significantly longer fatigue life with the NPR materials compared to the control coupons with non-NPR geometry. Digital image correlation techniques were used to measure strain during the test and showed that the slots used to obtain NPR behaviour resulted in crack arrest once cracks reach a critical size. Overall, coupon failure is the result of widespread fatigue damage, as opposed to the conventional structure that shows crack link-up and failure soon after crack nucleation.

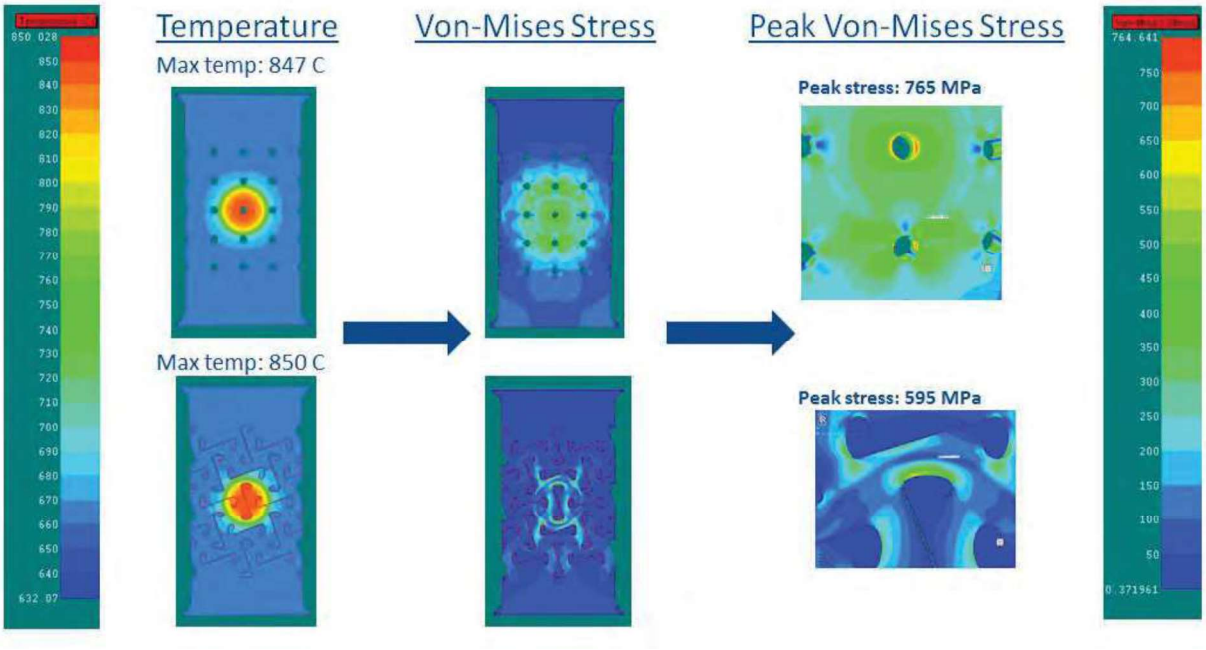

Figure 86 Design concept for NPR materials for high temperature applications

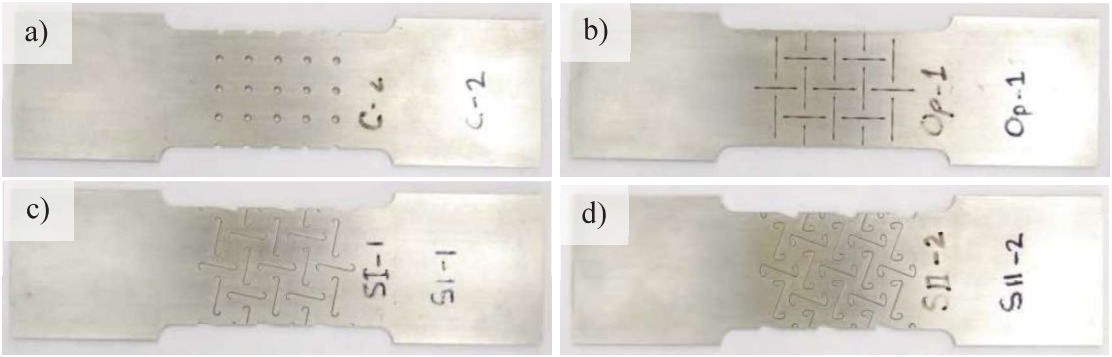

Figure 87 Test coupon geometries a) circular void (C coupon); b) optimized elliptical void (Op coupon); c) S-slot with circular tip (SI coupon); d) S-slot with elliptical tip (SII coupon)

9.2.1 REFERENCES

David Backman , Scott Yandt , Tyler Musclow , Minh Quan Pham, Ali Shanian, Christopher Morrison, Megan Schaenzer, Genevieve Bourgeois, Katia Bertoldi and Farhad Javid, "*Fatigue Testing of Negative Poisson Ratio Structures for Aerospace Applications*", 17th International ASTM/ESIS Symposium on Fatigue and Fracture Mechanics (41st National Symposium on Fatigue and Fracture Mechanics), May 10-12, 2017, Toronto, Canada.

9.3 FATIGUE OF A RARE-EARTH CONTAINING MAGNESIUM ALLOY

D.L. Chen, Department of Mechanical and Industrial Engineering, Ryerson University, Toronto, Ontario, Canada

Lightweighting of ground and aerospace vehicles is at present regarded as one of the most effective strategies to improve fuel economy and reduce climate-changing and environment-damaging emissions. Advanced high-strength steels, aluminum alloys, magnesium (Mg) alloys, and polymers are being used to reduce vehicle weight and the subsequent emissions, but substantial reductions could be achieved further by more applications of Mg alloys, which have been considered as a strategic ultra-lightweight material in the automotive and aerospace sectors due to their high strength-to-weight ratio, dimensional stability, good machinability and recyclability. In the structural applications of Mg alloys in the transportation industry, including camshaft covers, clutch and transmission housings, intake manifolds and automobile wheels, the components are inevitably subjected to cyclic stresses and strains for millions of cycles in service. Hence, knowledge on the cyclic deformation and fatigue behaviour of Mg alloys is of vital importance for the design and durability evaluation of structural engineering components.

Despite the potential of substantial reductions in weight, most wrought Mg alloys exhibited a high degree of anisotropy and tension-compression yield asymmetry due to the presence of strong crystallographic texture owing to their hexagonal close-packed (HCP) crystal structure with limited slip systems during extrusion or rolling processes. Indeed, for the vehicle components subjected to dynamic cyclic loading, such mechanical anisotropy and tension-compression yield asymmetry could lead to irreversibility of cyclic deformation, which may have an unfavorable influence on the performance and durability of structural components. These problems could be tackled through texture modification. One appealing approach of achieving this goal is via alloy composition adjustments, especially the addition of rare-earth (RE) elements into Mg alloys. The addition of RE elements in Mg alloys can lead to more random initial crystallographic texture compared with the RE-free wrought Mg alloys, which leads to improved ductility and strength at both room and elevated temperatures via solid solution strengthening and precipitation strengthening. While the texture weakening and the tension-compression yield asymmetry due to the RE elements additions have been extensively studied, more and more studies on the fatigue and fracture behaviour of these alloys have also been reported in recent years, since it is only possible to harness the full potential and benefits of weight reduction by using these RE-Mg alloys when the fatigue and fracture behaviour is properly understood.

Based on the strain-controlled low cycle fatigue tests results with different total strain amplitudes at room temperature, unlike the RE-free extruded AM30 magnesium alloy, the rare-earth containing extruded Mg-10Gd-3Y-0.5Zr (GW103K) magnesium alloy exhibited nearly symmetrical hysteresis loops in shape as shown in Figure 88, which were somewhat similar to those of face-centered cubic (FCC) metals (e.g., Al, Cu, Ni) as a result of the dislocation slip-

dominated deformation in most materials. This also suggested the absence of the tensile-compressive yield asymmetry which was predominantly due to the presence of the relatively weaker crystallographic texture and the lack of twinning-detwinning activities stemming from the fine grain size and RE-containing precipitates.

As shown in Figure 89, unlike the RE-free extruded alloys, where cyclic stabilization occurred only at lower strain amplitudes of 0.1% and 0.2%, the extruded GW103K alloy exhibited cyclic stabilization until failure up to a higher strain amplitude of 1.0% as well. Even at a strain amplitude of 1.2%, only a slight change, i.e., an initial slight cyclic hardening within the first three cycles and then minor cyclic softening, could be seen from Figure 89, which corresponded well to the variation of the plastic strain amplitude during cyclic deformation as shown in Figure 90 at different total strain amplitudes. Again, it is seen that cyclic stabilization basically occurred in the RE-containing GW103K alloy at all strain amplitudes applied up to as high as 1.2%. As a result, the addition of RE elements was able to change significantly the cyclic deformation behavior of the magnesium alloy.

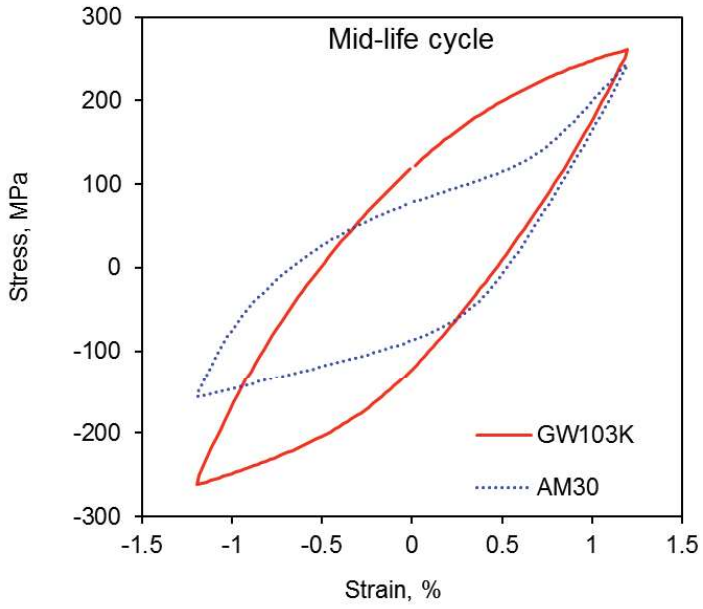

Figure 88 Typical stress-strain hysteresis loops of the mid-life cycle at a given total strain amplitude of 1.2% and strain ratio of R_ε= -1 for the extruded GW103K and AM30 alloys, respectively

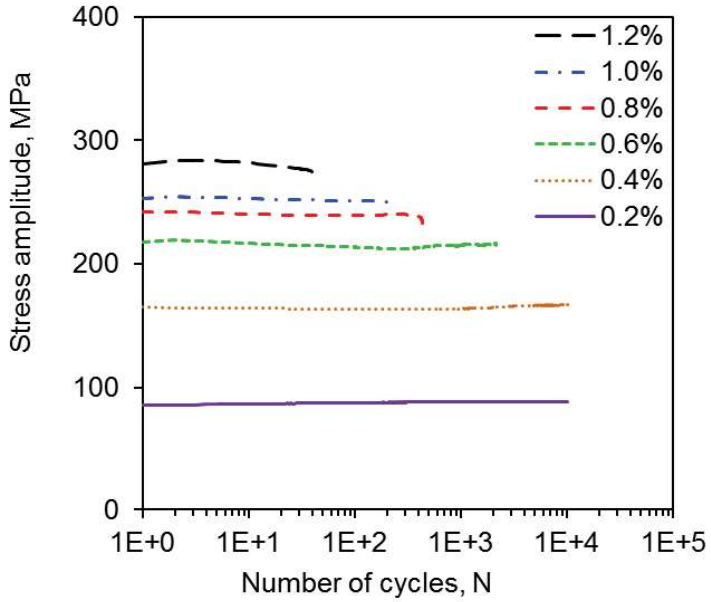

Figure 89 Stress amplitude vs. the number of cycles at different total strain amplitudes applied for the extruded GW103K alloy

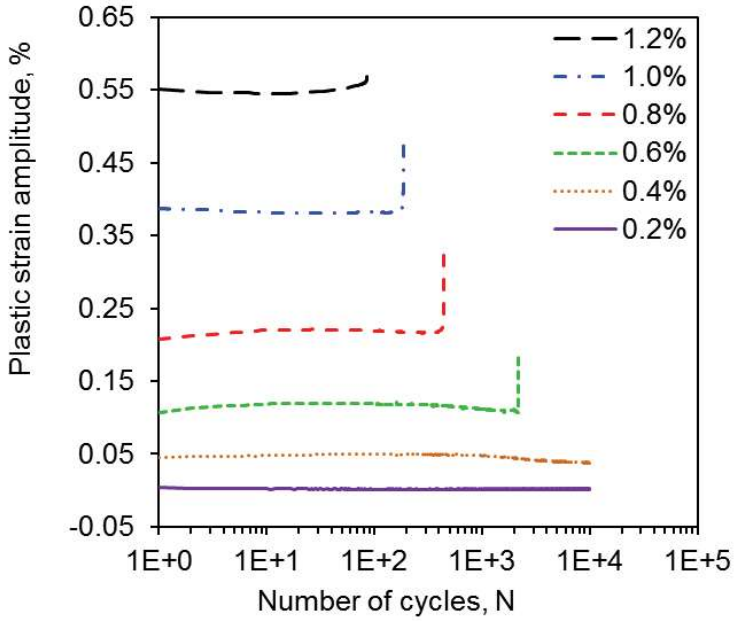

Figure 90 Plastic strain amplitude vs. the number of cycles at different total strain amplitudes applied for the extruded GW103K alloy

In addition, the fatigue life (i.e., the number of cycles to failure, N_f) as a function of the applied total strain amplitudes $(\Delta\varepsilon_t/2)$ of the extruded GW103K alloy is plotted in Figure 91, along with the experimental data reported in the literature for various extruded magnesium alloys for

comparison. The RE-containing GW103K alloy showed an improved fatigue life than the RE-free extruded magnesium alloys. Since RE-containing magnesium alloys are relatively new, while some data on the fatigue behaviour of such Mg alloys have been reported in the literature, our understanding of the cyclic deformation mechanisms is limited, and needs to be studied further so as to meet the needs in design and life prediction of structural components. Research efforts to determine fatigue crack growth behaviour and develop life prediction methodologies for the RE-Mg alloys are also needed.

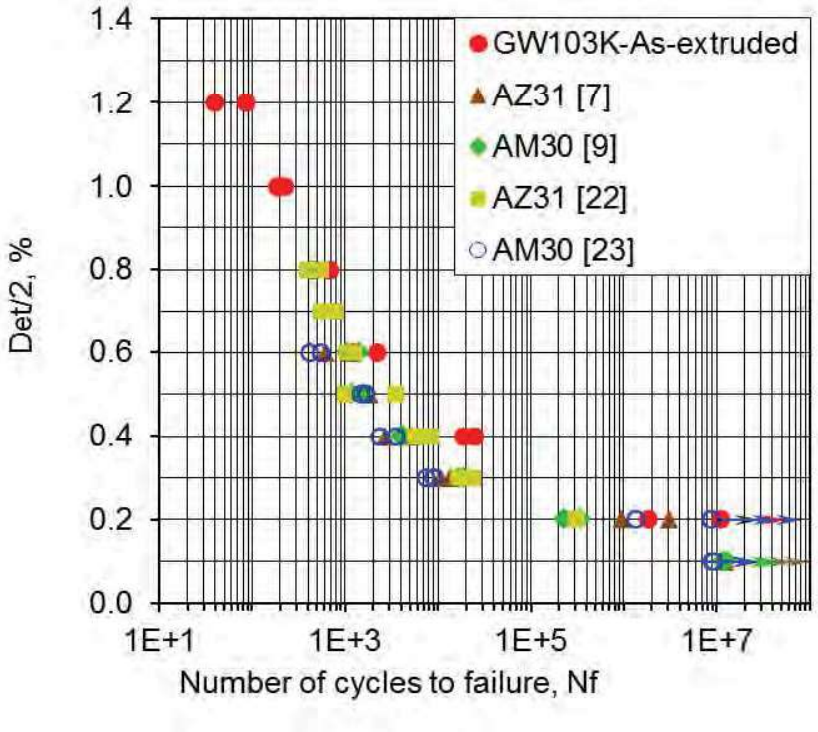

Figure 91 Total strain amplitude as a function of the number of cycles to failure for the extruded GW103K alloy, in comparison with the data reported in the literature for various extruded Mg alloys

9.3.1 REFERENCES

[64] Mirza F. A., and Chen D. L. (2014), Fatigue of rare-earth containing magnesium alloys: a review, Fatigue Fract Engng Mater Struct, 37, pages 831–853, doi: 10.1111/ffe.12198

9.4 LASER CONSOLIDATION - A NOVEL ADDITIVE MANUFACTURING PROCESS FOR MAKING NET-SHAPE FUNCTIONAL METALLIC COMPONENTS FOR VARIOUS APPLICATIONS

Lijue Xue, National Research Council Canada, London Ontario

Laser consolidation (LC) is a novel additive manufacturing process being developed by the National Research Council Canada (NRC) at its London facility. LC offers unique capabilities in the production of net-shape functional metallic parts requiring no further post-processing. NRC's LC technology has achieved dimensional accuracy of up to +/-0.05 mm with a surface finish up to 1 μm Ra (depending on the materials used in the manufacturing process). The LC process differs from other additive manufacturing technologies by its high precision deposition system that can build functional parts or build features using various alloys and high performance materials on top of an existing part. In this presentation, laser consolidation of various high performance materials (such as Ni-alloys, Co-alloys, Ti-alloys and Al-alloys) will be discussed in respect to their unique microstructure and mechanical properties (including fatigue/fracture properties). The examples will be given on building complex functional components and repairing parts otherwise unrepairable for aerospace, defense and other applications.

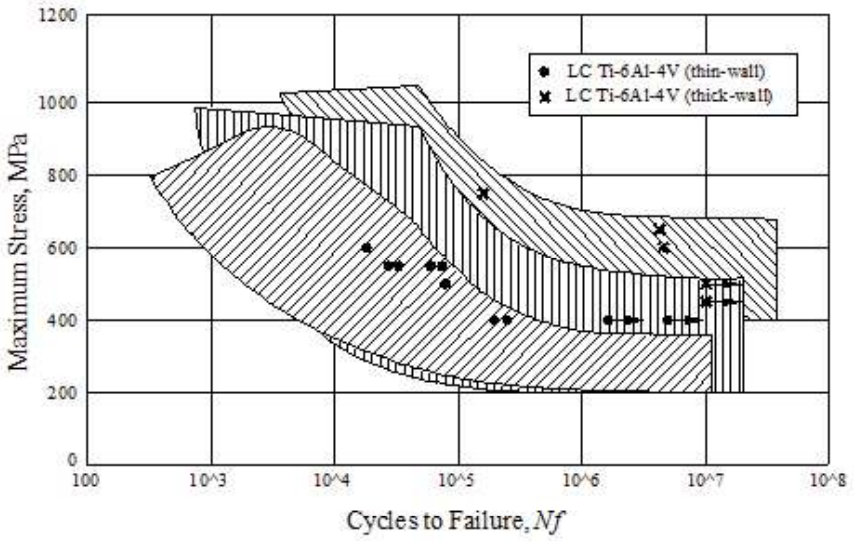

Figure 92 Fatigue data of LC Ti-6Al-4V compared with cast and wrought/annealed Ti-6Al-4V

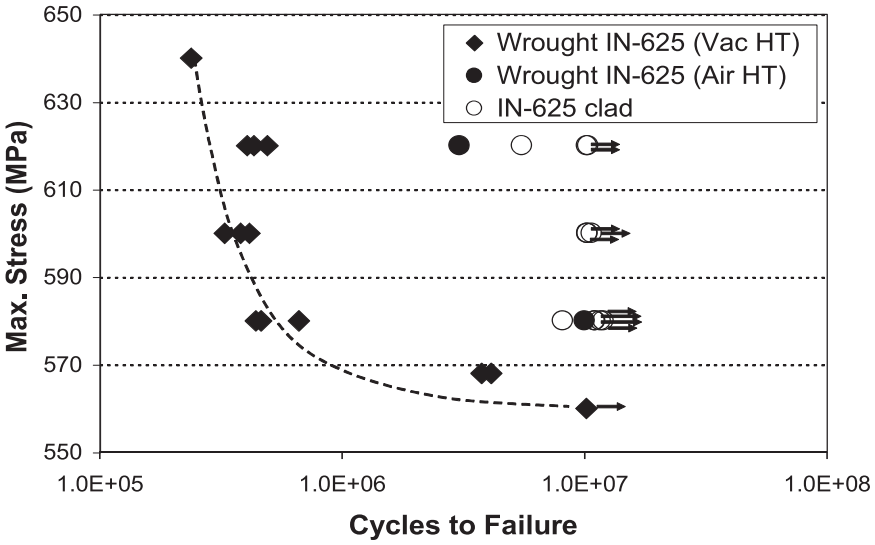

Figure 93 Room temperature fatigue testing results

(a) **(b)**

Figure 94 LC Ti-6Al-4V hollow ball: (a) top view, and (b) bottom view

Figure 95 Damaged fuel nozzle swirler

Figure 96 Laser clad repaired fuel nozzle swirler after final machining

The laser consolidated alloys present excellent mechanical properties, which allows the LC process to directly build functional components or to repair damaged components for aerospace applications. Compared to similar laser powder deposition processes, LC produces metallurgically sound samples with much better surface finish.

The LC process provides the unique capability to build net-shape functional metallic components or features on existing components that are difficult or even impossible to manufacture using conventional manufacturing processes. Compared to a similar laser powder deposition process, LC process has much smaller heat input and, therefore, much better control. It is especially suitable to perform “precision repair” of aerospace and defense components.

9.4.1 REFERENCES

[65] Xue, L. Keynote Presentation: Laser Consolidation - A Novel Additive Manufacturing Process for Making Net-Shape Functional Metallic Components for Various Applications, 17th International ASTM/ESIS Symposium on Fatigue and Fracture Mechanics (41st National Symposium on Fatigue and Fracture Mechanics), May 10-12, 2017, Toronto, Canada.

9.5 FATIGUE PERFORMANCE OF ADDITIVE MANUFACTURED 300M STEEL

Allison Nolting, Shannon Farrell, Department of National Defence, Halifax, NS, Canada
Lijue Xue, Jianyin Chen, Shaodong Wang, National Research Council Canada, London, ON.
Marc Genest, National Research Council Canada, Ottawa, ON.
Christophe Bescond, National Research Council Canada, Boucherville, QC.

The inherent variability with Additive Manufacturing (AM) processes is challenging from a quality assurance perspective, as the layer-by-layer fusion of feedstock (wire or powder) may engender defects, lack of fusion and porosity between layers in metallic alloys. As the morphology, size and distribution of these defects differ from those seen in conventionally manufactured materials, a better understanding of defect characteristics, detectability and their effect on mechanical performance is required to develop acceptance criteria for AM parts. This study was initiated to investigate the effect of typical AM microstructures and macrostructural features on fatigue performance and crack nucleation. The preliminary results of this on-going study are presented.

300M steel specimens were produced using a proprietary blown powder laser consolidation (LC) process being developed by the National Research Council of Canada at its London facility. Oversized specimens were manufactured, subjected to austenizing and double tempering heat treatments, and machined to the final specimen dimensions. Scanning electron microscopy conducted on the heat treated LC 300M samples revealed totally re-crystallized martensitic structure.

X-ray computed tomography (microCT) measurements, with a resolution of 5 μm^3, were performed in the gauge section of the flat specimens (Figure 97). The microCT scans revealed spherical and linear indications, examples of which are presented in Figure 97. Further microstructural analysis is required to determine if the spherical indications are pores or microstructural features, and if the linear indications were caused by microcracking, lack of fusion or alloy segregation. The volume of spherical indications in the gauge sections was typically measured to be less than 0.001 vol%, and the largest spherical indications ranged from 50 to 100 μm^3.

The average tensile properties of four heat treated samples were evaluated in accordance with ASTM E8. The material was found to have a 0.2% offset yield of 1710 MPa, UTS of 1972 MPa and 2.5% elongation at fracture.

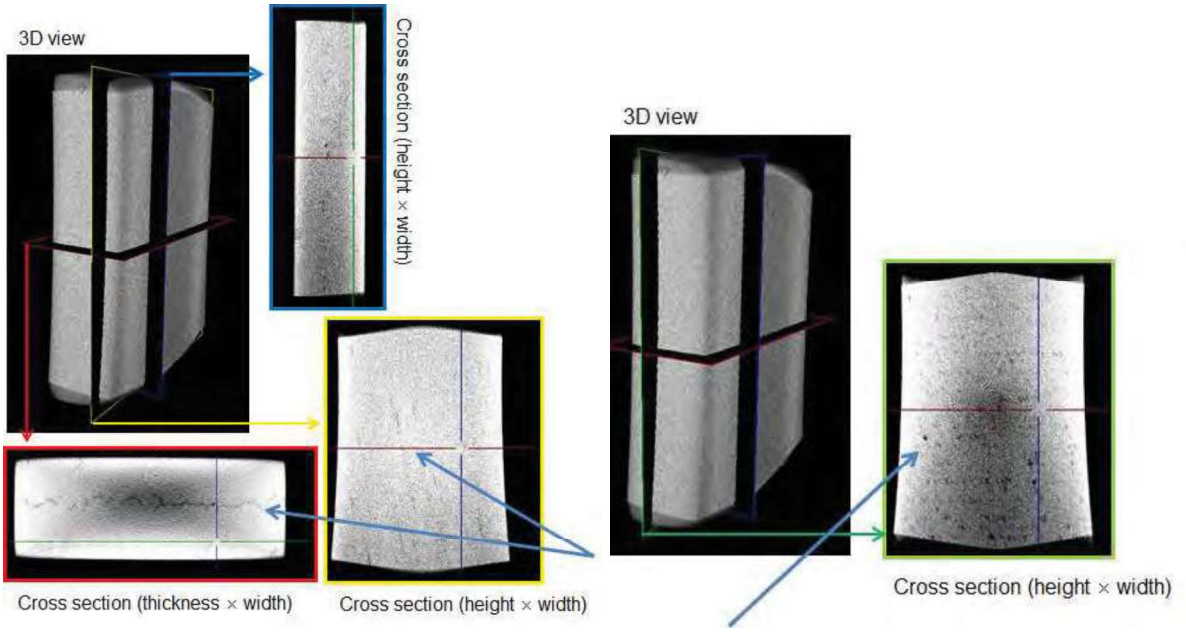

Figure 97 MicroCT results for a sample showing linear indications (left) and spherical indications (right)

Load controlled fatigue tests were conducted in accordance with ASTM E466 at a stress ratio of 0.05. Preliminary results for the heat treated LC 300M steel are shown, along with data on forged 300M tested at the same stress ratio, in Figure 98. The fracture surfaces of the LC 300M specimens exhibited multiple fatigue crack nucleation sites, shown in Figure 99, and were highly contoured, which implies that microstructural features or defects had an influence on fatigue crack nucleation.

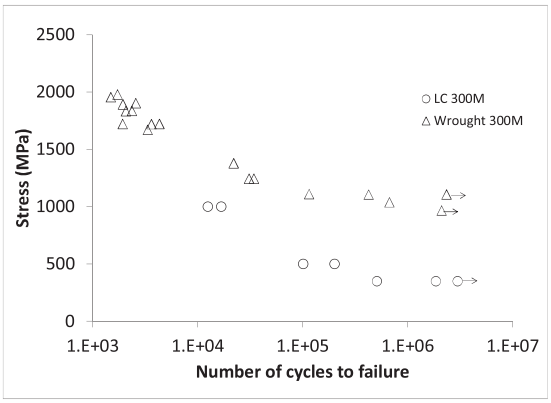

Figure 98 Preliminary S-N fatigue results for heat treated LC 300M steel. [4]

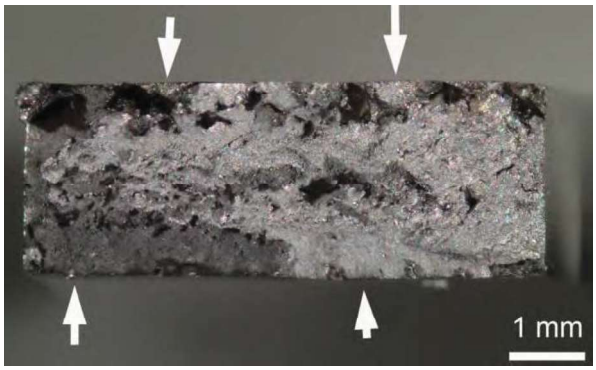

Figure 99 Fracture surface of a LC 300M fatigue specimen. White arrows provide examples of fatigue crack nucleation sites.

9.5.1 REFERENCES

[66] Allison Nolting, Shannon Farrell, Lijue Xue, Jianyin Chen, Shaodong Wang, Marc Genest, Christophe Bescond, Fatigue Performance of Additive Manufactured 300M Steel, 17th International ASTM/ESIS Symposium on Fatigue and Fracture Mechanics (41st National Symposium on Fatigue and Fracture Mechanics), May 10-12, 2017, Toronto, Canada.

9.6 ELECTRON BEAM WIRE ADDITIVE MANUFACTURING OF TI-6AL-4V

P. Wanjara[1], J. Gholipour[1] and C. Bescond[1]
K. Watanabe[2] and K. Nezaki[2]
[1]NRC – Aerospace;
[2]IHI Corporation

A multi-phase collaborative project between IHI Corporation (Japan) and the National Research Council Canada has focused on developing a repair technology using electron beam additive manufacturing (EBAM) to refurbish extensively damaged first stage titanium alloy fan blades. EBAM, also referred to as electron beam freeform fabrication (EB3F), deposits metallic materials using a wire feedstock through a layer by layer process to form near net shape components within a vacuum operational environment. The EBAM technology has advantages of a relatively large build envelop combined with the near 100% material efficiency of the wire-feed into the melt pool and high bulk material deposition rates of 200-600 mm^3/s depending on feature size and material. From a repair application perspective, the influence of the EBAM process on distortion of the Ti6Al4V is of particular signification. Specifically, distortion during AM repair can affect the geometrical characteristics, as well as the structural integrity of the assembly, both of which are critical for returning the part into service.

For the case of overhauling an extensively eroded Ti6Al4V fan blade, the EBAM process using Ti6Al4V wire feed was developed to deposit a thin wall build on a 3 mm-thick substrate (Figure 100). For quality assurance, the deposit was inspected using x-ray micro-computed tomography (Figure 101) that confirmed that the deposit, consisting of 142 layers, was fully dense and defect free. The distortion in the as-deposited and stress-relieved conditions was evaluated using a novel 3D optical strain measurement system (Figure 100 b)). The maximum out-of-plane displacement in the 3 mm-thick Ti6Al4V substrate after EBAM was about 0.70 mm (Figure 102 a)). After stress relieving, the maximum displacement increased to 1.15 mm, but the distribution in the central region of the Ti6Al4V substrate was more homogeneous relative to that in the as-deposited condition (Figure 102 b). These maximum displacement values measured in the Ti6Al4V substrate after EBAM and stress relieving were within the tolerance limit for the repair requirements of the fan blade. Fracture during static tensile loading occurred exclusively in the deposit through a ductile rupture fracture mechanism, which explains the relatively high plasticity of the Ti6Al4V build (i.e. total elongation of 13-15%). The mechanical property results

for the Ti6Al4V deposits fabricated by the EBAM met sufficiently the repair requirements and bode well for transitioning the process to the actual geometry of the fan blade. Presently, work to continue certification testing is ongoing to ascertain the residual stresses through hole drilling, as well as the low cycle and high cycle fatigue behavior for harmonic and random loading. From a processing perspective, the EBAM procedure is being scaled to demonstrate 3D repair of the actual fan blade geometry. Considering the relative size of the rebuilt part, in-line non-destructive inspection for real-time examination during the manufacturing process has been a consideration to allow early detection of any issues. Next, specific sub-scale and full-scale testing of the repaired fan blade will also be performed in accordance with IHI Corporation's requirements.

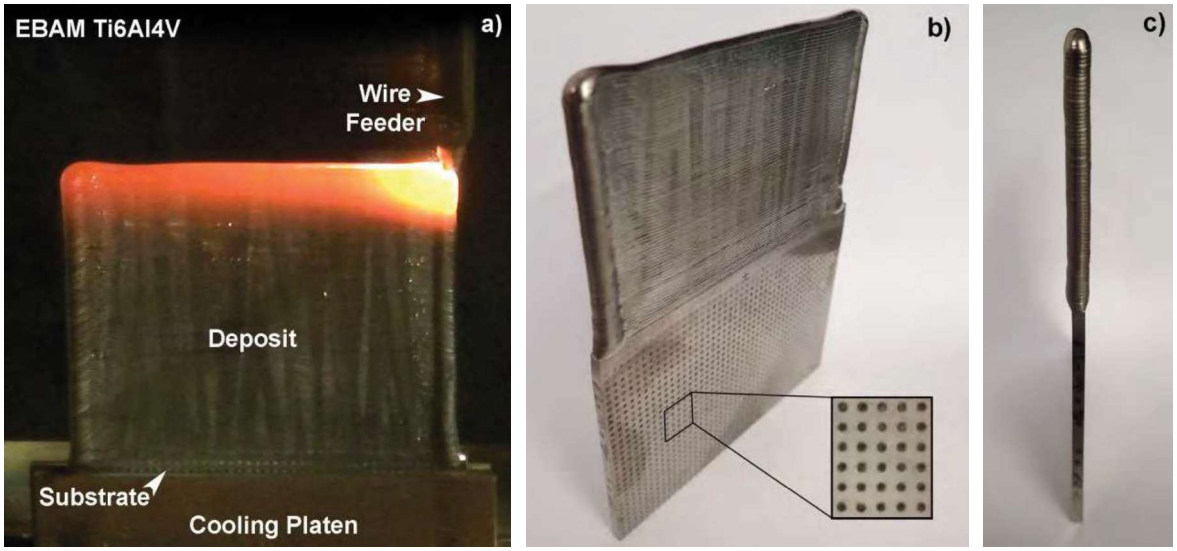

Figure 100 EBAM of a Ti6Al4V wall (50 mm in height) built on a 3 mm thick substrate etched for out-of-plane distortion measurement with a non-contact optical deformation measurement system

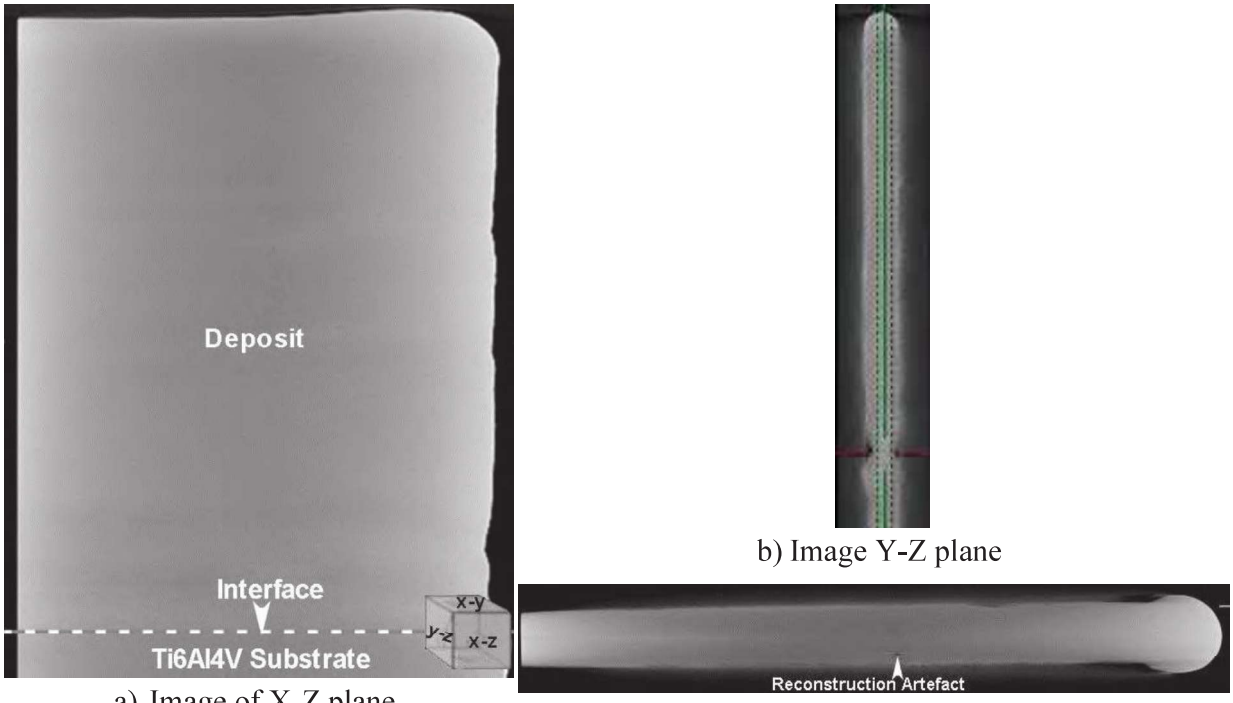

a) Image of X-Z plane

b) Image Y-Z plane

c) Image of X-Y plane (at mid-height)

Figure 101 X-ray micro-CT scan of Ti6Al4V deposited by EBAM exhibiting no indications

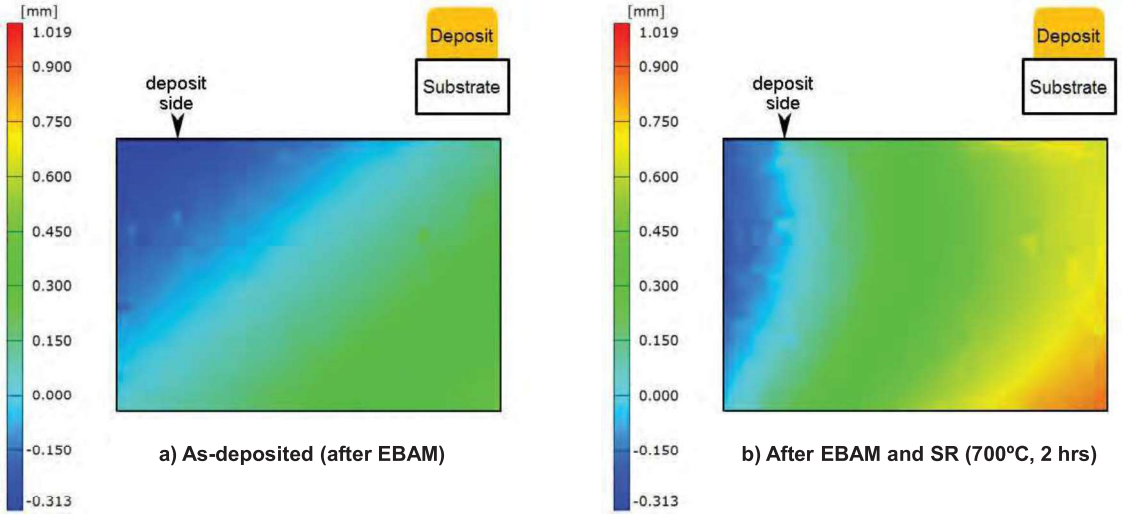

Figure 102 Map of out-plane displacement in Ti6Al4V substrate due to electron beam additive manufacturing with and without stress relieving at 700°C for 2 hours

9.6.1 REFERENCES

[67] P. Wanjara, J. Gholipour, C. Bescond, K. Watanabe and K. Nezaki, Characteristics of Ti6Al4V Repair using Electron Beam Additive Manufacturing, NATO-STO AVT-258 Specialists' Meeting Additive Manufacturing for Military Hardware, 27-29 April 2016, Tallinn, Estonia, pp. 16-1 – 16-14

9.7 FATIGUE OF ELECTRON BEAM WELDED TI-6AL-4V AND IMI834 TITANIUM ALLOY DISSIMILAR JOINTS

D.L. Chen, Department of Mechanical and Industrial Engineering, Ryerson University, Toronto, Ontario, Canada

Titanium and its alloys have been increasingly used as one of key structural materials in the aerospace applications due to their excellent combination of properties such as high strength-to-weight ratio, high fatigue life, toughness, excellent resistance to corrosion. The structural application of titanium alloys including their welded joints involves unavoidably fatigue and cyclic deformation characteristics, which results in the occurrence of fatigue failure. Hence, an understanding of fatigue and cyclic deformation of titanium alloy and its joints is critical for the design and durability evaluation of engineering components. The present study was, therefore, aimed at evaluating the microstructural characteristics, hardness, tensile and fatigue behaviour of electron beam (EB) welded Ti-6Al-4V/IMI834 alloys joints.

The results obtained showed that the cyclic stress-strain curve was in general consistent with the monotonic one for the dissimilar joint within the experimental scatter, as shown in Figure 103 extra space. The cyclic yield strength is about 9% lower than that of the monotonic yield strength of the dissimilar joint (i.e., 795 MPa vs. 868 MPa). This suggests that slight cyclic softening would occur, corresponding well to the change in the stress amplitude.

The fatigue tests revealed that the hysteresis loop became widened and its enclosed area increased with increasing strain amplitude, and the compressive stress was almost the same as the tensile stress, as shown in Figure 104, indicating the symmetry of hysteresis loops unlike the situation of conventional extruded magnesium alloys.

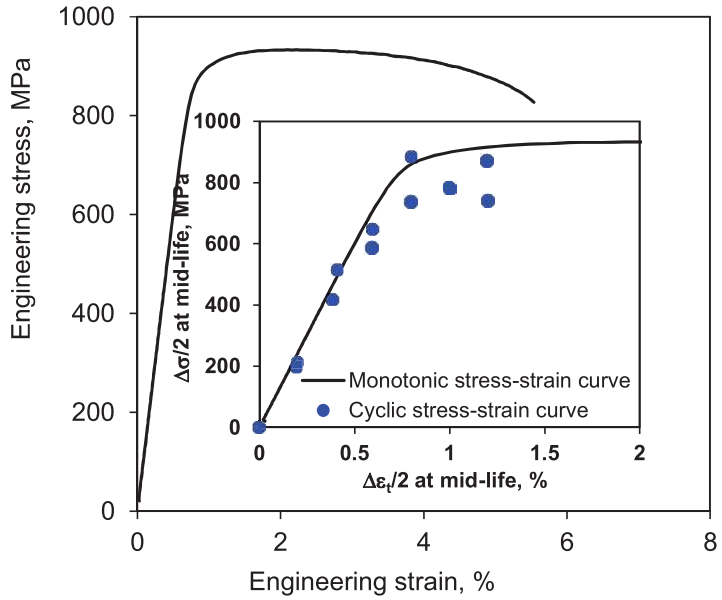

Figure 103 Monotonic stress-strain curves for the dissimilar joint, where the corresponding cyclic stress-strain curves are plotted for comparison

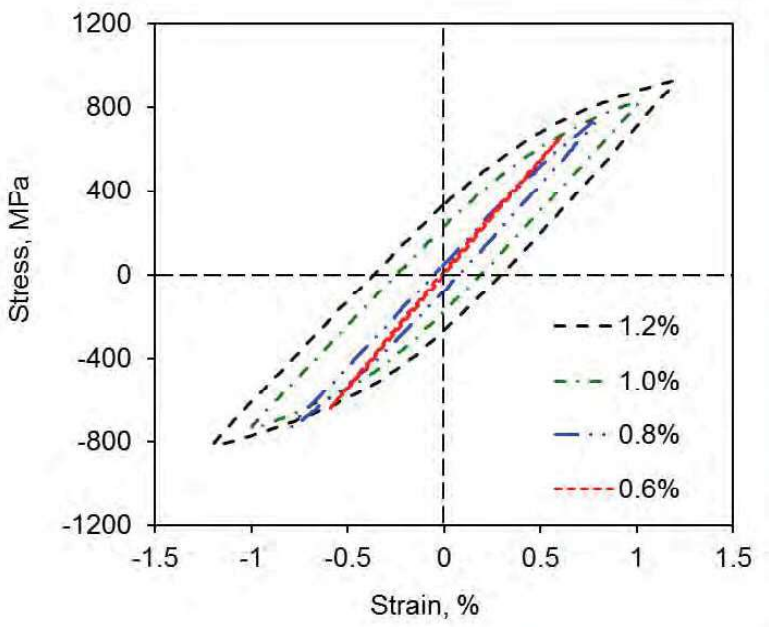

Figure 104 Mid-life stress-strain hysteresis loops at different total strain amplitudes

The response of cyclic stress amplitude as a function of the number of cycles at different strain amplitudes during strain-controlled fatigue tests for the dissimilar joints is shown in Figure 105. Generally cyclic stress amplitude increased and fatigue life decreased with increasing strain

amplitude in the dissimilar joints. At lower total strain amplitudes (0.2-0.6%) the stress amplitude remained basically constant or stable in the dissimilar joints throughout the entire fatigue life. At higher total strain amplitudes (0.8-1.2%), slight cyclic softening occurred in the dissimilar joints, which was in agreement with the results in Figure 103, where the cyclic stress-strain curve was positioned slightly below the monotonic cyclic stress-strain curve. This was likely due to the dislocation annihilation and rearrangement. The strain amplitude of 0.6% appeared to be a threshold, at or below which cyclic stabilization or saturation remained in the entire cyclic deformation process. Similar cyclic deformation characteristics have been reported for titanium alloys under strain-controlled fatigue tests. However, this was noticed to be in contrast to the cyclic deformation characteristics (secondary cyclic hardening) in the Ti-2Al-2.5Zr alloys fatigued at high temperatures due to the presence of multiple slip including prismatic plane and pyramidal plane, and also in magnesium alloys owing to the occurrence of twinning. Furthermore, the fatigue life of the dissimilar joints decreased with increasing strain amplitude, and was almost equal to that of the base metals (BMs) as shown in Figure 106. The fatigue life obtained in the present study was in good agreement with those presented in the literature referred in [68].

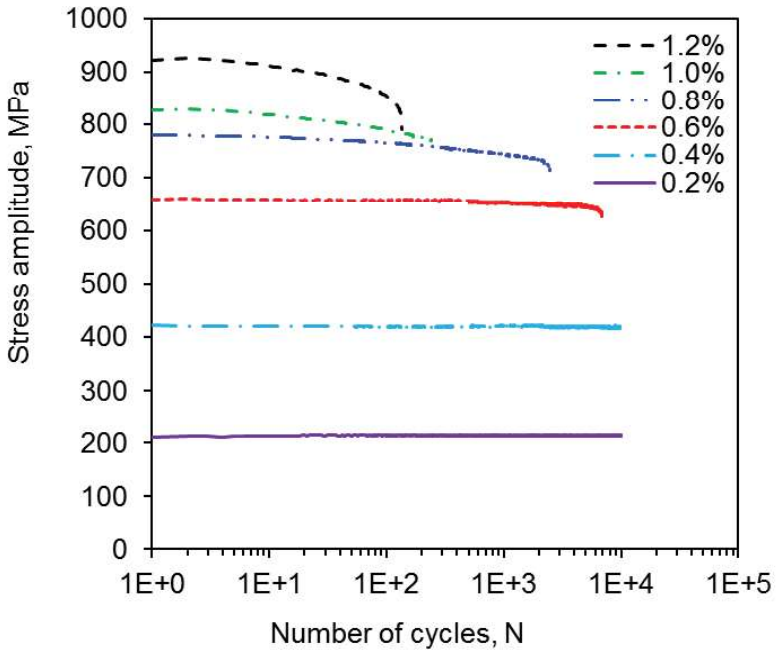

Figure 105 Stress amplitude vs. the number of cycles at different total strain amplitudes for the welded joints

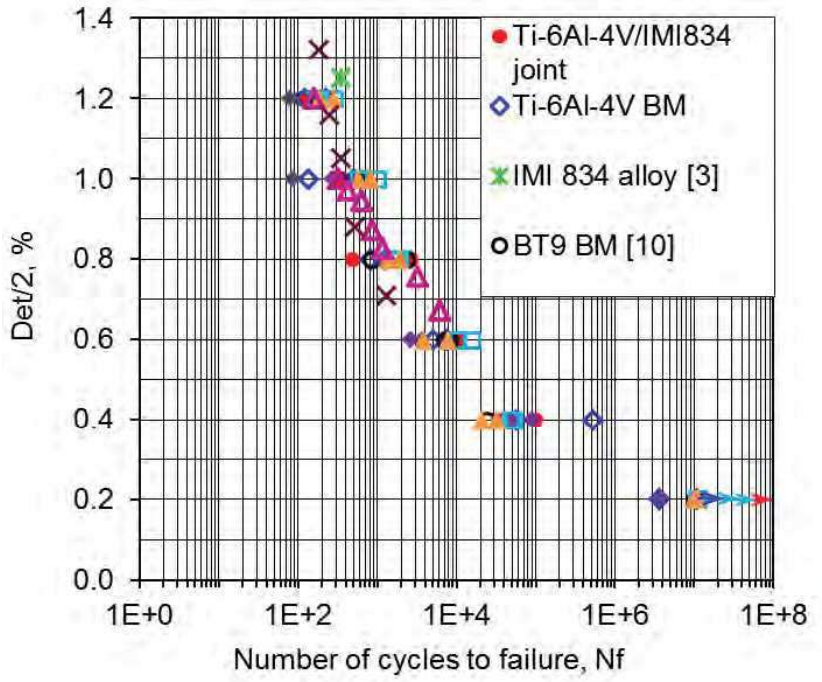

Figure 106 Total strain amplitude as a function of the number of cycles to failure for BMs and dissimilar joints, in comparison with the results reported in the literature

9.7.1 REFERENCES

[68] S.Q. Wang, W.Y. Li, Y. Zhou, X. Li, D.L. Chen, Tensile and fatigue behavior of electron beam welded dissimilar joints of Ti-6Al-4V and IMI834 titanium alloys, Materials Science and Engineering A, 2016, 649, 146-152.

9.8 DISCUSSION PAPER ON THE CERTIFICATION OF ADDITIVE MANUFACTURED COMPONENT

Min Liao, NRC Aerospace

Additive Manufacturing (AM) is one of the most attractive technology trends in aerospace and defence. Although AM will not replace conventional processes in the near future, it does have the potential to produce metallic parts for legacy systems, particularly for those that have gone out of production. This technology could sometime produce parts at significantly lower costs and with quick turnaround times. However, there are challenges that remain which need to be overcome before this technology can be readily adopted. One of the greatest challenges is how to certify/qualify AM parts for aerospace structural applications, especially for primary structural application. The goal of this task, shown in Figure 107, is to prepare a discussion paper on certification of AM components. In this study, both significant *potentials and challenges* are

presented for adopting and applying AM technology on primary/safety-critical metallic structures. To date, AM technologies have been applied to restore component geometry and to create secondary/non-critical structural replacement parts. Major challenges/issues exist, especially in qualification/certification of AM application, for primary metallic structures. This paper highlights the concerns/issues relating to AM, provides some considerations and R&D recommendations that will facilitate AM component certification and application.

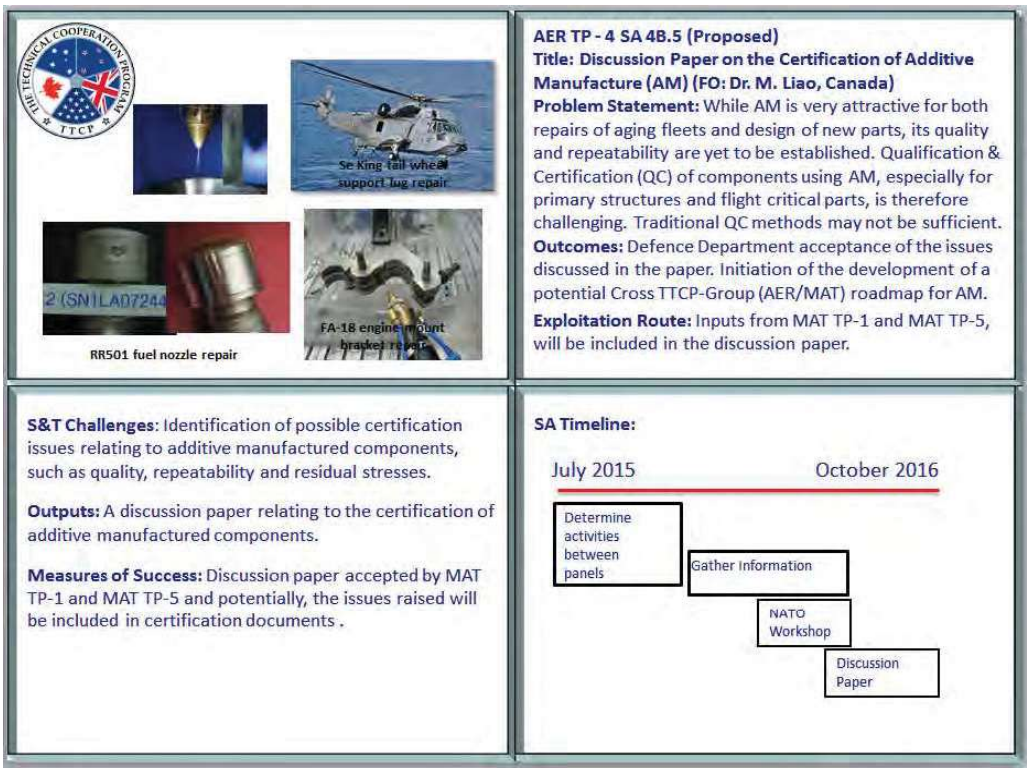

Figure 107 A TTCP AER (TP-4) Task on AM

9.8.1 REFERENCES

[69] Min Liao, Discussion Paper on the Certification of Additive Manufactured Component NRC Technical Report, LTR-SMM-2017-0037.

ACKNOWLEDGEMENTS

The NRC programs, Aeronautical Product Development Technologies (APDT) and Air Defence and Systems (ADS) provided support for some NRC's effort to prepare this ICAF National Review.

Special thanks to all the organizations and authors who contributed the input to the Canadian National Review for ICAF2017.